EPJ manuscript No.
(will be inserted by the editor)

Quest for precision in hadronic cross sections at low energies: Monte Carlo tools vs. experimental data

S. Actis[1], A. Arbuzov[2], G. Balossini[3], C. Bignamini[3], R. Bonciani[4], C.M. Carloni Calame[5], M. Czakon[6], H. Czyz[7], A. Denig[8], A. Ferroglia[9], G. Fetodovich[10], J. Gluza[7],, M. Gunia[7], A. Hafner[8], S. Jadach[11], P. Mastrolia[12], G. Montagna[3], F. Nguyen[13], O. Nicrosini[14], A. Penin[15], F. Piccinini[14], W. Płaczek[16], E. Remiddi[17], T. Riemann[18], A. Sibidanov[10], L. Trentadue[19], J. J. van der Bij[20], P. Wang[21], B.F.L. Ward[22], and M. Worek[23,7]

[1] Paul Scherrer Institut, Wuerenlingen and Villigen, CH-5232 Villigen PSI, Switzerland
[2] Bogoliubov Laboratory of Theoretical Physics, Joint Institute for Nuclear Research, 141980 Dubna, Russia
[3] Dipartimento di Fisica Nucleare e Teorica, Università di Pavia, and INFN, Sezione di Pavia, I-27100 Pavia, Italy
[4] Laboratoire de Physique Subatomique et de Cosmologie, Université Joseph Fourier/CNRS-IN2P3/INPG, F-38026 Grenoble, France
[5] School of Physics and Astronomy, University of Southampton, Southampton SO17 1BJ, UK and INFN, I-00044 Frascati, Italy
[6] Institut für Theoretische Physik E, RWTH Aachen Universität, D-52056 Aachen, Germany
[7] Department of Field Theory and Particle Physics, Institut of Physics, University of Silesia, PL-40007 Katowice, Poland
[8] Institut für Kernphysik, Johannes Gutenberg-Universität Mainz, D-55128 Mainz, Germany
[9] Institut für Physik (THEP), Johannes Gutenberg-Universität, D-55099 Mainz, Germany
[10] Budker Institute of Nuclear Physics, Novosibirsk, 630090 Russia
[11] Institute of Nuclear Physics, Polish Academy of Sciences, 31-342 Cracow, Poland
[12] CERN, Theory Department, CH-1211 Genève, Switzerland
[13] Dipartimento di Fisica dell'Università Roma Tre, and INFN, Sezione di Roma Tre, I-00146, Roma, Italy
[14] INFN, Sezione di Pavia, I-27100 Pavia, Italy
[15] Department of Physics, University of Alberta, Edmonton, AB T6G 2J1, Canada
[16] Marian Smoluchowski Institute of Physics, Jagiellonian University, 30-059 Cracow, Poland
[17] Dipartimento di Fisica dell'Università di Bologna, and INFN, Sezione di Bologna, I-40126 Bologna, Italy
[18] Deutsches Elektronen-Synchrotron, DESY, D-15738 Zeuthen, Germany
[19] Dipartimento di Fisica, Università di Parma, and INFN, Gruppo Collegato di Parma I-43100 Parma, Italy
[20] Physikalisches Institut, Albert-Ludwigs-Universität Freiburg, D-79104 Freiburg, Germany
[21] Institute of High Energy Physics, Beijing 10049, People's Republic of China
[22] Department of Physics, Baylor University, Waco, Texas 76798-7316, USA
[23] Fachbereich C, Bergische Universität Wuppertal, D-42097 Wuppertal, Germany

Received: date / Revised version: date

Abstract. Insert your abstract here.

PACS. PACS-key BU-HEPP-09-08 – PACS-key CERN-PH-TH/2009-201 – PACS-key DESY 09-092 – PACS-key FNT/T 2009/03 – PACS-key Freiburg-PHENO-09/07 – PACS-key HEPTOOLS 09-018 – PACS-key LPSC 09/157 – PACS-key PITHA-09/14 – PACS-key PSI-PR-09-14 – PACS-key SFB/CPP-09-53 – PACS-key WUB/09-07

1 Luminosity

The present Section addresses the most important experimental and theoretical issues involved in the precision determination of the luminosity at meson factories. The luminosity is the key ingredient underlying all the measurements and studies of the physics processes discussed in the other Sections. Particular emphasis is put on the theoretical accuracy inherent to the event generators used in the experimental analysis, in comparison with the most advanced perturbative calculations and experimental precision requirements. The effort done during the activity of the working group to perform tuned comparisons between the predictions of the most accurate programs is described in detail. New calculations, leading to an update of the theoretical error associated to the prediction of the luminosity cross section, are also presented. The aim of the Section is to provide a self-contained and up-to-date description of the progress occurred during the last few years towards high-precision luminosity monitor-

ing at flavour factories, as well as of the still open issues necessary for future advances.

The structure of the Section is as follows. After an introduction on the motivation for precision luminosity measurements at meson factories (Section 1.1), the leading-order (LO) cross sections of the two QED processes of major interest, i.e. Bhabha scattering and photon pair production, are presented in Section 1.2, together with the formulae for the next-to-leading-order (NLO) photonic corrections to the above processes. The remarkable progress on the calculation of next-to-next-leading-order (NNLO) QED corrections to the Bhabha cross section, as occurred in the last few years, is reviewed in Section 1.3. In particular, this Section presents new exact results on lepton and hadron pair corrections, taking into account realistic event selection criteria. Section 1.4 is devoted to the description of the theoretical methods used in the Monte Carlo (MC) generators for the simulation of multiple photon radiation. The matching of such contributions with NLO corrections is also described in Section 1.4. The main features of the MC programs used by the experimental collaborations are summarized in Section 1.5. Numerical results for the radiative corrections implemented into the MC generators are shown in Section 1.6 for both the Bhabha process and two-photon production. The tuned comparisons between the predictions of the most precise generators are presented and discussed in detail in Section 1.7, considering the Bhabha process at different centre-of-mass (c.m.) energies and with realistic experimental cuts. The theoretical accuracy presently reached by the luminosity tools is addressed in Section 1.8, where the most important sources of uncertainty are discussed quantitatively. The estimate of the total error affecting the calculation of the Bhabha cross section is given, as main conclusion of the present work, in Section 1.9, updating and making more robust results available in the literature. Some still open issues are drawn in Section 1.9 as well.

1.1 Motivation

The luminosity of a collider is the normalization constant between the event rate and the cross section of a given process. For an accurate measurement of the cross section of an electron-positron (e^+e^-) annihilation process, the precise knowledge of the collider luminosity is mandatory.

The luminosity depends on three factors: beam-beam crossing frequency, beam currents and the beam overlap area in the crossing region. However, the last quantity is difficult to determine accurately from the collider optics. Thus, experiments prefer to determine the luminosity by the counting rate of well selected events whose cross section is known with good accuracy, using the formula [1]

$$\int \mathcal{L}\,\mathrm{d}t = \frac{N}{\epsilon\,\sigma}, \tag{1}$$

where N is the number of events of the chosen reference process, ϵ the experimental selection efficiency and σ the theoretical cross section of the reference process. Therefore, the total luminosity error will be given by the sum in quadrature of the fractional experimental and theoretical uncertainties.

Since the advent of low luminosity e^+e^- colliders, a great effort was devoted to obtain good precision in the cross section of electromagnetic processes, extending the pioneering work of the earlier days [2]. At the e^+e^- colliders, operating in the c.m. energy range 1 GeV $< \sqrt{s} <$ 3 GeV, such as ACO at Orsay, VEPP-II at Novosibirsk and Adone at Frascati, the luminosity measurement was based on Bhabha scattering [3,4] with final-state electrons and positrons detected at small angles, or single and double bremsstrahlung processes [5], thanks to their high statistics. The electromagnetic cross sections scale as $1/s$, while elastic e^+e^- scattering has a steep dependence on the polar angle, $\sim 1/\theta^3$, thus providing high rate for small values of θ.

Also at high-energy accelerators running in the '90s around the Z pole to perform precision tests of the Standard Model (SM), as LEP at CERN and SLC at Stanford, the experiments used small-angle Bhabha scattering events as a luminosity monitoring process. Indeed, for the very forward angular acceptances considered by LEP/SLC collaborations, the Bhabha process is dominated by the electromagnetic interaction and, therefore, calculable, at least in principle, with very high accuracy. At the end of LEP and SLC operation, a total (experimental plus theoretical) precision of one per mille (or better) was achieved [6,7,8,9,10,11,12], thanks to the work of different theoretical groups and the excellent performance of precision luminometers.

At current low- and intermediate-energy high-luminosity meson factories, the small polar angle region is difficult to access for the presence of the low-beta insertions close to the beam crossing region, while wide-angle Bhabha scattering produces a large counting rate and can be exploited for a precise measurement of the luminosity.

Therefore, also in this latter case of $e^\pm$ scattered at large angles, e.g. larger than 55° for the KLOE experiment [1] running at DAΦNE, in Frascati and larger than 40° for the CLEO-c experiment [13] running at CESR, Cornell, the main advantages of Bhabha scattering are preserved:

1. large statistics. For example at DAΦNE, a statistical error $\delta\mathcal{L}/\mathcal{L} \sim 0.3\%$ is reached in about two hours of data taking, even at the lowest luminosities;
2. high accuracy for the calculated cross section;
3. clean event topology of the signal and small amount of background.

In Eq. (1) the cross section is usually evaluated by inserting event generators, which include radiative corrections at a high level of precision, into the MC code simulating the detector response. The code has to be developed to reproduce the detector performance (geometrical acceptance, reconstruction efficiency and resolution of the measured quantities) to a high level of confidence.

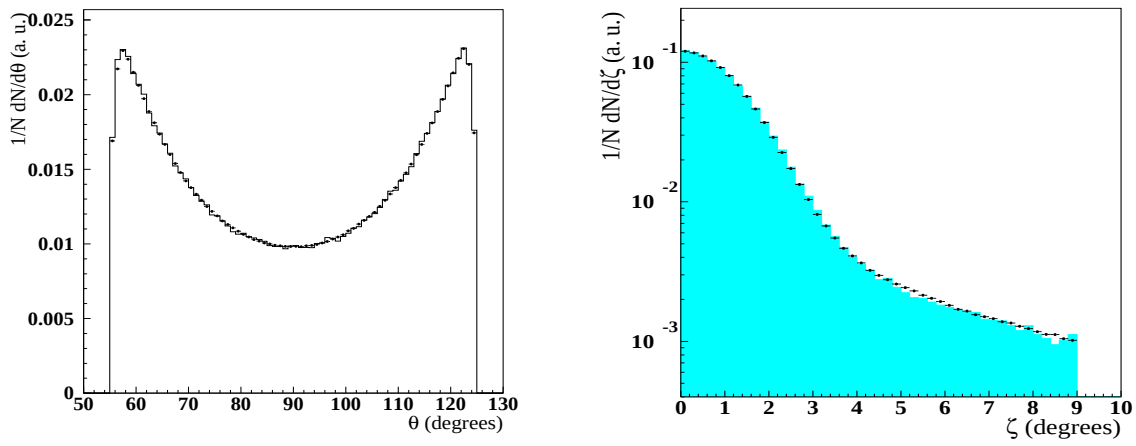

Fig. 1. Comparison between large-angle Bhabha KLOE data (points) and MC (histogram) distributions for the $e^{\pm}$ polar angle θ (left) and for the acollinearity, $\zeta = |\theta_{e^+} + \theta_{e^-} - 180°|$ (right), where the flight direction of the $e^{\pm}$ is given by the position of clusters in the calorimeter. In each case, MC and data histograms are normalized to unity. From [1].

In most cases the major sources of the systematic errors of the luminosity measurement are differences of efficiencies and resolutions between data and MC.

In the case of KLOE the largest experimental error of the luminosity measurement is due to a different polar angle resolution between data and MC which is observed at the edges of the accepted interval for Bhabha scattering events. Figure 1 shows a comparison between large angle Bhabha KLOE data and MC, at left for the polar angle and at right for the acollinearity $\zeta = |\theta_{e^+} + \theta_{e^-} - 180°|$. One observes a very good agreement between data and MC, but also the differences (of about 0.3 %) at the sharp interval edges. The analysis cut, $\zeta < 9°$, applied to the acollinearity distribution is very far from the bulk of the distribution and does not introduce noteworthy systematic errors. Also in the CLEO-c luminosity measurement with Bhabha scattering events, the detector modeling is the main source of experimental error. In particular, uncertainties include those due to finding and reconstruction of the electron shower, in part due to the nature of the electron shower, as well as the steep $e^{\pm}$ polar angle distribution.

The luminosity measured with Bhabha scattering events is often checked by using other QED processes, such as $e^+e^- \to \mu^+\mu^-$ or $e^+e^- \to \gamma\gamma$. In KLOE, the luminosity measured with $e^+e^- \to \gamma\gamma$ events differs by 0.3% with respect to Bhabha events. In CLEO-c, $e^+e^- \to \mu^+\mu^-$ events are also used and the luminosity determined from $\gamma\gamma$ ($\mu^+\mu^-$) is found to be 2.1% (0.6%) larger than that from Bhabha events. Figure 2 shows the CLEO-c data for the polar angle distributions of all three processes, compared with the corresponding MC predictions. The three QED processes are also used by the BaBar experiment at the PEP-II collider, Stanford, yielding a luminosity determination with an error of about 1% [14]. Large-angle Bhabha scattering is the normalization process adopted by the CMD-2 and SND collaborations at VEPP-2M, Novosibirsk, while both BES at BEPC, Beijing and BELLE at KEKB, Tsukuba measure luminosity using the processes $e^+e^- \to e^+e^-$ and $e^+e^- \to \gamma\gamma$ with the final-state particles detected at wide polar angles and an experimental accuracy of a few per cent. However, the BES-III aims at reaching a few per mille error in the luminosity measurement in the near future [15].

The need of precision, namely better than 1%, and possibly redundant measurements of the collider luminosity is of utmost importance to perform accurate measurements of the $e^+e^- \to$ hadrons cross sections, which are the key ingredient for evaluating the hadronic contribution to the running of the electromagnetic coupling constant α and the muon anomaly $g - 2$.

1.2 LO cross sections and NLO corrections

As remarked in Section 1.1, the processes of interest for luminosity measurement at meson factories are Bhabha scattering and electron-positron annihilation into two photons and muon pairs. Here we present the LO formulae of the cross section of the processes $e^+e^- \to e^+e^-$ and $e^+e^- \to \gamma\gamma$, as well as the QED corrections to their cross sections in the NLO approximation of the perturbation theory. The reaction $e^+e^- \to \mu^+\mu^-$ is discussed in Section 2.

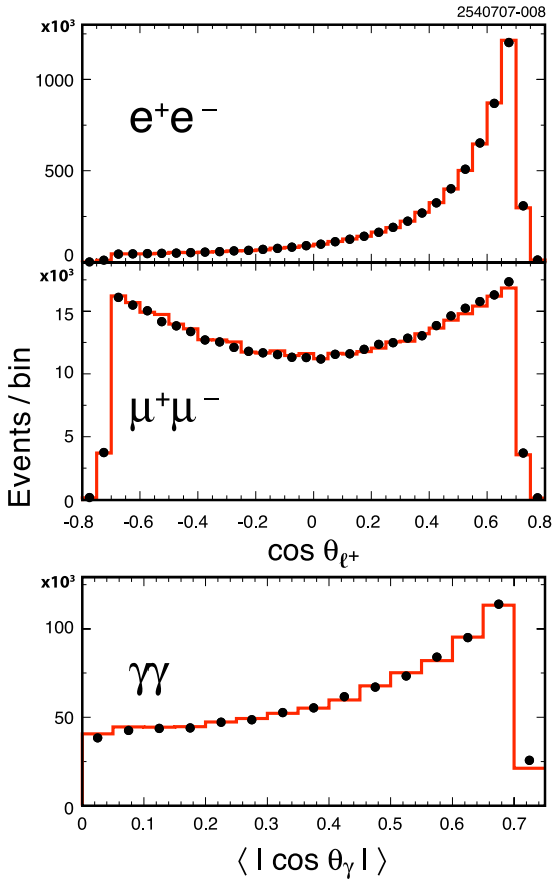

Fig. 2. Distributions of CLEO-c $\sqrt{s} = 3.774$ GeV data (circles) and MC simulations (histogram) for the polar angle of the positive lepton (upper two plots) in e^+e^- and $\mu^+\mu^-$ events, and the mean value of $|\cos\theta_\gamma|$ of the two photons in $\gamma\gamma$ events. MC histograms are normalized to the number of data events. From [13].

1.2.1 LO cross sections

For the Bhabha scattering process

$$e^-(p_-) + e^+(p_+) \to e^-(p'_-) + e^+(p'_+) \tag{2}$$

at the Born level with simple one-photon exchange (see Fig. 3) the differential cross section reads

$$\frac{\mathrm{d}\sigma_0^{\mathrm{Bhabha}}}{\mathrm{d}\Omega_-} = \frac{\alpha^2}{4s}\left(\frac{3+c^2}{1-c}\right)^2 + \mathcal{O}\left(\frac{m_e^2}{s}\right), \tag{3}$$

where

$$s = (p_- + p_+)^2, \qquad c = \cos\theta_-. \tag{4}$$

The angle θ_- is defined between the initial and final electron three-momenta, $\mathrm{d}\Omega_- = \mathrm{d}\phi_-\mathrm{d}\cos\theta_-$, and ϕ_- is the azimuthal angle of the outgoing electron. The small mass correction terms suppressed by the ratio m_e^2/s are negligible for the energy range and the angular acceptances which are of interest here.

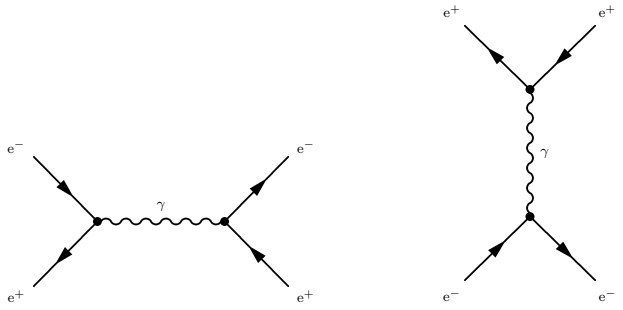

Fig. 3. LO Feynman diagrams for the Bhabha process in QED, corresponding to s-channel annihilation and t-channel scattering.

At meson factories the Bhabha scattering cross section is largely dominated by t-channel photon exchange, followed by s-t interference and s-channel annihilation. Furthermore, Z-boson exchange contributions and other electroweak effects are suppressed at least by a factor s/M_Z^2. In particular, for large-angle Bhabha scattering with a c.m. energy $\sqrt{s} = 1$ GeV the Z boson contribution amounts to about -1×10^{-5}. For $\sqrt{s} = 3$ GeV it amounts to -1×10^{-4} and -1×10^{-3} for $\sqrt{s} = 10$ GeV. So only at B-factories the electroweak effects should be taken into account at the tree level, when aiming at a per mille precision level.

The LO differential cross section of the two-photon annihilation channel (see Fig. 4)

$$e^+(p_+) + e^-(p_-) \to \gamma(q_1) + \gamma(q_2) \tag{5}$$

can be obtained by a crossing relation from the Compton scattering cross section computed by Brown and Feynman [16]. It reads as follows

$$\frac{\mathrm{d}\sigma_0^{\gamma\gamma}}{\mathrm{d}\Omega_1} = \frac{\alpha^2}{s}\left(\frac{1+c_1^2}{1-c_1^2}\right) + \mathcal{O}\left(\frac{m_e^2}{s}\right), \tag{6}$$

where $\mathrm{d}\Omega_1$ denotes the differential solid angle of the first photon. It is assumed that both final photons are registered in a detector, and that their polar angles with respect to the initial beam directions are not small ($\theta_{1,2} \gg m_e/E$, where E is the beam energy).

1.2.2 NLO corrections

The complete set of NLO radiative corrections, emerging at $\mathcal{O}(\alpha)$ of the perturbation theory, to Bhabha scattering and two-photon annihilation can be split into gauge-invariant subsets: QED corrections, due to emission of real photons off the charged leptons and exchange of virtual photons between them, and purely weak contributions arising from the electroweak sector of the SM.

The complete $\mathcal{O}(\alpha)$ QED corrections to Bhabha scattering are known since a long time [17,18]. The first complete NLO prediction in the electroweak SM was performed in [19], followed by [20] and several others. At the NNLO, the leading virtual weak corrections from the top

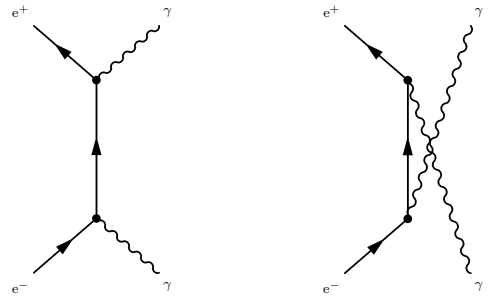

Fig. 4. LO Feynman diagrams for the process $e^+e^- \to \gamma\gamma$.

quark were derived first in [21] and are available in the fitting programs ZFITTER [22,23] and TOPAZ0 [24,25,26] extensively used by the experimentalists for the extraction of the electroweak parameters at LEP/SLC. The weak NNLO corrections in the Standard Model are also known for the ρ-parameter [27,28,29,30,31,32,33,34,35,36,37,38,39,40,41,42,43] and the weak mixing angle [44,45,46,47,48,49], as well as corrections from Sudakov logarithms [50,51,52,53,54,55,56,57]. Both NLO and NNLO weak effects are negligible at low energies and are not implemented yet in numerical packages for Bhabha scattering at meson factories. In pure QED, the situation is considerably different due to a remarkable progress made on NNLO corrections in recent years, as emphasized and discussed in detail in Section 1.3.

As usual, the photonic corrections can be split into two parts according to their kinematics. The first part preserves the Born-like kinematics and contains the effects due to one-loop amplitudes (virtual corrections) and single soft-photon emission. Examples of Feynman diagrams giving rise to such corrections are represented in Fig. 5. The energy of a soft photon is assumed not to exceed an energy ΔE, where E is the beam energy and the auxiliary parameter $\Delta \ll 1$ should be chosen in such a way that the validity of soft-photon approximation is guaranteed. The second contribution is due to hard photon emission, i.e. to single bremsstrahlung with photon energy above ΔE and corresponds to the radiative process $e^+e^- \to e^+e^-\gamma$.

Following [58,59], the soft plus virtual (SV) correction can be cast into the form

$$\frac{\mathrm{d}\sigma^{\mathrm{Bhabha}}_{B+S+V}}{\mathrm{d}\Omega_-} = \frac{\mathrm{d}\sigma^{\mathrm{Bhabha}}_{0}}{\mathrm{d}\Omega_-}\left\{1+\frac{2\alpha}{\pi}(L-1)\left[2\ln\Delta+\frac{3}{2}\right] - \frac{8\alpha}{\pi}\ln(\mathrm{ctg}\frac{\theta}{2})\ln\Delta+\frac{\alpha}{\pi}K^{\mathrm{Bhabha}}_{SV}\right\}, \quad (7)$$

where the factor K^{Bhabha}_{SV} is given by

$$K^{\mathrm{Bhabha}}_{SV} = -1-2\mathrm{Li}_2(\sin^2\frac{\theta}{2})+2\mathrm{Li}_2(\cos^2\frac{\theta}{2}) + \frac{1}{(3+c^2)^2}\left[\frac{\pi^2}{3}(2c^4-3c^3-15c)+2(2c^4-3c^3+9c^2 +3c+21)\ln^2(\sin\frac{\theta}{2})-4(c^4+c^2-2c)\ln^2(\cos\frac{\theta}{2}) -4(c^3+4c^2+5c+6)\ln^2(\mathrm{tg}\frac{\theta}{2})+2(c^3-3c^2+7c -5)\ln(\cos\frac{\theta}{2})+2(3c^3+9c^2+5c+31)\ln(\sin\frac{\theta}{2})\right], \quad (8)$$

and depends on the scattering angle, because of the contribution due to initial-final-state interference and box diagrams (see Fig. 6). It is worth noticing that the SV correction contains a leading logarithmic (LL) part enhanced by the collinear logarithm $L = \ln(s/m_e^2)$. Among the virtual corrections there is also a numerically important effect due to vacuum polarization in the photon propagator. Its contribution is omitted in Eq. (8) but can taken into account in the standard way by insertion of the resummed vacuum polarization operators in the photon propagators of the Born-level Bhabha amplitudes.

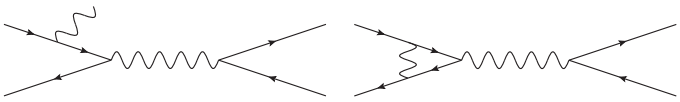

Fig. 5. Examples of Feynman diagrams for real and virtual NLO QED initial-state corrections to the s-channel contribution to the Bhabha process.

The differential cross section of the single hard bremsstrahlung process

$$e^+(p_+)+e^-(p_-)\to e^+(p'_+)+e^-(p'_-)+\gamma(k)$$

for scattering angles being large compared with m_e/E reads

$$\mathrm{d}\sigma^{\mathrm{Bhabha}}_{\mathrm{hard}} = \frac{\alpha^3}{2\pi^2 s}R_{e\bar{e}\gamma}\mathrm{d}\Gamma_{e\bar{e}\gamma}, \quad (9)$$

$$\mathrm{d}\Gamma_{e\bar{e}\gamma} = \frac{\mathrm{d}^3p'_+\mathrm{d}^3p'_-\mathrm{d}^3k}{\varepsilon'_+\varepsilon'_-k^0}\delta^{(4)}(p_++p_--p'_+-p'_--k),$$

$$R_{e\bar{e}\gamma} = \frac{WT}{4}-\frac{m_e^2}{(\chi'_+)^2}\left(\frac{s}{t}+\frac{t}{s}+1\right)^2 - \frac{m_e^2}{(\chi'_-)^2}\left(\frac{s}{t_1}+\frac{t_1}{s}+1\right)^2-\frac{m_e^2}{\chi_+^2}\left(\frac{s_1}{t}+\frac{t}{s_1}+1\right)^2 - \frac{m_e^2}{\chi_-^2}\left(\frac{s_1}{t_1}+\frac{t_1}{s_1}+1\right)^2,$$

where

$$W = \frac{s}{\chi_+\chi_-}+\frac{s_1}{\chi'_+\chi'_-}-\frac{t_1}{\chi'_+\chi_+}-\frac{t}{\chi'_-\chi_-}+\frac{u}{\chi'_+\chi_-}+\frac{u_1}{\chi'_-\chi_+},$$

$$T = \frac{ss_1(s^2+s_1^2)+tt_1(t^2+t_1^2)+uu_1(u^2+u_1^2)}{ss_1tt_1},$$

and the invariants are defined as

$$s_1 = 2p'_-p'_+, \quad t=-2p_-p'_-, \quad t_1=-2p_+p'_+,$$
$$u=-2p_-p'_+, \quad u_1=-2p_+p'_-, \quad \chi_\pm = kp_\pm, \quad \chi'_\pm = kp'_\pm.$$

NLO QED radiative corrections to the two-photon annihilation channel were obtained in [60,61,62,63], while weak corrections were computed in [64].

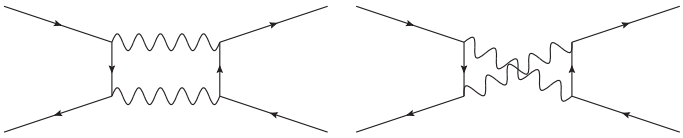

Fig. 6. Feynman diagrams for NLO QED box corrections to the s-channel contribution to the Bhabha process.

In the one-loop approximation the part of the differential cross section with the Born-like kinematics reads

$$\frac{\mathrm{d}\sigma^{\gamma\gamma}_{B+S+V}}{\mathrm{d}\Omega_1} = \frac{\mathrm{d}\sigma^{\gamma\gamma}_{0}}{\mathrm{d}\Omega_1}\left\{1+\frac{\alpha}{\pi}\left[(L-1)\left(2\ln\Delta+\frac{3}{2}\right)+K^{\gamma\gamma}_{SV}\right]\right\},$$

$$K^{\gamma\gamma}_{SV} = \frac{\pi^2}{3}+\frac{1-c_1^2}{2(1+c_1^2)}\left[\left(1+\frac{3}{2}\frac{1+c_1}{1-c_1}\right)\ln\frac{1-c_1}{2}+\left(1+\frac{1-c_1}{1+c_1}+\frac{1}{2}\frac{1+c_1}{1-c_1}\right)\ln^2\frac{1-c_1}{2}+(c_1\to -c_1)\right],$$

$$c_1=\cos\theta_1, \qquad \theta_1=\widehat{\boldsymbol{q}_1\boldsymbol{p}_-}\,. \tag{10}$$

In addition, the three-photon production process

$$e^+(p_+)\ +\ e^-(p_-)\ \to\ \gamma(q_1)\ +\ \gamma(q_2)\ +\ \gamma(q_3)$$

must be included. Its cross section is given by

$$\mathrm{d}\sigma^{e^+e^-\to 3\gamma} = \frac{\alpha^3}{8\pi^2 s}R_{3\gamma}\,\mathrm{d}\Gamma_{3\gamma}\,, \tag{11}$$

$$R_{3\gamma} = s\,\frac{\chi_3^2+(\chi_3')^2}{\chi_1\chi_2\chi_1'\chi_2'}-2m_e^2\left[\frac{\chi_1^2+\chi_2^2}{\chi_1\chi_2(\chi_3')^2}+\frac{(\chi_1')^2+(\chi_2')^2}{\chi_1'\chi_2'\chi_3^2}\right] + (\text{cyclic permutations}),$$

$$\mathrm{d}\Gamma_{3\gamma} = \frac{\mathrm{d}^3q_1\mathrm{d}^3q_2\mathrm{d}^3q_3}{q_1^0q_2^0q_3^0}\delta^{(4)}(p_++p_--q_1-q_2-q_3),$$

where

$$\chi_i = q_ip_-, \qquad \chi_i' = q_ip_+, \qquad i=1,2,3\,.$$

The process has to be treated as a radiative correction to the two-photon production. The energy of the third photon should exceed the soft-photon energy threshold ΔE. In practice, the tree photon contribution, as well as the radiative Bhabha process $e^+e^-\to e^+e^-\gamma$, should be simulated with the help of a MC event generator in order to take into account the proper experimental criteria of a given event selection.

In addition to the corrections discussed above, also the effect of vacuum polarization, due to the insertion of fermion loops inside the photon propagators, must be included in the precise calculation of the Bhabha scattering cross section. Its theoretical treatment, which faces the non-trivial problem of the non-perturbative contribution due to light quarks, is addressed in detail in Section 4. However, numerical results for such a correction are presented in Section 1.6 and Section 1.8.

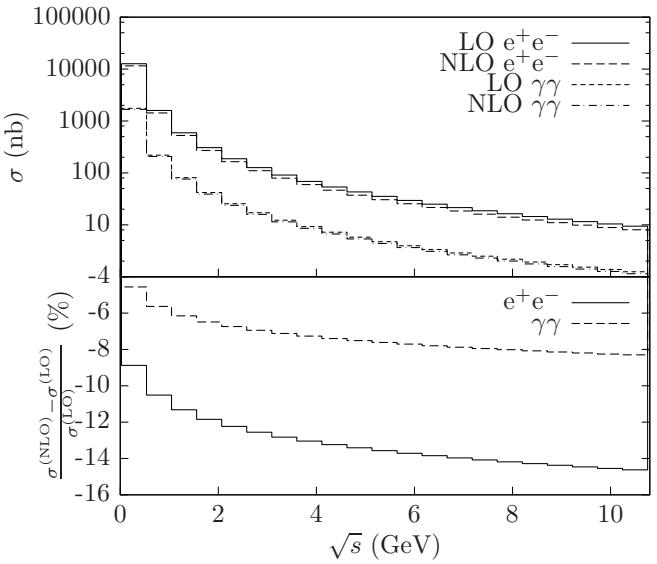

Fig. 7. Cross sections of the processes $e^+e^-\to e^+e^-$ and $e^+e^-\to\gamma\gamma$ in the LO and NLO approximations, as a function of the c.m. energy at meson factories (upper panel). In the lower panel, the relative contribution due to the NLO QED corrections (in per cent) to the two processes is shown.

In Fig. 7 the cross sections of the Bhabha and two-photon production processes in the LO and NLO approximations are shown as a function of the c.m. energy between $\sqrt{s}\simeq 2\,m_\pi$ and $\sqrt{s}\simeq 10$ GeV (upper panel). The results were obtained imposing the following cuts for the Bhabha process:

$$\theta_\pm^{\min}=45^\circ \qquad \theta_\pm^{\max}=135^\circ$$
$$E_\pm^{\min}=0.3\sqrt{s} \qquad \xi_{\max}=10^\circ \tag{12}$$

where $\theta_\pm^{\min,\max}$ are the angular acceptance cuts, $E_\pm^{\min}$ are the minimum energy thresholds for the detection of the final-state electron/positron and $\xi_{\max}$ is the maximum e^+e^- acollinearity. For the photon pair production processes we used correspondingly:

$$\theta_\gamma^{\min}=45^\circ \qquad \theta_\gamma^{\max}=135^\circ$$
$$E_\gamma^{\min}=0.3\sqrt{s} \qquad \xi_{\max}=10^\circ \tag{13}$$

where, as in Eq. (12), $\theta_\gamma^{\min,\max}$ are the angular acceptance cuts, $E_\gamma^{\min}$ is the minimum energy threshold for the detection of at least two photons and $\xi_{\max}$ is the maximum acollinearity between the most energetic and next-to-most energetic photon.

The cross sections display the typical $1/s$ QED behaviour. The relative effect of NLO corrections is shown in the lower panel. It can be seen that the NLO corrections are largely negative and increase with increasing c.m. energies, because of the growing importance of the collinear logarithm $L=\ln(s/m_e^2)$. The corrections to $e^+e^-\to\gamma\gamma$ are about one half of those to Bhabha scattering, because

of the absence of final-state radiation effects in photon pair production.

1.3 NNLO Corrections to the Bhabha Scattering Cross Section

Beyond the NLO corrections discussed in the previous Section, in recent years a significant effort was devoted to the calculation of the perturbative corrections to the Bhabha process at the NNLO in QED.

The calculation of the full NNLO corrections to the Bhabha scattering cross section requires three types of ingredients: *i)* the two-loop matrix elements for the $e^+e^- \to e^+e^-$ process; *ii)* the one-loop matrix elements for the $e^+e^- \to e^+e^-\gamma$ process, both in the case in which the additional photon is soft or hard; *iii)* the tree-level matrix elements for $e^+e^- \to e^+e^-\gamma\gamma$, with two soft, two hard or one soft and one hard photons. Also the process $e^+e^- \to e^+e^-e^+e^-$, with one of the two e^+e^- pairs remaining undetected, contributes to the Bhabha signature at NNLO. Depending on the kinematics, other final states like, e.g., $e^+e^-\mu^+\mu^-$ or those with hadrons are also possible.

The advent of new calculational techniques and a deeper understanding of the IR structure of unbroken gauge theories, such as QED or QCD, made the calculation of the complete set of two-loop QED corrections possible. The history of this calculation will be presented in Section 1.3.1.

Some remarks on the one-loop matrix elements with three particles in the final state are in order now. The diagrams involving the emission of a soft photon are known and they were included in the calculations of the two-loop matrix elements, in order to remove the IR soft divergencies. However, although the contributions due to a hard collinear photon are taken into account in logarithmic accuracy by the MC generators, a full calculation of the diagrams involving a hard photon in a general phase-space configuration is still missing. In Section 1.3.2, we shall comment on the possible strategies which can be adopted in order to calculate these corrections [1].

As a general comment, it must be noticed that the fixed-order corrections calculated up to NNLO are taken into account at the LL, and, partially, next-to-leading-log (NLL) level in the most precise MC generators, which include, as will be discussed in Section 1.4 and Section 1.5, the logarithmically enhanced contributions of soft and collinear photons at all orders in perturbation theory.

Concerning the tree level graphs with four particles in the final state, the production of a soft e^+e^- pair was considered in the literature by the authors of [66] by following the evaluation of pair production [67,68] within the calculation of the $\mathcal{O}(\alpha^2 L)$ single-logarithmic accurate small-angle Bhabha cross section [7], and it is included in the two-loop calculation (see Section 1.3.1). New results on lepton and hadron pair corrections which are at present approximately included in the available Bhabha codes are presented in Section 1.3.3.

[1] As it will be emphasized in Section 1.8 and Section 1.9 the complete calculation of this class of corrections became available [65] during the completion of the present work.

1.3.1 Virtual corrections for the $e^+e^- \to e^+e^-$ process

The calculation of the virtual two-loop QED corrections to the Bhabha scattering differential cross section was carried out in the last 10 years. This calculation was made possible by an improvement of the techniques employed in the evaluation of multiloop Feynman diagrams. An essential tool used to manage the calculation is the Laporta algorithm [69,70,71,72], which allows to reduce a generic combination of dimensionally-regularized scalar integrals to a combination of a small set of independent integrals called the "Master Integrals" (MIs) of the problem under consideration. The calculation of the MIs is then pursued by means of a variety of methods. Particularly important are the differential equations method [73,74,75,76,77,78,79] and the Mellin-Barnes techniques [80,81,82,83,84,85,86,87,88,89]. Both methods proved to be very useful in the evaluation of virtual corrections to Bhabha scattering since they are especially effective in problems with a small number of different kinematic parameters. They both allow one to obtain an analytic expression for the integrals, which must be written in terms of a suitable functional basis. A basis which was extensively employed in the calculation of multiloop Feynman diagrams of the type discussed here is represented by the Harmonic Polylogarithms [90,91,92,93,94,95,96,97,98] and their generalizations. Another fundamental achievement which allowed to complete the calculation of the QED two-loop corrections was an improved understanding of the IR structure of QED. In particular, the relation between the collinear logarithms in which the electron mass m_e plays the role of a natural cut-off and the corresponding poles in the dimensionally regularized massless theory was extensively investigated in [99,100,101,102].

The first complete diagrammatic calculation of the two-loop QED virtual corrections to Bhabha scattering can be found in [103]. However, this result was obtained in the fully massless approximation ($m_e = 0$), by employing dimensional regularization (DR) to regulate both soft and collinear divergencies. Today, the complete set of two-loop corrections to Bhabha scattering in pure QED have been evaluated using m_e as a collinear regulator, as required in order to include these fixed-order calculations in available Monte Carlo event generators. The Feynman diagrams involved in the calculation can be divided in three gauge-independent sets: *i)* diagrams without fermion loops ("photonic" diagrams), *ii)* diagrams involving a closed electron loop, and *iii)* diagrams involving a closed loop of hadrons or a fermion heavier than the electron. Some of the diagrams belonging to the aforementioned sets are shown in Figs. 8–11. These three sets are discussed in more detail below.

Photonic Corrections

A large part of the NNLO photonic corrections can be evaluated in a closed analytic form, retaining the full de-

pendence on m_e [104], by using the Laporta algorithm for the reduction of the Feynman diagrams to a combination of MIs, and then the differential equations method for their analytic evaluation. With this technique it is possible to calculate, for instance, the NNLO corrections to the form factors [105,106,107,108]. However, a calculation of the two-loop photonic boxes retaining the full dependence on m_e seems to be beyond the reach of this method. This is due to the fact that the number of MIs belonging to the same topology is, in some cases, large. Therefore, one must solve analytically large systems of first-order ordinary linear differential equations; this is not possible in general. Alternatively, in order to calculate the different MIs involved, one could use the Mellin-Barnes techniques, as shown in [86,87,108,109,110,111], or a combination of both methods. The calculation is very complicated and a full result is not available yet[2]. However, the full dependence on m_e is not phenomenologically relevant. In fact, the physical problem exhibits a well defined mass hierarchy. The mass of the electron is always very small compared to the other kinematic invariants and can be safely neglected everywhere, with the exception of the terms in which it acts as a collinear regulator. The ratio of the photonic NNLO corrections to the Born cross section is the following

$$\frac{d\sigma^{(2,\mathrm{PH})}}{d\sigma^{(\mathrm{Born})}} = \left(\frac{\alpha}{\pi}\right)^2 \sum_{i=0}^{2} \delta^{(\mathrm{PH},i)} \left(L_e\right)^i + \mathcal{O}\left(\frac{m_e^2}{s}, \frac{m_e^2}{t}\right) , \quad (14)$$

where $L_e = \ln\left(s/m_e^2\right)$ and the coefficients $\delta^{(\mathrm{PH},i)}$ contain infrared logarithms and are functions of the scattering angle θ. The approximation given by Eq. (14) is sufficient for a phenomenological description of the process[3]. The coefficients of the double and single collinear logarithm in Eq. (14), $\delta^{(\mathrm{PH},2)}$ and $\delta^{(\mathrm{PH},1)}$, were obtained in [112, 113]. However, the precision required for luminosity measurements at e^+e^- colliders demands the calculation of the non-logarithmic coefficient, $\delta^{(\mathrm{PH},0)}$. The latter was obtained in [99,100] by reconstructing the differential cross section in the $s \gg m_e^2 \neq 0$ limit from the dimensionally regularized massless approximation [103]. The main idea of the method developed in [99,100] is outlined below. As far as the leading term in the small electron mass expansion is considered, the difference between the massive and the dimensionally regularized massless Bhabha scattering can be viewed as a difference between two regularization schemes for the infrared divergences. With the known massless two-loop result at hand, the calculation of the massive one is reduced to constructing the *infrared matching* term which relates the two above mentioned regularization schemes. To perform the matching an auxiliary amplitude is constructed, which has the same structure of the infrared singularities but it is sufficiently simple to be evaluated at least at the leading order in the small mass expansion. A particular form of the auxiliary amplitude is dictated by the general theory of infrared singularities in QED and involves the exponent of the one-loop correction as well as the two-loop corrections to the logarithm of the electron form factor. The difference between the full and the auxiliary amplitudes is infrared finite. It can be evaluated by using dimensional regularization for each amplitude and then taking the limit of four space-time dimensions. The infrared divergences, which induce the asymptotic dependence of the virtual corrections on the electron and photon masses, are absorbed into the auxiliary amplitude while the technically most nontrivial calculation of the full amplitude is performed in the massless approximation. The matching of the massive and massless results is then necessary only for the auxiliary amplitude and it is straightforward. Thus the two-loop massless result for the scattering amplitude along with the two-loop massive electron form factor [114] are sufficient to obtain the two-loop photonic correction to the differential cross section in the small electron mass limit.

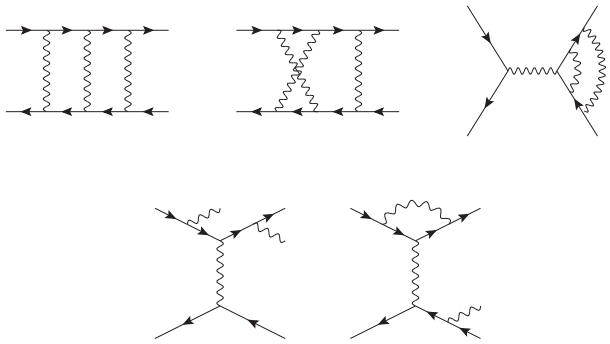

Fig. 8. Some of the diagrams belonging to the class of the "photonic" NNLO corrections to the Bhabha scattering differential cross section. The additional photons in the final state are soft.

A method based on a similar principle was subsequently developed in [101,102]; the authors of [102] confirmed the result of [99,100] for the NNLO photonic corrections to the Bhabha scattering differential cross section.

Electron Loop Corrections

The NNLO electron loop corrections arise from the interference of two-loop Feynman diagrams with the tree-level amplitude as well as from the interference of one-loop diagrams, as long as one of the diagrams contributing to each term involves a closed electron loop. This set of corrections presents a single two-loop box topology, and it is therefore technically less challenging to evaluate with respect to the photonic correction set. The calculation of the electron loop corrections was completed a few years ago [115, 116,117,118]; the final result retains the full dependence of the differential cross section on the electron mass m_e. The MIs involved in the calculation were identified by means of

[2] For the planar double box diagrams, all the MIs are known [109] for small m_e, while the MIs for the non-planar double box diagrams are not completed.

[3] It can be shown that the terms suppressed by a positive power of m_e^2/s do not play any phenomenological role already at very low c.m. energies, $\sqrt{s} \sim 10$ MeV. Moreover, the terms m_e^2/t (or m_e^2/u) become important in the extremely forward (backward) region, unreachable for the experimental setup.

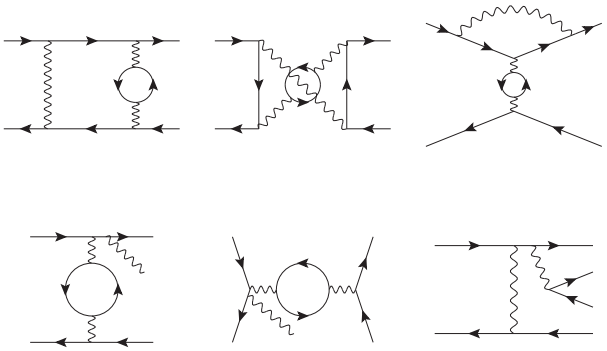

Fig. 9. Some of the diagrams belonging to the class of the "electron loop" NNLO corrections. The additional photons or electron-positron pair in the final state are soft.

the Laporta algorithm and evaluated with the differential equation method. As expected, after UV renormalization the differential cross section presented only residual IR poles which were removed by adding the contribution of the soft photon emission diagrams. The resulting NNLO differential cross section could be conveniently written in terms of 1- and 2-dimensional Harmonic Polylogarithms (HPLs) of maximum weight three. Expanding the cross section in the limit $s, |t| \gg m_e^2$, the ratio of the NNLO corrections to the Born cross section can be written as in Eq. (14):

$$\frac{d\sigma^{(2,\mathrm{EL})}}{d\sigma^{(\mathrm{Born})}} = \left(\frac{\alpha}{\pi}\right)^2 \sum_{i=0}^{3} \delta^{(\mathrm{EL,i})} \left(L_e\right)^i + \mathcal{O}\left(\frac{m_e^2}{s}, \frac{m_e^2}{t}\right) . \quad (15)$$

Note that the series now contains a cubic collinear logarithm. This logarithm appears, with an opposite sign, in the corrections due to the production of an electron-positron pair (the soft-pair production was considered in [66]). When the two contributions are considered together in the full NNLO, the cubic collinear logarithms cancel. Therefore, the physical cross section includes at most a double logarithm, as in Eq. (14).

The explicit expression of all the coefficients $\delta^{(\mathrm{EL,i})}$, obtained by expanding the results of [115,116,117] was confirmed by two different groups [102,118]. In [102] the small electron mass expansion was performed within the soft-collinear effective theory (SCET) framework, while the analysis in [118] employed the asymptotic expansion of the MIs.

Heavy-Flavor and Hadronic Corrections

Finally, we consider the corrections originating from two-loop Feynman diagrams involving a heavy flavor fermion loop[4]. Since this set of corrections involves one more mass scale with respect to the corrections analyzed in the previous sections, a direct diagrammatic calculation is in principle a more challenging task. Recently, in [102] the authors applied their technique based on SCET to Bhabha scattering and obtained the heavy flavor NNLO corrections in the limit in which $s, |t|, |u| \gg m_f^2 \gg m_e^2$, where m_f^2 is the mass of the heavy fermion running in the loop. Their result was very soon confirmed in [118] by means of a method based on the asymptotic expansion of Mellin-Barnes representation of the MIs involved in the calculation. However, the results obtained in the approximation $s, |t|, |u| \gg m_f^2 \gg m_e^2$ cannot be applied to the case in which $\sqrt{s} < m_f$ (as in the case of a tau loop at $\sqrt{s} \sim 1$ GeV), and they apply only to a relatively narrow angular region perpendicular to the beam direction when $\sqrt{s}$ is not very much larger than m_f (as in the case of top-quark loops at ILC). It was therefore necessary to calculate the heavy flavor corrections to Bhabha scattering assuming only that the electron mass is much smaller than the other scales in the process, but retaining the full dependence on the heavy mass, $s, |t|, |u|, m_f^2 \gg m_e^2$.

The calculation was carried out in two different ways: in [119,120] it was done analytically, while in [121,122] it was done numerically with dispersion relations.

The technical problem of the diagrammatic calculation of Feynman integrals with four scales can be simplified by considering carefully, once more, the structure of the collinear singularities of the heavy-flavor corrections. The ratio of the NNLO heavy flavor corrections to the Born cross section is given by

$$\frac{d\sigma^{(2,\mathrm{HF})}}{d\sigma^{(\mathrm{Born})}} = \left(\frac{\alpha}{\pi}\right)^2 \sum_{i=0}^{1} \delta^{(\mathrm{HF,i})} \left(L_e\right)^i + \mathcal{O}\left(\frac{m_e^2}{s}, \frac{m_e^2}{t}\right) , \quad (16)$$

where now the coefficients $\delta^{(i)}$ are functions of the scattering angle θ and, in general, of the mass of the heavy fermions involved in the virtual corrections. It is possible to prove that, in a physical gauge, all the collinear singularities factorize and can be absorbed in the external field renormalization [123]. This observation has two consequences in the case at hand. The first one is that box diagrams are free of collinear divergencies in a physical gauge; since the sum of all boxes forms a gauge independent block, it can be concluded that the sum of all box diagrams is free of collinear divergencies in any gauge. The second consequence is that the single collinear logarithm in Eq. (16) arises from vertex corrections only. Moreover, if one chooses on-shell UV renormalization conditions, the irreducible two-loop vertex graphs are free of collinear singularities. Therefore, among all the two-loop diagrams contributing to the NNLO heavy flavor corrections to Bhabha scattering, only the reducible vertex corrections are logarithmically divergent in the $m_e \to 0$ limit[5]. The latter are easily evaluated even if they depend on two different masses. By exploiting these two facts, one can obtain the NNLO heavy-flavor corrections to the Bhabha scattering differential cross section assuming only that $s, |t|, |u|, m_f^2 \gg m_e^2$. In particular, one can set

[4] Here by "heavy flavor" we mean a muon or a τ-lepton, as well as a heavy quark, like the top, the b- or the c-quark, depending on the c.m. energy range that we are considering.

[5] Additional collinear logarithms arise also from the interference of one-loop diagrams in which at least one vertex is present.

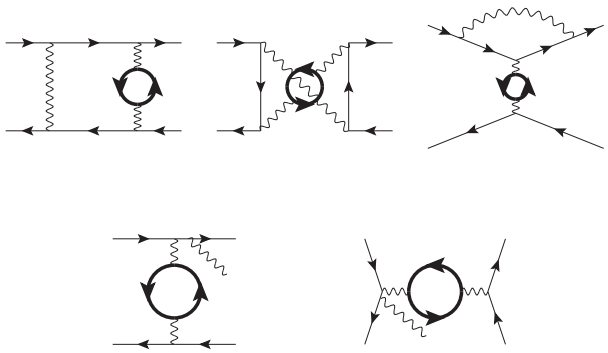

Fig. 10. Some of the diagrams belonging to the class of the "heavy fermion" NNLO corrections. The additional photons in the final state are soft.

$m_e = 0$ from the beginning in all the two-loop diagrams with the exception of the reducible ones. This procedure allows one to effectively eliminate one mass scale from the two-loop boxes, so that these graphs can be evaluated with the techniques already employed in the diagrammatic calculation of the electron loop corrections[6]. In the case in which the heavy flavor fermion is a quark, it is straightforward to modify the calculation of the two-loop self-energy diagrams to obtain the mixed QED-QCD corrections to Bhabha scattering [120].

An alternative approach to the calculation of the heavy flavor corrections to Bhabha scattering, is based on dispersion relations. This method also applies to hadronic corrections. The hadronic and heavy-fermion corrections to the Bhabha-scattering cross section can be obtained by appropriately inserting the renormalized irreducible photon vacuum-polarization function Π in the photon propagator:

$$\frac{g_{\mu\nu}}{q^2 + i\,\delta} \;\to\; \frac{g_{\mu\alpha}}{q^2 + i\,\delta}\,\left(q^2\,g^{\alpha\beta} - q^\alpha\,q^\beta\right)\,\Pi(q^2)\,\frac{g_{\beta\nu}}{q^2 + i\,\delta}. \tag{17}$$

The vacuum polarization Π can be represented by a once-subtracted dispersion integral [2],

$$\Pi(q^2) = -\frac{q^2}{\pi}\int_{4M^2}^{\infty} dz\,\frac{\mathrm{Im}\,\Pi(z)}{z}\,\frac{1}{q^2 - z + i\,\delta}. \tag{18}$$

The contributions to Π may then be determined from a (properly normalized) production cross section by the optical theorem [127],

$$\mathrm{Im}\,\Pi_{\rm had}(z) = -\frac{\alpha}{3}\,R_{\rm had}(z). \tag{19}$$

In this way, the hadronic vacuum polarization may be obtained from the experimental data for $R_{\rm had}$:

$$R_{\rm had}(z) = \frac{\sigma(\{e^+e^- \to \gamma^\star \to \text{hadrons}\}; z)}{(4\pi\alpha^2)/(3z)}. \tag{20}$$

[6] The necessary MIs can be found in [120,124,125,126].

In the low-energy region the inclusive experimental data may be used [128,129]. Around a narrow hadronic resonance with mass $M_{\rm res}$ and width $\Gamma_{\rm res}^{e^+e^-}$ one may use the relation

$$R_{\rm res}(z) = \frac{9\pi}{\alpha^2} M_{\rm res}\Gamma_{\rm res}^{e^+e^-}\,\delta(z - M_{\rm res}^2), \tag{21}$$

and in the remaining regions the perturbative QCD prediction [130]. Contributions to Π arising from leptons and heavy quarks with mass m_f, charge Q_f and color C_f can be computed directly in perturbation theory:

$$R_f(z; m_f) = Q_f^2\,C_f\,\left(1 + 2\,\frac{m_f^2}{z}\right)\,\sqrt{1 - 4\,\frac{m_f^2}{z}}. \tag{22}$$

As a result of the above formulas, the massless photon propagator gets replaced by a massive propagator, whose effective mass z is subsequently integrated over:

$$\frac{g_{\mu\nu}}{q^2 + i\delta} \to \frac{\alpha}{3\pi}\int_{4M^2}^{\infty}\frac{dz\;R(z)}{z(q^2 - z + i\delta)}\left(g_{\mu\nu} - \frac{q_\mu q_\nu}{q^2 + i\delta}\right). \tag{23}$$

For self-energy corrections to Bhabha scattering at one-loop order, the dispersion relation approach was first employed in [131]. Two-loop applications of this technique, prior to Bhabha scattering, are the evaluation of the hadronic vertex correction [132] and of two-loop hadronic corrections to the lifetime of the muon [133]. The approach was also applied to the evaluation of the two-loop form factors in QED in [134,135,136].

The fermionic and hadronic corrections to Bhabha scattering at one-loop accuracy come only from the self-energy diagram; see for details Section 4. At two-loop level there are reducible and irreducible self-energy contributions, vertices and boxes. The reducible corrections are easily treated. For the evaluation of the irreducible two-loop diagrams, it is advantageous that they are one-loop diagrams with self-energy insertions, because the application of the dispersion technique as described here is possible.

The kernel function for the irreducible two-loop vertex was derived in [132] and verified in e.g. [122] and the three kernel functions for the two-loop box functions were first obtained in [137,121,122] and verified in [138]. A complete collection of all the relevant formulae may be found in [122], and the corresponding Fortran code bhbhnnlohf is publicly available at the web page [139] `www-zeuthen.desy.de/theory/research/bhabha/`.

In [122], the dependence of the various heavy-fermion NNLO corrections on $\ln(s/m_f^2)$ for $s, |t|, |u| \gg m_f^2$ was studied. The irreducible vertex behaves (before a combination with real pair emission terms) like $\ln^3(s/m_f^2)$ [132], while the sum of the various infrared divergent diagrams as a whole behaves like $\ln(s/m_f^2)\ln(s/m_e^2)$. This is in accordance with Eq. (16), but the limit plays no effective role at the energies studied here.

As a result of efforts of recent years we have now for all the non-photonic virtual two-loop contributions at least two completely independent calculations. The net result,

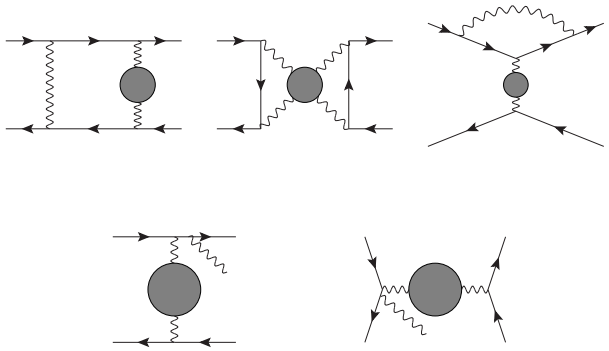

Fig. 11. Some of the diagrams belonging to the class of the "hadronic" corrections. The additional photons in the final state are soft.

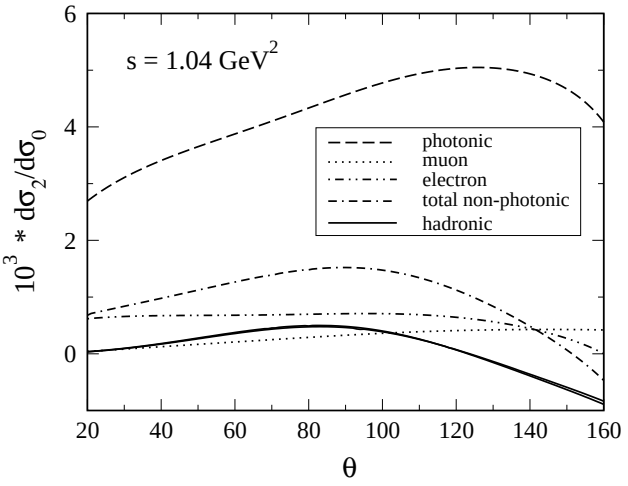

Fig. 12. Two-loop photonic and non-photonic corrections to Bhabha scattering at $\sqrt{s} = 1.02$ GeV, normalized to the QED tree-level cross section, as a function of the electron polar angle. No cuts. The parameterizations of R_{had} due to [140] and [128, 129, 130] are very close to each other.

as a ratio of the NNLO corrections to the Born cross section in per mille, is shown in Fig. 12 for KLOE and in Fig. 13 for BaBar/Belle[7]. While the non-photonic corrections stay at 1 per mille or less for KLOE, they reach a few per mille at the BaBar/Belle energy range. The NNLO photonic corrections are the dominant contributions and amount to some per mille, both at Φ and B factories. However, as already emphasized, the bulk of both photonic and non-photonic corrections is incorporated into the generators used by the experimental collaborations. Hence, the consistent comparison between the results of NNLO calculations and the MC predictions at the same perturbative level allows to assess the theoretical accuracy of the luminosity tools, as will be discussed quantitatively in Section 1.8.

[7] The pure self-energy corrections deserve a special discussion and are thus omitted in the plots.

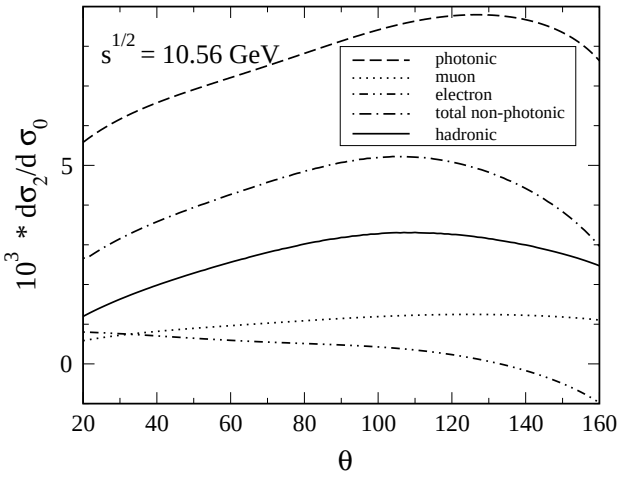

Fig. 13. Two-loop photonic and non-photonic corrections to Bhabha scattering at $\sqrt{s} = 10.56$ GeV, normalized to the QED tree-level cross section, as a function of the electron polar angle. No cuts. The parameterizations of R_{had} is due to [140].

1.3.2 Fixed-Order Calculation of the Hard Photon Emission at One Loop

The one-loop matrix element for the process $e^+e^- \to e^+e^-\gamma$ is one of the contributions to the complete set of NNLO corrections to Bhabha scattering. Its evaluation requires the non-trivial computation of one-loop tensor integrals associated to pentagon-diagrams.

According to the standard Passarino-Veltman (PV) approach [141], one-loop tensor integrals can be expressed in terms of MIs with trivial numerators that are independent of the loop variable, each multiplied by a Lorentz structure depending only on combinations of the external momenta and the metric tensor. The achievement of the complete PV-reduction amounts to solve a non-trivial system of equations. Due to its size, it is reasonable replacing the analytic techniques by numerical tools. It is difficult to implement the PV-reduction numerically, since it gives rise to Gram determinants. The latter naturally arise in the procedure of inverting a system and they can vanish at special phase space points. This fact requires a proper modification of the reduction algorithm [142, 143, 144, 145, 146, 147, 148]. A viable solution for the complete algebraic reduction of tensor-pentagon (and tensor-hexagon) integrals was formulated in [149, 150, 151], by exploiting the algebra of signed minors [152]. In this approach the cancelation of powers of inverse Gram determinants was performed recently in [153, 154].

The computation of the one-loop five-point amplitude $e^+e^- \to e^+e^-\gamma$ can be alternatively performed by using generalized-unitarity cutting rules (see [155] for a detailed compilation of references). In the following we propose two ways to achieve the result, *via* an analytical and *via* a semi-numerical method. The application of generalized cutting-rules as an on-shell method of calculation is based on two fundamental properties of scattering amplitudes:

i) analyticity, according to which any amplitude is determined by its singularity structure [156,157,158,127,159]; *ii)* and unitarity, according to which the residues at the singularities are determined by products of simpler amplitudes. Turning these properties into a tool for computing scattering amplitudes is possible because of the underlying representation of the amplitude in terms of Feynman integrals and their PV-reduction, which grants the existence of a representation of any one-loop amplitudes as linear combination of MIs, each multiplied by a rational coefficient. In the case of $e^+e^- \to e^+e^-\gamma$, pentagon-integrals may be expressed, through PV-reduction, by a linear combination of 17 MIs (including 3 boxes, 8 triangles, 5 bubbles, and 1 tadpole). Since the required MIs are analytically known [160,161,162,150,144,163,164], the determination of their coefficients is needed for reconstructing the amplitude as a whole. To this aim, one may use the Mathematica program hexagon [153,154]. Also matching the generalized cuts of the amplitude with the cuts of the MIs provides an efficient way to extract their (rational) coefficients out of the amplitude itself. In general the fulfillment of multiple-cut conditions requires loop momenta with complex components. The effect of the cut conditions is to freeze some of its components, when not all, according to the number of the cuts. With the quadruple-cut [165] the loop momentum is completely frozen, yielding the algebraic determination of the coefficients of n-point functions with $n \geq 4$. In cases where fewer than four denominators are cut, like triple-cut [166,167,168], double-cut [169,170,171,172,173,167], and single-cut [174], the loop momentum is not frozen: the free-components are left over as phase-space integration variables.

For each multiple-cut, the evaluation of the phase-space integral would generate, in general, logarithms and a non-logarithmic term. The coefficient of a given n-point MI finally appears in the non-logarithmic term of the corresponding n-particle cut, where all the internal lines are on-shell (while the logarithms correspond to the cuts of higher-point MIs which share that same cut). Therefore all the coefficients of MIs can be determined in a *top-down* algorithm, starting from the quadruple-cuts for the extraction of the 4-point coefficients, and following with the triple-, double-, and single-cuts, for the coefficients of 3-, 2- and 1-point, respectively. The coefficient of an n-point MI ($n \geq 2$) can be also obtained by specializing to the case at hands the generating formulas given in [175] for general one-loop amplitudes.

Instead of the analytic evaluation of the multiple-cut phase-space integrals, it is worth considering the feasibility of computing the process $e^+e^- \to e^+e^-\gamma$ with a seminumerical technique by now known as OPP-reduction [176,177], based on the decomposition of the numerator of any one-loop integrand in terms of its denominators [178,179,180,181]. Within this approach the coefficients of the MIs can be found simply by solving a system of numerical equations, avoiding any explicit integration. The OPP-reduction algorithm exploits the polynomial structures of the integrand when evaluated at values of the loop-momentum fulfilling multiple cut-conditions: *i)* for each n-point MI, one considers the n-particle cut obtained by setting all the propagating lines on-shell; *ii)* such a cut is associated to a polynomial in terms of the free components of the loop-momentum, which corresponds to the numerator of the integrand evaluated at the solution of the on-shell conditions; *iii)* the constant-term of that polynomial *is* the coefficient of the MI.
Hence the difficult task of evaluating one-loop Feynman integrals is reduced to the much simpler problem of polynomial fitting, recently optimized by using a projection technique based on the Discrete Fourier Transform [182].

In general the result of a dimensional-regulated amplitude in the 4-dimensional limit, being D ($= 4-2\epsilon$) the regulating parameter, is expected to contain (poly)logarithms, often referred to as the cut-constructible term, and a pure rational term. In a later paper [183], which completed the OPP-method, the rising of the rational term was attributed to two potential sources (of UV-divergent integrals): one, defined R_1, due to the D-dimensional completion of the 4-dimensional contribution of the numerator; a second one, called R_2, due to the (-2ϵ)-dimensional algebra of Dirac-matrices. Therefore in the OPP-approach the calculation of the one-loop amplitude $e^+e^- \to e^+e^-\gamma$ can proceed through two computational stages:

1. the coefficients of the MIs that are responsible both for the cut-constructible and for the R_1-rational terms can be determined by applying the OPP-reduction discussed above [176,177,182];
2. the R_2-rational term can be computed by using additional tree-level-like diagrammatic rules, very much resembling the computation of the counter terms needed for the renormalization of UV-divergencies [183].

The numerical influence of the radiative loop diagrams, including the pentagon diagrams, is expected not to be particularly large. However, the calculation of such corrections would greatly help to assess the physical precision of existing luminosity programs.

1.3.3 Pair Corrections

As was mentioned in the paragraph on virtual heavy flavor and hadronic corrections of Section 1.3.1, these virtual corrections have to be combined with real corrections in order to get physically sensible results. The virtual NNLO electron, muon, tau and pion corrections have to be combined with the emission of real electron, muon, tau and pion pairs, respectively. The real pair production cross sections are finite, but cut dependent. We consider here the pion pair production as it is the dominant part of the hadronic corrections and can serve as an estimate of the role of the whole set of hadronic corrections. The description of all relevant hadronic contributions is much more involved task and will not be covered in this review. As was first explicitly shown for Bhabha scattering in [66] for electron pairs, and also discussed in [122], there appear exact cancellations of terms of the order $\ln^3(s/m_e^2)$ or $\ln^3(s/m_f^2)$, so that the leading terms are at most of order $\ln^2(s/m_e^2), \ln^2(s/m_f^2)$.

Table 1. The NNLO lepton and pion pair corrections to the Bhabha scattering Born cross section σ_B: virtual corrections σ_v , soft and hard real photon emissions σ_s, σ_h, and pair emission contributions σ_{pairs}. Total pair correction cross sections obtainable from the sum $\sigma_{s+v+h} + \sigma_{pairs}$. All cross sections in nanobarns according to the cuts given in the text.

Electron pair corrections					
	σ_B	σ_h	σ_{v+s}	σ_{v+s+h}	σ_{pairs}
KLOE	529.469	9.502	-11.567	-2.065	0.271
BaBar	6.744	0.246	-0.271	-0.025	0.017
Muon pair corrections					
	σ_B	σ_h	σ_{v+s}	σ_{v+s+h}	σ_{pairs}
KLOE	529.469	1.494	-1.736	-0.241	–
BaBar	6.744	0.091	-0.095	-0.004	0.0005
Tau pair corrections					
	σ_B	σ_h	σ_{v+s}	σ_{v+s+h}	σ_{pairs}
KLOE	529.469	0.020	-0.023	-0.003	–
BaBar	6.744	0.016	-0.017	-0.0007	$< 10^{-7}$
Pion pair corrections					
	σ_B	σ_h	σ_{v+s}	σ_{v+s+h}	σ_{pairs}
KLOE	529.469	1.174	-1.360	-0.186	–
BaBar	6.744	0.062	-0.065	-0.003	0.00003

In Table 1 we show NNLO lepton and pion pair contributions with typical kinematical cuts for the KLOE and BaBar experiments. Besides contributions from unresolved pair emissions σ_{pairs}, we also add unresolved real hard photon emission contributions σ_h. The corrections σ_{pairs} from fermions have been calculated with the Fortran package HELAC-PHEGAS [184,185,186,187], the real pion corrections with EKHARA [188,189], the NNLO hard photonic corrections σ_h with a program [190] based on the generator BHAGEN-1PH [191]. The latter depend, technically, on the soft photon cut-off $E_\gamma^{\min} = \omega$. After adding up with σ_{v+s}, the sum of the two σ_{v+s+h} is independent of that; in fact we use here $\omega/E_{\rm beam} = 10^{-4}$. The σ_{v+s} is determined with an updated version of the Fortran package bhbhnnlohf [122,139] in order to cover also pion pair corrections. The cuts applied in Table 1 for the KLOE experiment are

- $\sqrt{s} = 1.02$ GeV
- $E_{\min} = 0.4$ GeV
- $55^\circ < \theta_\pm < 125^\circ$
- $\xi_{\max} = 9^\circ$,

and for the BaBaR experiment

- $\sqrt{s} = 10.56$ GeV
- $|\cos(\theta_\pm)| < 0.7$ and $|\cos(\theta_+)| < 0.65$ or $|\cos(\theta_-)| < 0.65$
- $|\boldsymbol{p}_+|/E_{\rm beam} > 0.75$ and $|\boldsymbol{p}_-|/E_{\rm beam} > 0.5$ or $|\boldsymbol{p}_-|/E_{\rm beam} > 0.75$ and $|\boldsymbol{p}_+|/E_{\rm beam} > 0.5$
- $\xi^{3d}_{\max} = 30^\circ$.

Here $E_{\min}$ is the energy threshold for the final-state electron/positron, $\theta_\pm$ are the electron/positron polar angles and ξ_{max} is the maximum allowed polar angle acollinearity:

$$\xi = |\theta_+ + \theta_- - 180^\circ|\,, \tag{24}$$

and $\xi^{3d}_{\max}$ is the maximum allowed three dimensional acollinearity:

$$\xi^{3d} = \left|\arccos\left(\frac{p_+ \cdot p_-}{(|\boldsymbol{p}_-||\boldsymbol{p}_+|}\right) \times \frac{180^\circ}{\pi} - 180^\circ\right|. \tag{25}$$

For $e^+e^- \to e^+e^-\mu^+\mu^-$, cuts are applied only to the e^+e^- pair. In the case of $e^+e^- \to e^+e^-e^+e^-$, all possible $e^\pm e^\mp$ combinations are checked and if at least one pair fulfils the cuts the event is accepted.

At KLOE the electron pair corrections contribute about 3×10^{-3} and at BaBar about 1×10^{-3}, while all the other contributions of pair production are even smaller. Like in small-angle Bhabha scattering at LEP/SLC the pair corrections [192] are largely dominated by the electron pair contribution.

1.4 Multiple photon effects and matching with NLO corrections

1.4.1 Universal methods for leading logarithmic corrections

From inspection of Eq. (7) and Eq.(10) for the SV NLO QED corrections to the cross section of the Bhabha scattering and $e^+e^- \to \gamma\gamma$ process, it can be seen that large logarithms $L = \ln(s/m_e^2)$, due to collinear photon emission, are present. Similar large logarithmic terms arise after integration of the hard photon contributions from the kinematical domains of photon emission at small angles with respect to charged particles. For the energy range of meson factories the logarithm is large numerically, i.e. $L \sim 15$ at the Φ-factories and $L \sim 20$ at the B-factories, and the corresponding terms give the bulk of the total radiative correction. These contributions represent also the dominant part of the NNLO effects discussed in Section 1.3. Therefore the logarithmically enhanced contributions due to emission of soft and collinear photons must be taken into account at all orders in perturbation theory, to achieve the required theoretical accuracy.

The methods for the calculation of higher-order (HO) QED corrections on the basis of the generators employed nowadays at flavour factories were already widely and successfully used in the 90s at LEP/SLC for electroweak tests of the SM. They were adopted for the calculation of both the small-angle Bhabha scattering cross section (necessary for the high-precision luminosity measurement) and Z-boson observables. Hence, the theory accounting for the control of HO QED corrections at meson factories can be considered particularly robust, having passed the very stringent tests of LEP/SLC era.

The most popular and standard methods to keep under control multiple photon effects are the QED Structure Function (SF) approach [193,194,195,196] and Yennie-Frautschi-Suura (YFS) exponentiation [197]. The former is used in all the versions of the generator BabaYaga [198,199,200] and MCGPJ [201] (albeit according to different realizations), while the latter is the theoretical recipe adopted in BHWIDE [202]. Actually, analytical QED SFs $D(x, Q^2)$, valid in the strictly collinear approximation,

are implemented in MCGPJ, whereas BabaYaga is based on a MC Parton Shower (PS) algorithm to reconstruct $D(x,Q^2)$ numerically.

The Structure Function approach

Let us consider the annihilation process $e^-e^+ \to X$, where X is some given final state and $\sigma_0(s)$ its LO cross section. Initial-state (IS) QED radiative corrections can be described according to the following picture. Before arriving at the annihilation point, the incoming electron (positron) of four-momentum $p_{-(+)}$ radiates real and virtual photons. These photons, due to the dynamical features of QED, are mainly radiated along the direction of motion of the radiating particles, and their effect is mainly to reduce the original four-momentum of the incoming electron (positron) to $x_{1(2)}p_{-(+)}$. After this pre-emission, the hard scattering process $e^-(x_1p_-)e^+(x_2p_+) \to X$ takes place, at a reduced squared c.m. energy $\hat{s} = x_1x_2s$. The resulting cross section, corrected for IS QED radiation, can be represented as follows [193,194,195]

$$\sigma(s) = \int_0^1 dx_1dx_2D(x_1,s)D(x_2,s)\sigma_0(x_1x_2s)\Theta(\text{cuts}), \tag{26}$$

where $D(x,s)$ is the electron SF, representing the probability that an incoming electron (positron) radiates a collinear photon, retaining a fraction x of its original momentum at the energy scale $Q^2 = s$, and $\Theta(\text{cuts})$ stands for a rejection algorithm taking care of experimental cuts. When considering photonic radiation only the non-singlet part of the SF is of interest. If the running of the QED coupling constant is neglected, the non-singlet part of the SF is the solution of the following Renormalization Group (RG) equation, analogous to the Dokshitzer-Gribov-Lipatov-Altarelli-Parisi (DGLAP) equation of QCD [203,204,205]:

$$s\frac{\partial}{\partial s}D(x,s) = \frac{\alpha}{2\pi}\int_x^1 \frac{dz}{z}P_+(z)D\left(\frac{x}{z},s\right), \tag{27}$$

where $P_+(z)$ is the regularized Altarelli-Parisi (AP) splitting function electron $\to$ electron + photon, given by

$$\begin{aligned} P_+(z) &= P(z) - \delta(1-z)\int_0^1 dxP(x), \\ P(z) &= \frac{1+z^2}{1-z}. \end{aligned} \tag{28}$$

Equation (27) can be also transformed into an integral equation, subject to the boundary condition $D(x,m_e^2) = \delta(1-x)$:

$$D(x,s) = \delta(1-x) + \frac{\alpha}{2\pi}\int_{m_e^2}^s \frac{dQ^2}{Q^2}\int_x^1 \frac{dz}{z}P_+(z)D\left(\frac{x}{z},Q^2\right). \tag{29}$$

Equation (29) can be solved exactly by means of numerical methods, such as the inverse Mellin transform method. However, this derivation of $D(x,s)$ turns out be problematic in view of phenomenological applications. Therefore, approximate (but very accurate) analytical representations of the solution of the evolution equation are of major interest for practical purposes. This type of solution was the one typically adopted in the context of LEP/SLC phenomenology. A first analytical solution can be obtained in the soft photon approximation, i.e. in the limit $x \simeq 1$. This solution, also known as Gribov-Lipatov (GL) approximation, exponentiates at all perturbative orders the large logarithmic contributions of infrared and collinear origin, but it does not take into account hard-photon (collinear) effects. This drawback can be overcome by solving the evolution equation iteratively. At the n-th step of the iteration, one obtains the $\mathcal{O}(\alpha^n)$ contribution to the SF for any value of x. By combining the GL solution with the iterative one, in which the soft-photon part has been eliminated in order to avoid double counting, one can build a hybrid solution of the evolution equation. It exploits all the positive features of the two kinds of solutions and is not affected by the limitations intrinsic to each of them. Two classes of hybrid solutions, namely the additive and factorized ones, are known in the literature and both were adopted for applications to LEP/SLC precision physics. A typical additive solution, where the GL approximation $D_{GL}(x,s)$ is supplemented by finite-order terms present in the iterative solution, is given by [206]

$$\begin{aligned} D_A(x,s) &= \sum_{i=0}^3 d_A^{(i)}(x,s), \\ d_A^{(0)}(x,s) &= \frac{\exp\left[\frac{1}{2}\beta\left(\frac{3}{4}-\gamma_E\right)\right]}{\Gamma\left(1+\frac{1}{2}\beta\right)}\frac{1}{2}\beta(1-x)^{\frac{1}{2}\beta-1}, \\ d_A^{(1)}(x,s) &= -\frac{1}{4}\beta(1+x), \\ d_A^{(2)}(x,s) &= \frac{1}{32}\beta^2\left[(1+x)\left(-4\ln(1-x)+3\ln x\right)\right. \\ &\quad \left. -4\frac{\ln x}{1-x} - 5 - x\right], \\ d_A^{(3)}(x,s) &= \frac{1}{384}\beta^3\left\{(1+x)\left[18\zeta(2) - 6\text{Li}_2(x)\right.\right. \\ &\quad \left. -12\ln^2(1-x)\right] + \frac{1}{1-x}\left[-\frac{3}{2}(1+8x+3x^2)\ln x\right. \\ &\quad +\frac{1}{2}(1+7x^2)\ln^2 x - 12(1+x^2)\ln x\ln(1-x) \\ &\quad -6(x+5)(1-x)\ln(1-x) \\ &\quad \left.\left.\left. -\frac{1}{4}(39-24x-15x^2)\right]\right\}, \end{aligned} \tag{30}$$

where Γ is the Euler gamma-function, $\gamma_E \approx 0.5772$ the Euler-Mascheroni constant, ζ the Riemann ζ-function and β is the large collinear factor

$$\beta = \frac{2\alpha}{\pi}\left[\ln\left(\frac{s}{m_e^2}\right) - 1\right]. \tag{31}$$

Explicit examples of factorized solutions, which are obtained by multiplying the GL solution by finite-order terms, in such a way that, order by order, the iterative

contributions are exactly recovered, can be found in [207]. For the calculation of HO corrections with a per mille accuracy analytical SFs in additive and factorized form containing up to $\mathcal{O}(\alpha^3)$ finite-order terms are sufficient and in excellent agreement. They also agree with the accuracy much better than 0.1 with the exact numerical solution of the QED evolution equation. Explicit solutions up to the fifth order in α were calculated in [208,209].

The RG method described above was applied in [210] for the treatment of LL QED radiative corrections to various processes of interest for physics at meson factories. Such a formulation was later implemented in the generator MCGPJ. For example, according to [210], the Bhabha scattering cross section, accounting for LL terms in all orders, $\mathcal{O}(\alpha^n L^n)$, $n = 1, 2, \ldots$, of perturbation theory, is given by

$$\begin{aligned}
\mathrm{d}\sigma^{\mathrm{Bhabha}}_{\mathrm{LLA}} &= \sum_{a,b,c,d=e^{\pm},\gamma} \int_{\bar{z}_1}^{1} \mathrm{d}z_1 \int_{\bar{z}_2}^{1} \mathrm{d}z_2 D^{\mathrm{str}}_{ae^-}(z_1) D^{\mathrm{str}}_{be^+}(z_2) \\
&\times \mathrm{d}\sigma_0^{ab\to cd}(z_1, z_2) \int_{\bar{y}_1}^{1} \frac{\mathrm{d}y_1}{Y_1} D^{\mathrm{frg}}_{e^-c}\left(\frac{y_1}{Y_1}\right) \int_{\bar{y}_2}^{1} \frac{\mathrm{d}y_2}{Y_2} D^{\mathrm{frg}}_{e^+d}\left(\frac{y_2}{Y_2}\right) \\
&+ \mathcal{O}\left(\alpha^2 L, \alpha \frac{m_e^2}{s}\right), \qquad (32)
\end{aligned}$$

where $\mathrm{d}\sigma_0^{ab\to cd}(z_1, z_2)$ is the differential LO cross section of the process $ab \to cd$ with energy fractions of the incoming particles being scaled by factors z_1 and z_2 with respect to the initial electron and positron, respectively. In the notation of [210], the electron SF $D^{\mathrm{str}}_{ab}(z)$ is distinguished from the electron fragmentation function $D^{\mathrm{frg}}_{ab}(z)$ to point out the role played by IS radiation (described by $D^{\mathrm{str}}_{ab}(z)$) with respect to the one due to final-state radiation (described by $D^{\mathrm{frg}}_{ab}(z)$). However, because of their probabilistic meaning, the electron structure and fragmentation functions coincide. In Eq. (32) the quantities $Y_{1,2}$ are the energy fractions of particles c and d with respect to the beam energy. Explicit expressions for $Y_{1,2} = Y_{1,2}(z_1, z_2, \cos\theta)$ and other details on the kinematics can be found in [210]. The lower limits of the integrals, $\bar{z}_{1,2}$ and $\bar{y}_{1,2}$, should be defined according to the experimental conditions of particle detection and kinematical constraints. For the case of the $e^+e^- \to \gamma\gamma$ process, one has to change the master formula (32) by picking up the two-photon final state. Formally it can be done just by choosing the proper fragmentation functions, $D^{\mathrm{frg}}_{\gamma c}$ and $D^{\mathrm{frg}}_{\gamma d}$.

The photonic part of the non-singlet electron structure (fragmentation) function in $\mathcal{O}(\alpha^n L^n)$ considered in [210] reads as follows

$$\begin{aligned}
D^{NS,\gamma}_{ee}(z) &= \delta(1-z) + \sum_{i=1}^{n} \left(\frac{\alpha}{2\pi}(L-1)\right)^i \frac{1}{i!} \left[P^{(0)}_{ee}(z)\right]^{\otimes i}, \\
D_{\gamma e}(z) &= \frac{\alpha}{2\pi}(L-1) P_{\gamma e}(z) + \mathcal{O}(\alpha^2 L^2), \\
D_{e\gamma}(z) &= \frac{\alpha}{2\pi} L P_{\gamma e}(z) + \mathcal{O}(\alpha^2 L^2), \\
P^{(0)}_{ee}(z) &= \left[\frac{1+z^2}{1-z}\right]_+ \\
&= \lim_{\Delta\to 0} \left\{ \delta(1-z)(2\ln\Delta + \frac{3}{2}) + \Theta(1-z-\Delta)\frac{1+z^2}{1-z} \right\}, \\
\left[P^{(0)}_{ee}(z)\right]^{\otimes i} &= \int_z^1 \frac{\mathrm{d}t}{t} P^{(i-1)}_{ee}(t) P^{(0)}_{ee}\left(\frac{z}{t}\right), \qquad (33) \\
P_{e\gamma}(z) &= z^2 + (1-z)^2, \quad P_{\gamma e}(z) = \frac{1+(1-z)^2}{z}.
\end{aligned}$$

Starting from the second order in α there appear also non-singlet and singlet e^+e^- pair contributions to the structure function:

$$\begin{aligned}
D^{NS,e^+e^-}_{ee}(z) &= \frac{1}{3}\left(\frac{\alpha}{2\pi}L\right)^2 P^{(1)}_{ee}(z) + \mathcal{O}(\alpha^3 L^3), \\
D^{S,e^+e^-}_{ee}(z) &= \frac{1}{2!}\left(\frac{\alpha}{2\pi}L\right)^2 R(z) + \mathcal{O}(\alpha^3 L^3), \\
R(z) &= P_{e\gamma} \otimes P_{\gamma e}(z) = \frac{1-z}{3z}(4 + 7z + 4z^2) \\
&\quad + 2(1+z)\ln z. \qquad (34)
\end{aligned}$$

Note that radiation of a real pair, *i.e.* appearance of additional electrons and positrons in the final state, require the application of nontrivial conditions of experimental particle registration. Unambiguously, that can be done only within a MC event generator based on four-particle matrix elements, as already discussed in Section 1.3.

In the same way as in QCD, the LL cross sections depend on the choice of the factorization scale Q^2 in the argument of the large logarithm $L = \ln(Q^2/m_e^2)$, which is not fixed a priori by the theory. However, the scale should be taken of the order of the characteristic energy transfer in the process under consideration. Typical choices are $Q^2 = s$, $Q^2 = -t$, and $Q^2 = st/u$. The first one is good for annihilation channels, like $e^+e^- \to \mu^+\mu^-$, the second one is optimal for small-angle Bhabha scattering, where the t-channel exchange dominates, see [211]. The last choice allows to exponentiate the leading contribution due to initial-final state interference [212] and is particularly suited for large-angle Bhabha scattering in QED. The option $Q^2 = st/u$ is adopted in all the versions of the generator BabaYaga. Reduction of the scale dependence can be achieved by taking into account next-to-leading corrections in $\mathcal{O}(\alpha^n L^{n-1})$, next-to-next-to-leading ones in $\mathcal{O}(\alpha^n L^{n-2})$ *etc.*

The Parton Shower algorithm

The PS algorithm is a method for providing a MC iterative solution of the evolution equation, at the same time generating the four-momenta of the electron and photon at a given step of the iteration. It was developed within the context of QCD and later applied in QED too.

In order to implement the algorithm, it is first necessary to assume the existence of an upper limit for the energy fraction x, in such a way that the AP splitting function is regularized as follows

$$P_+(z) = \theta(x_+ - z)P(z) - \delta(1-z)\int_0^{x_+} dx P(x). \qquad (35)$$

Of course, in the limit $x_+ \to 1$ Eq. (35) recovers the usual definition of the AP splitting function given in Eq. (28). By inserting the modified AP vertex into Eq. (27), one obtains

$$s\frac{\partial}{\partial s}D(x,s) = \frac{\alpha}{2\pi}\int_x^{x_+}\frac{dz}{z}P(z)D\left(\frac{x}{z},s\right) - \frac{\alpha}{2\pi}D(x,s)\int_x^{x_+}dzP(z). \quad (36)$$

Separating the variables and introducing the Sudakov form factor

$$\Pi(s_1,s_2) = \exp\left[-\frac{\alpha}{2\pi}\int_{s_2}^{s_1}\frac{ds'}{s'}\int_0^{x_+}dzP(z)\right], \quad (37)$$

which is the probability that the electron evolves from virtuality $-s_2$ to $-s_1$ without emitting photons of energy fraction larger than $1-x_+ \equiv \epsilon$ ($\epsilon \ll 1$), Eq. (36) can be recast into integral form as follows

$$D(x,s) = \Pi(s,m_e^2)D(x,m_e^2) + \frac{\alpha}{2\pi}\int_{m_e^2}^{s}\frac{ds'}{s'}\Pi(s,s')\int_x^{x_+}\frac{dz}{z}P(z)D\left(\frac{x}{z},s'\right). \quad (38)$$

The formal iterative solution of Eq. (38) can be represented by the following infinite series

$$D(x,s) = \sum_{n=0}^{\infty}\prod_{i=1}^{n}\left\{\int_{m_e^2}^{s_{i-1}}\frac{ds_i}{s_i}\Pi(s_{i-1},s_i) \times\frac{\alpha}{2\pi}\int_{x/(z_1\cdots z_{i-1})}^{x_+}\frac{dz_i}{z_i}P(z_i)\right\}\Pi(s_n,m_e^2)D\left(\frac{x}{z_1\cdots z_n},m_e^2\right). \quad (39)$$

The particular form of Eq. (39) allows to exploit a MC method for building the solution iteratively. The steps of the algorithm are as follows:

1 – set $Q^2 = m_e^2$, and fix $x = 1$ according to the boundary condition $D(x,m_e^2) = \delta(1-x)$;
2 – generate a random number ξ in the interval $[0,1]$;
3 – if $\xi < \Pi(s,Q^2)$ stop the evolution; otherwise
4 – compute Q'^2 as solution of the equation $\xi = \Pi(Q'^2,Q^2)$;
5 – generate a random number z according to the probability density $P(z)$ in the interval $[0,x_+]$;
6 – substitute $x \to xz$ and $Q^2 \to Q'^2$; go to 2.

The x distribution of the electron SF as obtained by means of the PS algorithm and a numerical solution (based on the inverse Mellin transform method) of the QED evolution equation is shown in Fig. 14. Perfect agreement is seen. Once $D(x,s)$ has been reconstructed by the algorithm, the master formula of Eq. (26) can be used for the calculation of LL corrections to the cross section of interest. This cross section must be independent of the soft-hard photon separator ϵ, in the limit of small ϵ values. This can be clearly seen in Fig. 15, where the QED

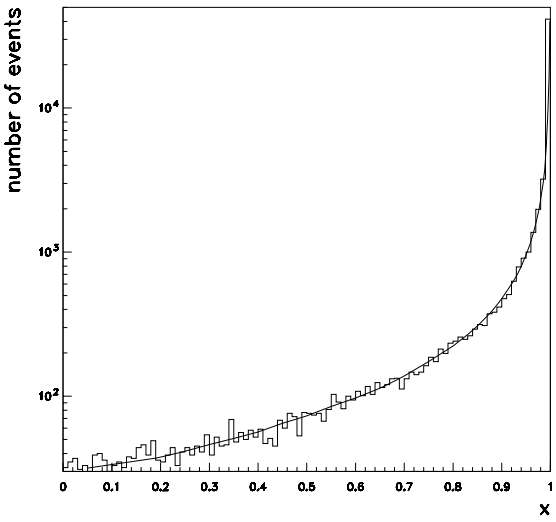

Fig. 14. Comparison for the x distribution of the electron SF as obtained by means of a numerical solution of the QED evolution equation (solid line) and the PS algorithm (histogram). From [198].

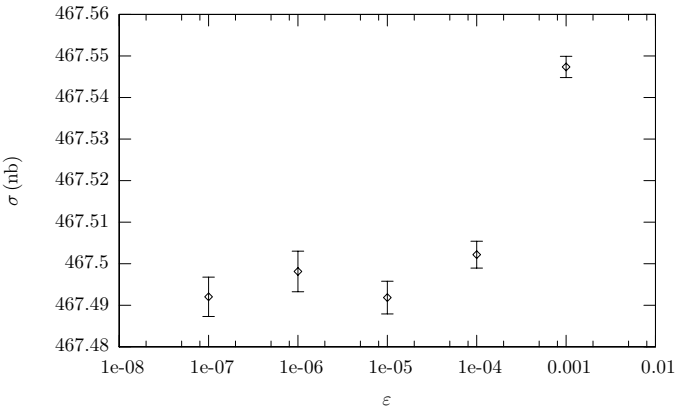

Fig. 15. QED corrected Bhabha cross section at DAΦNE as a function of the infrared regulator ε of the PS approach, according to the setup of Eq. (12). The error bars correspond to 1σ MC errors. From [200].

corrected Bhabha cross section as a function of the fictitious parameter ε is shown for DAΦNE energies with the cuts of Eq. (12), but for an angular acceptance $\theta_\pm$ of $55° \div 125°$. The cross section reaches a plateau for ϵ smaller than 10^{-4}.

The main advantage of the PS algorithm with respect to the analytical solutions of the electron evolution is the possibility of going beyond the strictly collinear approximation and generating transverse momentum $p_\perp$ of electrons and photons at each branching. In fact, the kinematics of the branching process $e(p) \to e'(p') + \gamma(q)$ can be written as

$$p = (E, \mathbf{0}, p_z)$$

$$p' = (zE, \boldsymbol{p}_\perp, p'_z)$$
$$q = ((1-z)E, -\boldsymbol{p}_\perp, q_z). \quad (40)$$

Once the variables p^2, p'^2 and z are generated by the PS algorithm, the on-shell condition $q^2 = 0$, together with the longitudinal momentum conservation, allows to obtain an expression for the $p_\perp$ variable:

$$p_\perp^2 = (1-z)(zp^2 - p'^2), \quad (41)$$

at first order in $p^2/E^2 \ll 1$, $p_\perp^2/E^2 \ll 1$.

However, some not correct behaviour of the exclusive photon kinematics reconstruction is related to this PS picture, due to the approximations inherent to Eq. (41). First of all, since within the PS algorithm the generation of p'^2 and z are independent, it can happen that in some branching the $p_\perp^2$ as given by Eq. (41) is negative. In order to avoid this problem, the introduction of any kinematical cut on p^2 or z generation (or the regeneration of the whole event) would mean a not correct reconstruction of the SF x distribution, which is important for a precise cross section calculation. Furthermore, in the PS scheme, each fermion produces its photon cascade independently of the other ones, missing the effects due to the interference of radiation coming from different charged particles. As far as inclusive cross sections (i.e., no cuts are imposed on the generated photons) are considered, these effects are largely integrated out but they become important when more exclusive variables distributions are looked at, as shown in [213]

Concerning the first problem, it can be overcome choosing a generation of $p_\perp$ of the photons different from Eq. (41). For example, one can choose to extract the photon $\cos\vartheta_\gamma$ according to the universal leading poles $1/p\cdot k$ present in the matrix element for photon emission. Namely, one can generate $\cos\vartheta_\gamma$ as

$$\cos\vartheta_\gamma \propto \frac{1}{1-\beta\cos\vartheta_\gamma} \quad , \quad (42)$$

where β is the speed of the emitting particle. In this way, photon energy and angle are generated independently, different from Eq. (41). The nice feature of this prescription is that $p_\perp^2 = E_\gamma^2 \sin^2\vartheta_\gamma$ is always well defined and the x distribution reproduces exactly the SF, because any further kinematical cuts must be imposed to avoid unphysical events. At this stage, the PS is used only to generate the energies and multiplicity of the photons. The problem of including the radiation interference is still unsolved, because the variables of photons emitted by a fermion are still uncorrelated with those of the other charged particles. The issue of including photon interference can be successfully worked out looking at the YFS formula [197]:

$$d\sigma_n \approx d\sigma_0 \frac{e^{2n}}{n!}\prod_{l=1}^{n}\frac{d^3\mathbf{k}_l}{(2\pi)^3 2k_l^0}\sum_{i,j=1}^{N}\eta_i\eta_j\frac{-p_i\cdot p_j}{(p_i\cdot k_l)(p_j\cdot k_l)} \quad . \quad (43)$$

It gives the differential cross section $d\sigma_n$ for the emission of n photons, whose momenta are $k_1,\cdots,k_n$, from a kernel process described by $d\sigma_0$ and involving N fermions, whose momenta are $p_1,\cdots,p_N$. In Eq. (43) η_i is a charge factor, which is $+1$ for incoming e^- or outgoing e^+ and -1 for incoming e^+ or outgoing e^-. Note that Eq. (43) is valid in the soft limit ($k_i \to 0$). The important point is that it also accounts for coherence effects. From the YFS formula it is straightforward to read out the angular spectrum of the l^{th} photon:

$$\cos\vartheta_l \propto -\sum_{i,j=1}^{N}\eta_i\eta_j\frac{1-\beta_i\beta_j\cos\vartheta_{ij}}{(1-\beta_i\cos\vartheta_{il})(1-\beta_j\cos\vartheta_{jl})} \quad . \quad (44)$$

It is worth noticing that in the LL prescription, the same quantity writes as

$$\cos\vartheta_l \propto \sum_{i=1}^{N}\frac{1}{1-\beta_i\cos\vartheta_{il}}, \quad (45)$$

whose terms are of course contained in Eq. (44).

In order to consider also coherence effects in the angular distribution of the photons, one can generate $\cos\vartheta_\gamma$ according to Eq. (44), rather than to Eq. (45). This recipe [213] is adopted in BabaYaga v3.5 and BabaYaga@NLO.

Yennie-Frautschi-Suura exponentiation

The YFS exponentiation procedure, implemented in the code BHWIDE, is a technique for summing up all the infrared (IR) singularities present in any process accompanied by photonic radiation [197]. It is inherently exclusive, i.e. all the summations of the IR singular contributions are done before any phase-space integration over the virtual or real photon four-momenta are performed. The method was mainly developed by S. Jadach, B.F.L. Ward and collaborators to realize precision MC tools. In the following, the general ideas underlying the procedure are summarized.

Let us consider the scattering process $e^+(p_1)e^-(p_2) \to f_1(q_1)\cdots f_n(q_n)$, where $f_1(q_1)\cdots f_n(q_n)$ represents a given arbitrary final state, and let $\mathcal{M}_0$ be its tree-level matrix element. By using standard Feynman-diagram techniques, it is possible to show that the same process, when accompanied by l additional real photons radiated by the IS particles, and under the assumption that the l additional photons are soft, i.e. their energy is much smaller that any energy scale involved in the process, can be described by the factorized matrix element built up by the LO one, $\mathcal{M}_0$, times the product of l eikonal currents, namely

$$\mathcal{M} \simeq \mathcal{M}_0\prod_{i=1}^{l}\left[e\left(\frac{\varepsilon_i(k_i)\cdot p_2}{k_i\cdot p_2} - \frac{\varepsilon_i(k_i)\cdot p_1}{k_i\cdot p_1}\right)\right], \quad (46)$$

where e is the electron charge, k_i are the momenta of the photons and $\varepsilon_i(k_i)$ their polarization vectors. Taking the square of the matrix element in Eq. (46) and multiplying by the proper flux factor and the Lorentz-invariant phase space volume, the cross section for the process $e^+(p_1)e^-(p_2) \to f_1(q_1)\cdots f_n(q_n) + l$ real photons

can be written as

$$d\sigma_r^{(l)} = d\sigma_0 \frac{1}{l!} \prod_{i=1}^{l} \left[k_i dk_i d\cos\vartheta_i d\varphi_i \frac{1}{2(2\pi)^3} \sum_{\varepsilon_i} e^2 \left(\frac{\varepsilon_i(k_i)\cdot p_2}{k_i\cdot p_2} - \frac{\varepsilon_i(k_i)\cdot p_1}{k_i\cdot p_1} \right)^2 \right]. \quad (47)$$

By summing over the number of final-state photons, one obtains the cross section for the original process accompanied by an arbitrary number of real photons, namely

$$\begin{aligned} d\sigma_r^{(\infty)} &= \sum_{l=0}^{\infty} d\sigma_r^{(l)} \\ &= d\sigma_0 \exp\left[kdkd\cos\vartheta d\varphi \frac{1}{2(2\pi)^3} \sum_{\varepsilon} e^2 \left(\frac{\varepsilon(k)\cdot p_2}{k\cdot p_2} - \frac{\varepsilon(k)\cdot p_1}{k\cdot p_1} \right)^2 \right]. \end{aligned} \quad (48)$$

Equation (48), being limited to real radiation only, is IR divergent once the phase space integrations are performed down to zero photon energy. This problem, as well known, finds its solution in the matching between real and virtual photonic radiation. Equation (48) already shows the key feature of exclusive exponentiation, i.e. summing up all the perturbative contributions before performing any phase space integration.

In order to get meaningful radiative corrections, besides IS real photon corrections it is necessary to consider also IS virtual photon corrections, i.e. the corrections due to additional internal photon lines connecting the IS electron and positron. For a vertex-type amplitude, the result can be written as

$$\mathcal{M}_{V_1} = -i\frac{e^2}{(2\pi)^4} \int d^4k \; \frac{1}{k^2+i\varepsilon} \bar{v}(p_1)\gamma^\mu \frac{-(\not{p}_1 - \not{k}) + m}{2p_1\cdot k + k^2 + i\varepsilon} \times \Gamma \frac{(\not{p}_2 + \not{k}) + m}{2p_2\cdot k + k^2 + i\varepsilon} \gamma_\mu u(p_2), \quad (49)$$

where Γ stands for the Dirac structure of the LO process, in such a way that $\mathcal{M}_0 = \bar{v}(p_1)\Gamma u(p_2)$. The soft-photon part of the amplitude can be extracted by taking $k^\mu \simeq 0$ in all the numerators. In this approximation, the amplitude of Eq. (49) becomes

$$\begin{aligned} &\mathcal{M}_{V_1} = \mathcal{M}_0 \times V, \\ &V = \frac{2i\alpha}{(2\pi)^3} \int d^4k \frac{4p_1\cdot p_2}{(2p_1\cdot k + k^2 + i\varepsilon)(2p_2\cdot k + k^2 + i\varepsilon)} \times \frac{1}{k^2+i\varepsilon}. \end{aligned} \quad (50)$$

It can be seen that, as in the real case, the IR virtual correction factorizes off the LO matrix element so that it is universal, i.e. independent of the details of the process under consideration, and divergent in the IR portion of the phase space.

The correction given by n soft virtual photons can be seen to factorize with an additional $1/n!$ factor, namely

$$\mathcal{M}_{V_n} = \mathcal{M}_0 \times \frac{1}{n!} V^n, \quad (51)$$

so that by summing over all the additional soft virtual photons one obtains

$$\mathcal{M}_V = \mathcal{M}_0 \times \exp[V]. \quad (52)$$

As already noticed both the real and virtual factors are IR divergent. In order to obtain meaningful expressions one has to adopt some regularization procedure. One possibility is to give the photon a (small) mass λ and modify Eqs. (47) and (50) accordingly. Once all the expressions are properly regularized, one can write down the YFS master formula, which takes into account real and virtual photonic corrections to the LO process. In virtue of the factorization properties discussed above, the master formula can be obtained from Eq. (48) with the substitution $d\sigma_0 \to d\sigma_0 |\exp(V)|^2$, i.e.

$$d\sigma = d\sigma_0 |\exp(V)|^2 \exp\left[kdkd\cos\vartheta d\varphi \frac{1}{2(2\pi)^3} \sum_{\varepsilon} e^2 \left(\frac{\varepsilon(k)\cdot p_2}{k\cdot p_2} - \frac{\varepsilon(k)\cdot p_1}{k\cdot p_1} \right)^2 \right]. \quad (53)$$

As a last step it is possible to perform analytically the IR cancellation between virtual and very soft real photons. Actually, since very soft real photons do not affect the kinematics of the process, the real photon exponent can be split into a contribution coming from photons with energy less than a cutoff k_{min} plus a contribution from photons with energy above it. The first contribution can be integrated over all its phase space and then combined with the virtual exponent. After this step it is possible to remove the regularizing photon mass by taking the limit $\lambda \to 0$, so that Eq. (53) becomes

$$d\sigma = d\sigma_0 \exp(Y) \exp\left[kdkd\Theta(k-k_{min}) \cos\vartheta d\varphi \frac{1}{2(2\pi)^3} \sum_{\varepsilon} e^2 \left(\frac{\varepsilon(k)\cdot p_2}{k\cdot p_2} - \frac{\varepsilon(k)\cdot p_1}{k\cdot p_1} \right)^2 \right], \quad (54)$$

where Y is given by

$$Y = 2V + \int kdkd\Theta(k_{min}-k) \cos\vartheta d\varphi \frac{1}{2(2\pi)^3} \sum_{\varepsilon} e^2 \left(\frac{\varepsilon(k)\cdot p_2}{k\cdot p_2} - \frac{\varepsilon(k)\cdot p_1}{k\cdot p_1} \right)^2. \quad (55)$$

The explicit form of Y can be derived by performing all the details of the calculation, and reads

$$\begin{aligned} Y &= \beta \ln\frac{k_{min}}{E} + \delta_{YFS}, \\ \delta_{YFS} &= \frac{1}{4}\beta + \frac{\alpha}{\pi}\left(\frac{\pi^2}{3} - \frac{1}{2} \right). \end{aligned} \quad (56)$$

1.4.2 Matching NLO and higher-order corrections

As it will be shown numerically in Section 1.6, NLO corrections must be combined with multiple photon emission effects to achieve a theoretical accuracy at the per mille level. This combination, technically known as *matching*, is on the grounds of the most precise generators used for luminosity monitoring, i.e. BabaYaga@NLO, BHWIDE and MCGPJ. Although the matching is implemented according to different theoretical details, some general aspects are common to all the recipes and must be emphasized:

1. it is possible to match NLO and HO corrections consistently, avoiding double counting of LL contributions at order α and preserving the advantages of resummation of soft and collinear effects beyond $\mathcal{O}(\alpha)$;
2. the convolution of NLO corrections with HO terms allows to include the dominant part of NNLO corrections, given by infrared-enhanced $\alpha^2 L$ sub-leading contributions. This was argued and demonstrated analytically and numerically in [8] through comparison with the available $\mathcal{O}(\alpha^2)$ corrections to s-channel processes and t-channel Bhabha scattering. Such an aspect of the matching procedure is crucial to settle the theoretical accuracy of the generators by means of explicit comparisons with the exact NNLO perturbative corrections discussed in Section 1.3, and will be addressed in Section 1.8
3. BabaYaga@NLO and BHWIDE implement a fully factorized matching recipe, while MCGPJ includes some terms in additive form, as will be visible in the formulae to be reported.

In the following we summarize the basic features of the matching procedure as implemented in the codes MCGPJ, BabaYaga@NLO and BHWIDE.

The matching approach realized in the MC event generator MCGPJ was developed in [201]. In particular Bhabha scattering with complete $\mathcal{O}(\alpha)$ and HO LL photonic corrections is represented in the following way:

$$
\begin{aligned}
\frac{\mathrm{d}\sigma^{e^+e^-\to e^+e^-(\gamma)}}{\mathrm{d}\Omega_-} &= \int\limits_{\bar z_1}^1 \mathrm{d}z_1 \int\limits_{\bar z_2}^1 \mathrm{d}z_2\; D_{ee}^{NS,\gamma}(z_1) D_{ee}^{NS,\gamma}(z_2) \\
&\times \frac{\mathrm{d}\hat\sigma_0^{\mathrm{Bhabha}}(z_1,z_2)}{\mathrm{d}\Omega_-}\left(1+\frac{\alpha}{\pi}K_{SV}\right)\Theta(\mathrm{cuts}) \\
&\times \int\limits_{y_{\mathrm{th}}}^{Y_1}\frac{\mathrm{d}y_1}{Y_1}\int\limits_{y_{\mathrm{th}}}^{Y_2}\frac{\mathrm{d}y_2}{Y_2}\; D_{ee}^{NS,\gamma}\!\left(\frac{y_1}{Y_1}\right) D_{ee}^{NS,\gamma}\!\left(\frac{y_2}{Y_2}\right) \\
&+\frac{\alpha}{\pi}\int\limits_{\Delta}^1\frac{\mathrm{d}x}{x}\left\{\left[\left(1-x+\frac{x^2}{2}\right)\ln\frac{\theta_0^2(1-x)^2}{4}+\frac{x^2}{2}\right]\right. \\
&\times 2\frac{\mathrm{d}\sigma_0^{\mathrm{Bhabha}}}{\mathrm{d}\Omega_-}+\left[\left(1-x+\frac{x^2}{2}\right)\ln\frac{\theta_0^2}{4}+\frac{x^2}{2}\right] \\
&\left.\times\left[\frac{\mathrm{d}\hat\sigma_0^{\mathrm{Bhabha}}(1-x,1)}{\mathrm{d}\Omega_-}+\frac{\mathrm{d}\hat\sigma_0^{\mathrm{Bhabha}}(1,1-x)}{\mathrm{d}\Omega_-}\right]\right\}\Theta(\mathrm{cuts}) \\
&-\frac{\alpha^2}{4s}\left(\frac{3+c^2}{1-c}\right)^2\frac{8\alpha}{\pi}\ln(\mathrm{ctg}\frac{\theta}{2})\ln\frac{\Delta\varepsilon}{\varepsilon} \\
&+\frac{\alpha^3}{2\pi^2 s}\int\limits_{\substack{k^0>\Delta\varepsilon\\ \theta_i>\theta_0}}\frac{WT}{4}\Theta(\mathrm{cuts})\frac{\mathrm{d}\Gamma_{e\bar e\gamma}}{\mathrm{d}\Omega_-}\,. \qquad (57)
\end{aligned}
$$

Here the step functions $\Theta(\mathrm{cuts})$ stand for the particular cuts applied. The auxiliary parameter θ_0 defines cones around the directions of the motion of the charged particles in which the emission of hard photons is approximated by the factorized form by convolution of collinear radiation factors [214] with the Born cross section. The dependence on the parameters Δ and θ_0 cancels out in the sum with the last term of Eq. (57), where the photon energy and emission angles with respect to all charged particles are limited from below ($k^0>\Delta\varepsilon, \theta_i>\theta_0$). Taking into account vacuum polarization the Born level Bhabha cross section with reduced energies of the incoming electron and positron can be cast in the following form:

$$
\begin{aligned}
\frac{\mathrm{d}\hat\sigma_0^{\mathrm{Bhabha}}(z_1,z_2)}{\mathrm{d}\Omega_-} &= \frac{4\alpha^2}{sa^2}\left\{\frac{1}{|1-\Pi(\hat t)|^2}\,\frac{a^2+z_2^2(1+c)^2}{2z_1^2(1-c)^2}\right. \\
&+\frac{1}{|1-\Pi(\hat s)|^2}\,\frac{z_1^2(1-c)^2+z_2^2(1+c)^2}{2a^2} \\
&\left.-\mathrm{Re}\,\frac{1}{(1-\Pi(\hat t))(1-\Pi(\hat s))^*}\,\frac{z_2^2(1+c)^2}{az_1(1-c)}\right\}\mathrm{d}\Omega_-\,, \\
\hat s = z_1z_2s, &\quad \hat t = -\frac{sz_1^2z_2(1-c)}{z_1+z_2-(z_1-z_2)c}\,. \qquad (58)
\end{aligned}
$$

where $\Pi(Q^2)$ is the photon self-energy correction. Note that in the cross section above the cosine of the scattering angle, c, is given for the original c.m. reference frame of the colliding beams.

For the two-photon production channel, a similar representation is used in MCGPJ:

$$
\begin{aligned}
\mathrm{d}\sigma^{e^+e^-\to\gamma\gamma(\gamma)} &= \int\limits_{\bar z_1}^1 \mathrm{d}z_1 D_{ee}^{NS,\gamma}(z_1)\int\limits_{\bar z_2}^1 \mathrm{d}z_2 D_{ee}^{NS,\gamma}(z_2) \\
&\times \mathrm{d}\hat\sigma_0^{\gamma\gamma}(z_1,z_2)\left(1+\frac{\alpha}{\pi}K_{SV}^{\gamma\gamma}\right)+\frac{\alpha}{\pi}\int\limits_{\Delta}^1\frac{\mathrm{d}x}{x} \\
&\times\left[\left(1-x+\frac{x^2}{2}\right)\ln\frac{\theta_0^2}{4}+\frac{x^2}{2}\right]\left[\mathrm{d}\hat\sigma_0(1-x,1)\right. \\
&\left.+\mathrm{d}\hat\sigma_0(1,1-x)\right]+\frac{1}{3}\,\frac{4\alpha^3}{\pi^2 s^2}\int\limits_{\substack{z_i\ge\Delta\\ \pi-\theta_0\ge\theta_i\ge\theta_0}}\mathrm{d}\Gamma_{3\gamma} \\
&\times\left[\frac{z_3^2(1+c_3^2)}{z_1^2z_2^2(1-c_1^2)(1-c_2^2)}+\text{two cyclic permutations}\right], \\
z_i = \frac{q_i^0}{\varepsilon}, &\quad c_i=\cos\theta_i, \quad \theta_i = \widehat{\boldsymbol{p}_-\boldsymbol{q}_i}\,, \qquad (59)
\end{aligned}
$$

where the cross section with reduced energies has the form

$$
\frac{\mathrm{d}\hat\sigma_0^{\gamma\gamma}(z_1,z_2)}{\mathrm{d}\Omega_1} = \frac{2\alpha^2}{s}\,\frac{z_1^2(1-c_1)^2+z_2^2(1+c_1)^2}{(1-c_1^2)(z_1+z_2+(z_2-z_1)c_1)^2}\,,
$$

and the factor 1/3 in the last term of Eq. (59) takes into account the identity of the final-state photons. The sum of the last two terms does not depend on Δ and θ_0.

Concerning BabaYaga@NLO the matching starts from the observation that Eq. (26) for the QED corrected all-order cross section can be rewritten in terms of the PS ingredients as

$$d\sigma^{\infty}_{LL} = \Pi(Q^2,\varepsilon)\ \sum_{n=0}^{\infty}\frac{1}{n!}\ |\mathcal{M}_{n,LL}|^2\ d\Phi_n, \qquad (60)$$

The expansion at $\mathcal{O}(\alpha)$ of Eq. (60) does not coincide, by construction, with an exact $\mathcal{O}(\alpha)$ result. In fact

$$\begin{aligned} d\sigma^{\alpha}_{LL} &= \left[1-\frac{\alpha}{2\pi}\ I_+\ \log\frac{Q^2}{m^2}\right]|\mathcal{M}_0|^2 d\Phi_0 + |\mathcal{M}_{1,LL}|^2 d\Phi_1 \\ &\equiv [1+C_{\alpha,LL}]\,|\mathcal{M}_0|^2 d\Phi_0 + |\mathcal{M}_{1,LL}|^2 d\Phi_1, \end{aligned} \qquad (61)$$

where $I_+ \equiv \int_0^{1-\epsilon} P(z)dz$, whereas an exact NLO cross section can be always cast in the form

$$d\sigma^{\alpha} = [1+C_{\alpha}]\,|\mathcal{M}_0|^2 d\Phi_0 + |\mathcal{M}_1|^2 d\Phi_1. \qquad (62)$$

The coefficients C_α contain the complete $\mathcal{O}(\alpha)$ virtual and soft-bremsstrahlung corrections in units of the Born squared amplitude and $|\mathcal{M}_1|^2$ is the exact squared matrix element with the emission of one hard photon. We remark that $C_{\alpha,LL}$ has the same logarithmic structure as C_α and that $|\mathcal{M}_{1,LL}|^2$ has the same singular behaviour like $|\mathcal{M}_1|^2$.

In order to match the LL and NLO calculations the following correction factors, which are by construction infrared safe and free of collinear logarithms, are introduced

$$F_{SV} = 1+(C_\alpha - C_{\alpha,LL}), \quad F_H = 1+\frac{|\mathcal{M}_1|^2-|\mathcal{M}_{1,LL}|^2}{|\mathcal{M}_{1,LL}|^2}, \qquad (63)$$

so that the exact $\mathcal{O}(\alpha)$ cross section can be expressed, up to terms of $\mathcal{O}(\alpha^2)$, in terms of its LL approximation as

$$d\sigma^{\alpha} = F_{SV}(1+C_{\alpha,LL})|\mathcal{M}_0|^2 d\Phi_0 + F_H|\mathcal{M}_{1,LL}|^2 d\Phi_1. \qquad (64)$$

Driven by Eq. (64), Eq. (60) can be improved by writing the resummed matched cross section as

$$\begin{aligned} d\sigma^{\infty}_{\rm matched} = {} & F_{SV}\ \Pi(Q^2,\varepsilon) \\ & \sum_{n=0}^{\infty}\frac{1}{n!}\ \left(\prod_{i=0}^{n}F_{H,i}\right)\ |\mathcal{M}_{n,LL}|^2\ d\Phi_n. \end{aligned} \qquad (65)$$

The correction factors $F_{H,i}$ follow from the definition (63) for each photon emission. The $\mathcal{O}(\alpha)$ expansion of Eq. (65) coincides now with the exact NLO cross section of Eq. (62) and all HO LL contributions are the same as in Eq. (60). This formulation is implemented in BabaYa@NLO for both Bhabha scattering and photon pair production, using, of course, the appropriate SV and hard bremsstrahlung formulae. This matching formulation has been also applied to the study of Drell-Yan-like processes, by combining the complete $\mathcal{O}(\alpha)$ electroweak corrections with QED shower evolution in the generator HORACE [215,216,217,218].

As far as BHWIDE is concerned, this MC event generator realizes the process

$$e^+(p_1)+e^-(q_1) \longrightarrow e^+(p_2)+e^-(q_2)+\gamma_1(k_1)+\ldots+\gamma_n(k_n) \qquad (66)$$

via the YFS exponentiated cross section formula

$$\begin{aligned} d\sigma = {} & e^{2\alpha\Re B+2\alpha\tilde{B}}\ \sum_{n=0}^{\infty}\frac{1}{n!}\int\prod_{j=1}^{n}\frac{d^3k_j}{k_j^0}\int\frac{d^4y}{(2\pi)^4} \\ & e^{iy(p_1+q_1-p_2-q_2-\sum_j k_j)+D}\,\bar{\beta}_n(k_1,\ldots,k_n)\,\frac{d^3p_2 d^3q_2}{p_2^0 q_2^0}, \end{aligned} \qquad (67)$$

where the real infrared function $\tilde{B}$ and the virtual infrared function B are given presently [202], and here we note the usual connections

$$\begin{aligned} 2\alpha\tilde{B} &= \int^{k\le K_{max}}\frac{d^3k}{k_0}\,\tilde{S}(k), \\ D &= \int d^3k\,\frac{\tilde{S}(k)}{k^0}\left(e^{-iy\cdot k}-\theta(K_{\rm max}-k)\right), \end{aligned} \qquad (68)$$

for the standard YFS infrared real emission factor

$$\tilde{S}(k) = \frac{\alpha}{4\pi^2}\left[Q_f Q_{f'}\left(\frac{p_1}{p_1\cdot k}-\frac{q_1}{q_1\cdot k}\right)^2+\ldots\right], \qquad (69)$$

if Q_f is the electric charge of f in units of the positron charge. Here, the "..." represent the remaining terms in $\tilde{S}(k)$ obtained from the one given by respective substitutions of Q_f, p_1, $Q_{f'}$, q_1 with corresponding values for the other pairs of the respective external charged legs according to the YFS prescription in Ref. [197,219] (wherein due attention is taken to obtain the correct relative sign of each of the terms in $\tilde{S}(k)$ according to this latter prescription). We have explicitly the representations

$$\begin{aligned} & 2\alpha\Re B(p_1,q_1,p_2,q_2)+2\alpha\tilde{B}(p_1,q_1,p_2,q_2;k_m) = \\ & R_1(p_1,q_1;k_m)+R_1(p_2,q_2;k_m)+R_2(p_1,p_2;k_m)+ \\ & R_2(q_1,q_2;k_m)-R_2(p_1,q_2;k_m)-R_2(q_1,p_2;k_m), \end{aligned} \qquad (70)$$

with

$$R_1(p,q;k_m) = R_2(p,q;k_m)+\left(\frac{\alpha}{\pi}\right)\frac{\pi^2}{2}, \qquad (71)$$

$$\begin{aligned} R_2(p,q;k_m) = {} & \frac{\alpha}{\pi}\left\{\left(\ln\frac{2pq}{m_e^2}-1\right)\ln\frac{k_m^2}{p^0q^0}+\frac{1}{2}\ln\frac{2pq}{m_e^2}\right. \\ & -\frac{1}{2}\ln^2\frac{p^0}{q^0}-\frac{1}{4}\ln^2\frac{(\Delta+\delta)^2}{4p^0q^0}-\frac{1}{4}\ln^2\frac{(\Delta-\delta)^2}{4p^0q^0} \\ & -\Re\,\mathrm{Li}_2\left(\frac{\Delta+\omega}{\Delta+\delta}\right)-\Re\,\mathrm{Li}_2\left(\frac{\Delta+\omega}{\Delta-\delta}\right) \\ & -\Re\,\mathrm{Li}_2\left(\frac{\Delta-\omega}{\Delta+\delta}\right)-\Re\,\mathrm{Li}_2\left(\frac{\Delta-\omega}{\Delta-\delta}\right) \\ & \left.+\frac{\pi^2}{3}-1\right\}, \end{aligned} \qquad (72)$$

where $\Delta = \sqrt{2pq+(p^0-q^0)^2}$, $\omega = p^0+q^0$, $\delta = p^0-q^0$, and k_m is a soft photon cut-off in the CMS ($E_\gamma^{\rm soft} < k_m \ll E_{\rm beam}$).

The YFS hard photon residuals $\bar{\beta}_i$ in (67), $i=0,1$, are given exactly through $\mathcal{O}(\alpha)$ in Ref. [202] for BHWIDE, so

that this latter event generator calculates the YFS exponentiated exact $\mathcal{O}(\alpha)$ cross section for $e^+e^- \to e^+e^- + n(\gamma)$ with multiple initial, initial-final, and final state radiation using a corresponding MC realization of Eq. (67) in the wide angle regime. The $\mathcal{O}(\alpha)$ electroweak corrections library, relevant for higher energies, is taken from Refs. [220,59].

The result (67) is an exact re-arrangement of the loop expansion for the respective cross section and it is independent of the dummy parameter $K_{\max}$. To see how to derive it, one may proceed as follows. Let the amplitude for the emission of n real photons in the Bhabha process be

$$\mathcal{M}^{(n)} = \sum_{\ell} M_{\ell}^{(n)}, \tag{73}$$

$M_{\ell}^{(n)}$ is the contribution to $\mathcal{M}^{(n)}$ from Feynman diagrams with ℓ virtual loops. The key result in the YFS theory of Ref. [197,219] on virtual corrections is that we may rewrite Eq. (73) as the exact representation

$$\mathcal{M}^{(n)} = e^{\alpha B} \sum_{j=0}^{\infty} \mathsf{m}_j^{(n)}, \tag{74}$$

where we have defined

$$\alpha B = \int \frac{d^4k}{(k^2 - \lambda^2 + i\epsilon)} S(k), \tag{75}$$

with the virtual infrared emission factor given by

$$S(k) = \frac{-i\alpha}{8\pi^2} \sum_{i'<j} Z_{i'}\theta_{i'} Z_j \theta_j \left(\frac{(2\bar{p}_{i'}\theta_{i'} - k)_\mu}{k^2 - 2k\bar{p}_{i'}\theta_{i'} + i\epsilon} + \frac{(2\bar{p}_j\theta_j + k)_\mu}{k^2 + 2k\bar{p}_j\theta_j + i\epsilon} \right)^2. \tag{76}$$

Here, λ is an infrared regulator mass, and we follow Ref. [197, 219] and identify the sign of the j-th external line charge here as $Z_j = Q_j$ and $\theta_j = +(-)$ for outgoing (incoming) 4-momentum $\bar{p}_j$, so that here $\bar{p}_1 = p_1$, $\bar{p}_2 = q_1$, $\bar{p}_3 = p_2$, $\bar{p}_4 = q_2$, $Z_1 = +1$, $\theta_1 = -$, $Z_2 = -1$, $\theta_2 = -$, $Z_3 = +1$, $\theta_3 = +$, $Z_4 = -1$, $\theta_4 = +$. The amplitudes $\{\mathsf{m}_j^{(n)}\}$ are free of all virtual infrared divergences.

Using the result (74) for $\mathcal{M}^{(n)}$, we get the attendant differential cross section by the standard methods as

$$d\hat{\sigma}^n = \frac{e^{2\alpha \Re B}}{n!} \int \prod_{l=1}^{n} \frac{d^3k_l}{(k_l^2 + \lambda^2)^{1/2}} \times \bar{\rho}^{(n)}(p_1, q_1, p_2, q_2, k_1, \cdots, k_n) \frac{d^3p_2 d^3q_2}{p_2^0 q_2^0} \times \delta^{(4)} \left(p_1 + q_1 - p_2 - q_2 - \sum_{i=1}^{n} k_i \right), \tag{77}$$

where we have defined

$$\bar{\rho}^{(n)}(p_1, q_1, p_2, q_2, k_1, \cdots, k_n) = \sum_{\text{spin}} \left| \sum_{j=0}^{\infty} \mathsf{m}_j^{(n)} \right|^2, \tag{78}$$

in the incoming e^+e^- CMS system, and we have absorbed the remaining kinematical factors for the initial state flux and spin averages into the normalization of the amplitudes $\mathcal{M}^{(n)}$ for pedagogical reasons, so that the $\bar{\rho}^{(n)}$ are averaged over initial spins and summed over final spins. We then use the key result of Ref. [197,219] on real corrections to write the exact result

$$\bar{\rho}^{(n)}(p_1, q_1, p_2, q_2, k_1, \cdots, k_n) = \prod_{i=1}^{n} \tilde{S}(k_i)\bar{\beta}_0 + \cdots + \sum_{i=1}^{n} \tilde{S}(k_i)\bar{\beta}_{n-1}(k_1, \ldots, k_{i-1}, k_{i+1}, \ldots, k_n) + \bar{\beta}_n(k_1, \ldots, k_n), \tag{79}$$

where the hard photon residuals $\{\bar{\beta}_j\}$ are determined recursively [197,219] and are free all virtual and all real infrared singularities to all orders in α. Introducing the result (79) into Eq. (77) and summing over the number of real photons n leads directly to master formula (67). We see that it allows for exact exclusive treatment of hard photonic effects on an event-by-event basis.

1.5 Monte Carlo generators

To measure the luminosity, event generators, rather than analytical calculations, are mandatory to provide theoretical results of real experimental interest. The software tools used in early measurements of the luminosity at flavour factories (and sometimes still used in recent experimental publications) include generators such as BHAGENF [221], BabaYaga v3.5 [199] and BKQED [222,223]. These MC programs, however, are based either on a fixed NLO calculation (such as BHAGENF and BKQED) or include corrections to all orders in perturbation theory, but in the LL approximation only (like BabaYaga v3.5). Therefore the precision of these codes can be estimated to lie in the range 0.5÷1%, depending on the adopted experimental cuts.

The increasing precision reached on the experimental side during the last years led to the development of new dedicated theoretical tools, such as BabaYaga@NLO and MCGPJ, and the adoption of already well-tested codes, like BHWIDE, the latter extensively used at high-energy LEP/SLC colliders for the simulation of the large-angle Bhabha process. As already emphasized in Section 1.4.2, all these three codes include NLO corrections in combination with multiple photon contributions and have, therefore, a precision tag of $\sim 0.1\%$. As described in the following, the experiments typically use more than one generator, to keep the luminosity theoretical error under control through the comparison of independent predictions.

A list of the MC tools used in the luminosity measurement at meson factories is given in Tab. 2, which summarizes the main ingredients of their formulation for radiative corrections and the estimate of their theoretical accuracy.

The basic theoretical and phenomenological features of the different generators are summarized in the following.

Table 2. MC generators used for luminosity monitoring at meson factories.

Generator	Theory	Accuracy
BabaYaga v3.5	Parton Shower	$\sim 0.5 \div 1\%$
BabaYaga@NLO	$\mathcal{O}(\alpha) + \mathrm{PS}$	$\sim 0.1\%$
BHAGENF	$\mathcal{O}(\alpha)$	$\sim 1\%$
BHWIDE	$\mathcal{O}(\alpha)$ YFS	$\sim 0.5\%$(LEP1)
BKQED	$\mathcal{O}(\alpha)$	$\sim 1\%$
MCGPJ	$\mathcal{O}(\alpha) + \mathrm{SF}$	$< 0.2\%$

1. BabaYaga v3.5 – It is a MC generator developed by the Pavia group at the starting of DAΦNE operation using a QED PS approach for the treatment of LL QED corrections to luminosity processes and later improved to account for the interference of radiation emitted by different charged legs in the generation of the momenta of the final-state particles. The main drawback of BabaYaga v3.5 is the absence of $\mathcal{O}(\alpha)$ non-log contributions, resulting in a theoretical precision of $\sim 0.5\%$ for large-angle Bhabha scattering and of about 1% for $\gamma\gamma$ and $\mu^+\mu^-$ final states. It is used by the CLEO-c collaboration for the study of all the three luminosity processes.
2. BabaYaga@NLO – It is the presently released version of BabaYaga, based on the matching of exact $\mathcal{O}(\alpha)$ corrections with QED PS, as described in Section 1.4.2. The accuracy of the current version is estimated to be at 0.1% level for large-angle Bhabha scattering, two-photon and $\mu^+\mu^-$ [8] production. It is presently used by the KLOE and BaBar collaborations, and under consideration by the BES-III experiment. Like BabaYaga v3.5, BabaYaga@NLO is available at the web page of the Pavia phenomenology group `www.pv.infn.it/~hepcomplex/babayaga.html`.
3. BHAGENF/BKQED – BKQED is the event generator developed by Berends and Kleiss and based on the classical exact NLO calculations of [222,223] for all QED processes. It was intensively used at LEP to perform tests of QED through the analysis of the $e^+e^- \to \gamma\gamma$ process and is adopted by the BaBar collaboration for the simulation of the same reaction. BHAGENF is a code realized by Drago and Venanzoni at the beginning of DAΦNE operation to simulate Bhabha events, adapting the calculations of [222] to include the contribution of the Φ resonance. Both generators lack the effect of HO corrections and, as such, have a precision accuracy of about 1%. The BHAGENF code is available at the web address `www.lnf.infn.it/~graziano/bhagenf/bhabha.html`.
4. BHWIDE – It is a MC code realized in Krakow-Knoxwille at the time of LEP/SLC operation and described in [202]. In this generator exact $\mathcal{O}(\alpha)$ corrections are matched with the resummation of soft and collinear logarithms through the YFS exponentiation approach. According to the authors the precision is estimated to be about 0.5% for c.m. energies around the Z resonance. This accuracy estimate was derived through detailed comparisons of the BHWIDE predictions with those of other LEP tools in the presence of the full set of NLO corrections, including purely weak corrections. However since the latter are phenomenologically unimportant at e^+e^- accelerators of moderately high energies and the QED theoretical ingredients of BHWIDE are very similar to the formulation of both BabaYaga@NLO and MCGPJ, one can argue that BHWIDE accuracy for physics at flavour factories is at the level of 0.1%. It is adopted by the KLOE, BaBar and BES collaborations. The code is available at `placzek.home.cern.ch/placzek/bhwide/`.
5. MCGPJ – It is the generator developed by the Dubna-Novosibirsk collaboration and used at VEPP-2M collider. This program includes exact $\mathcal{O}(\alpha)$ corrections supplemented with HO LL contributions related to the emission of collinear photon jets and taken into account through analytical QED collinear SF, as described in Section 1.4.2. The theoretical precision is estimated to be better than 0.2%. The generator is available at the web address `cmd.inp.nsk.su/~sibid/`.

It is worth noticing that the theoretical uncertainty of the most accurate generators based on the matching of exact NLO with LL resummation starts at the level of $\mathcal{O}(\alpha^2)$ NNL contributions, as far as photonic corrections are concerned. Other sources of error affecting their physical precision are discussed in detail in Section 1.8

1.6 Numerical results

Before showing the results which enable us to settle the technical and theoretical accuracy of the generators, it is worth discussing the impact of various sources of radiative corrections implemented in the programs used in the experimental analysis. This allows one to understand which corrections are strictly necessary to achieve a precision at the per mille level for both the calculation of integrated cross section and the simulation of more exclusive distributions.

1.6.1 Integrated cross sections

The first set of phenomenological results about radiative corrections refer to the Bhabha cross section, as obtained by means of the code BabaYaga@NLO, according to different perturbative and precision levels. In Tab. 3 we show the values for the Born cross section σ_0, the $\mathcal{O}(\alpha)$ PS and exact cross section, $\sigma_\alpha^{\mathrm{PS}}$ and $\sigma_\alpha^{\mathrm{NLO}}$, respectively, as well as the LL PS cross section σ^{PS} and the matched cross section $\sigma_{\mathrm{matched}}$. Furthermore, the cross section in the presence of the vacuum polarization correction σ_0^{VP}

[8] At present, finite mass effects in the virtual corrections to $e^+e^- \to \mu^+\mu^-$, which should be included for precision simulations at the Φ-factories, are not included in BabaYaga@NLO.

Table 3. Bhabha cross section (in nb) at meson factories according to different precision levels and using the cuts of Eq. (12), but with an angular acceptance of $55^\circ \leq \theta_\pm \leq 125^\circ$. The numbers in parentheses are 1σ MC errors.

$\sqrt{s}$(GeV)	1.02	4	10
σ_0	529.4631(2)	44.9619(1)	5.5026(2)
$\sigma_0^{\rm VP}$	542.657(6)	46.9659(1)	5.85526(3)
$\sigma_{\rm NLO}$	451.523 (6)	37.1654 (6)	4.4256 (2)
$\sigma_\alpha^{\rm PS}$	454.503 (6)	37.4186 (6)	4.4565 (1)
$\sigma_{\rm matched}$	455.858 (5)	37.6731 (4)	4.5046 (3)
$\sigma^{\rm PS}$	458.437 (4)	37.8862 (4)	4.5301 (2)

is also shown. The results correspond to the c.m. energies $\sqrt{s} = 1, 4, 10$ GeV, and were obtained with the selection criteria of Eq. (12), but for an angular acceptance of $55^\circ \leq \theta_\pm \leq 125^\circ$ resembling realistic data taking at meson factories. One should keep in mind that the cuts of Eq. (12) tend to single out quasi-elastic Bhabha events and that the energy of final-state electron/positron corresponds to a so-called "bare" event selection (i.e. without photon recombination), which corresponds to what is done in practice at flavour factories. In particular the rather stringent energy and acollinearity cuts enhance the impact of soft and collinear radiation with respect to a more inclusive setup.

From these cross section values, it is possible to calculate the relative effect of various corrections, namely the contribution of vacuum polarization and exact $\mathcal{O}(\alpha)$ QED corrections, of non-logarithmic (NLL) terms entering the $\mathcal{O}(\alpha)$ cross section, of HO corrections in the $\mathcal{O}(\alpha)$ matched PS scheme and finally of NNL effects beyond order α largely dominated by $\mathcal{O}(\alpha^2 L)$ contributions. The above per cent corrections are shown in Tab. 4 and can be derived from the cross section results of Tab. 3 according to the following definitions

$$\delta_{\rm VP} \equiv \frac{\sigma_0^{\rm VP} - \sigma_0}{\sigma_0}, \qquad \delta_\alpha \equiv \frac{\sigma_{\rm NLO} - \sigma_0}{\sigma_0},$$
$$\delta_\alpha^{\rm NLL} \equiv \frac{\sigma_{\rm NLO} - \sigma_\alpha^{\rm PS}}{\sigma_{\rm NLO}}, \qquad \delta_{\rm HO} \equiv \frac{\sigma_{\rm matched} - \sigma_{\rm NLO}}{\sigma_{\rm NLO}},$$
$$\delta_{\alpha^2 L} \equiv \frac{\sigma_{\rm matched} - \sigma_{\rm NLO} - \sigma^{\rm PS} + \sigma_\alpha^{\rm PS}}{\sigma_{\rm NLO}}.$$

From Tab. 4 it can be seen that $\mathcal{O}(\alpha)$ corrections decrease the Bhabha cross section by about 15÷17% at the Φ and τ-charm factories, and by about 20% at the B–factories. Within the full set of $\mathcal{O}(\alpha)$ corrections, non–log terms are of the order of 0.5%, almost independently of c.m. energy, as expected, and with a mild dependence on the angular acceptance cuts as due to box/interference contributions. The effect of HO corrections due to multiple photon emission is about 1% at the Φ and τ-charm factories and reaches about 2% at the B–factories. The contribution of (approximate) $\mathcal{O}(\alpha^2 L)$ corrections is at the 0.1% level, while the vacuum polarization increases the cross section by about 2% around 1 GeV, and of about 5% and 6% at 4 GeV and 10 GeV, respectively. Concerning the latter correction the non-perturbative hadronic contribution to the running of α was parameterized in terms of the HADR5N routine [224,225,226] included in BabaYaga@NLO both in the LO and NLO diagrams. We have checked that the results obtained for the vacuum polarization correction in terms of the parametrization [129] agree at the 10^{-4} level with those obtained with HADR5N, as shown in detail in Section 1.8. Those routines return a data driven error thus affecting the theoretical precision of the calculation of the Bhabha cross cross section as will be discussed in Section 1.9.

Analogous results about the size of radiative corrections to the process $e^+e^- \to \gamma\gamma$ are given in Tab. 5 [227]. They were obtained using BabaYaga@NLO, according to the experimental cuts of Eq. (13) for the c.m. energies $\sqrt{s} = 1, 3, 10$ GeV.

Table 4. Relative size of different sources of correction (in per cent) to the large-angle Bhabha cross section for typical selection cuts at Φ, τ-charm and B factories.

$\sqrt{s}$(GeV)	1.02	4.	10.
δ_α	−14.73	−17.32	−19.57
$\delta_\alpha^{\rm NLL}$	−0.66	−0.68	−0.70
$\delta_{\rm HO}$	0.97	1.35	1.79
$\delta_{\alpha^2 L}$	0.09	0.09	0.11
$\delta_{\rm VP}$	2.43	4.46	6.03

Table 5. Photon pair production cross sections (in nb) at different accuracy levels and relative corrections (in per cent) for the setup of Eq. (13) and the c.m. energies $\sqrt{s} = 1, 3, 10$ GeV.

$\sqrt{s}$ (GeV)	1	3	10
σ_0	137.53	15.281	1.3753
$\sigma_{\rm NLO}$	129.45	14.211	1.2620
$\sigma_\alpha^{\rm PS}$	128.55	14.111	1.2529
$\sigma_{\rm matched}$	129.77	14.263	1.2685
$\sigma^{\rm PS}$	128.92	14.169	1.2597
δ_α	−5.87	−7.00	−8.24
$\delta_\alpha^{\rm NLL}$	0.70	0.71	0.73
$\delta_{\rm HO}$	0.24	0.37	0.51

The numerical errors coming from the MC integration are not shown in Tab. 4 because they are beyond the quoted digits. From Tab. 4 it can be seen that the exact $\mathcal{O}(\alpha)$ corrections lower the Born cross section by about 5.9% (Φ resonance), 7.0% (at $\sqrt{s} = 3$ GeV) and 8.2% (Υ resonance). The effect due to $\mathcal{O}(\alpha^n L^n)$ (with $n \geq 2$) terms is quantified by the contribution $\delta_{\rm HO}$, which is a positive correction of about 0.2% (at the Φ resonance), 0.4% (τ-charm factories) and 0.5% (at the Υ resonance), and therefore important in the light of the aimed per mille accuracy. On the other hand also next-to-leading $\mathcal{O}(\alpha)$ cor-

rections, quantified by the contribution $\delta_\alpha^{\rm NLL}$, are necessary at the precision level of 0.1%, since their contribution is of about 0.7% almost independently of the c.m. energy. To further corroborate the precision reached in the cross section calculation of $e^+e^- \to \gamma\gamma$, we also evaluated the effect due to the most important sub-leading $\mathcal{O}(\alpha^2)$ photonic corrections and given by order $\alpha^2 L$ contributions. It turns out that the effect due to $\mathcal{O}(\alpha^2 L)$ corrections does not exceed the 0.05% level. Obviously, the contribution of vacuum polarization is absent in $\gamma\gamma$ production and this is an advantage for particularly precise predictions as the uncertainty associated with the hadronic part of vacuum polarization does not affect the cross section calculation.

1.6.2 Distributions

Besides the integrated cross section, various differential cross sections are used by the experimentalists to monitor the collider luminosity. In Fig. 16 and Fig. 17 we show two distributions which are particularly sensitive to the details of photon radiation, i.e. the e^+e^- invariant mass and acollinearity distribution, in order to quantify the size of NLO and HO corrections. The distributions are obtained according to the exact $\mathcal{O}(\alpha)$ calculation and with the two BabaYaga versions, BabaYaga v3.5 and BabaYaga@NLO. From Fig. 16 and Fig. 17 it can be clearly seen that multiple photon corrections introduce significant deviations with respect to an $\mathcal{O}(\alpha)$ simulation, especially in the hard tails of the distributions where they amount to several per cent. To make clearly visible the contribution of exact $\mathcal{O}(\alpha)$ non-log terms the inset shows the relative differences between the predictions of BabaYaga v3.5 (denoted as OLD) and BabaYaga@NLO (denoted as NEW). Actually as discussed in Section 1.4.2 these differences mainly come from non-log NLO contributions and to a smaller extent from $\mathcal{O}(\alpha^2 L)$ terms. Their effect is flat and at the level of 0.5% for the acollinearity distribution while they reach the several per cent level in the hard tail of the invariant mass distribution.

It is also worth noticing that LL radiative corrections beyond α^2 can be quite important for accurate simulations at least when considering differential distributions. This means that even with a complete NNLO calculation at hand it would be desirable to match such corrections with the resummation of all the remaining LL effects. In Fig. 18, the relative effect of HO corrections beyond α^2 dominated by the α^3 contributions (dashed line) is shown in comparison with that of the α^2 corrections (solid line) on the acollinearity distribution for the Bhabha process at DAΦNE. As it can be seen the α^3 effect can be as large as 10% in the phase space region of soft photon emission, corresponding to small acollinearity angles with almost back-to-back final-state fermions.

Concerning the process $e^+e^- \to \gamma\gamma$ we show in Fig. 19 the energy distribution of the most energetic photon, while the acollinearity distribution of the two most energetic photons is represented in Fig. 20. The distributions refer to exact $\mathcal{O}(\alpha)$ corrections matched with the PS algorithm (solid line), to the exact NLO calculation (dashed

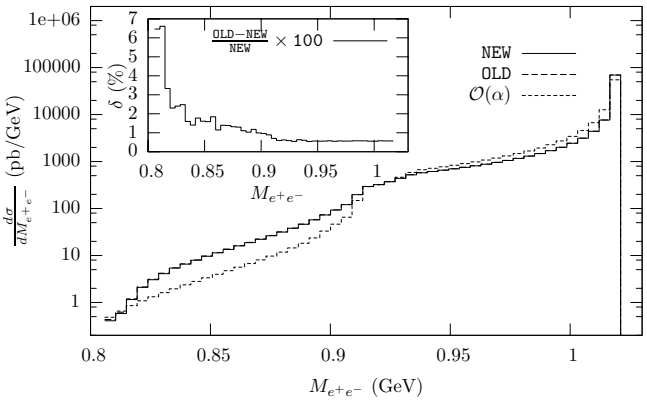

Fig. 16. Invariant mass distribution of the Bhabha process at KLOE, according to BabaYaga v3.5 (OLD), BabaYaga@NLO (NEW) and an exact NLO calculation. The inset shows the relative effect of NLO corrections, given by the difference of BabaYaga v3.5 and BabaYaga@NLO predictions. From [200].

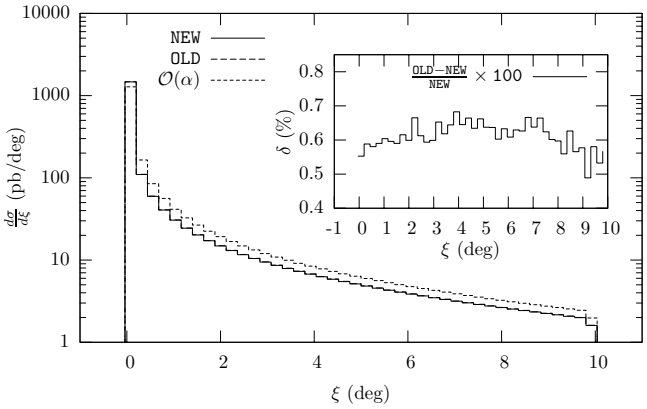

Fig. 17. Acollinearity distribution of the Bhabha process at KLOE, according to BabaYaga v3.5 (OLD) and BabaYaga@NLO (NEW). The inset shows the relative effect of NLO corrections, given by the difference of BabaYaga v3.5 and BabaYaga@NLO predictions. From [200].

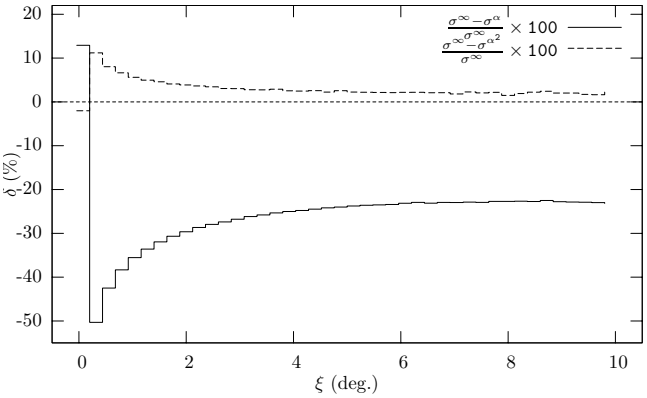

Fig. 18. Relative effect of HO corrections $\alpha^2 L^2$ and $\alpha^n L^n$ ($n \geq 3$) to the acollinearity distribution of the Bhabha process at KLOE. From [200].

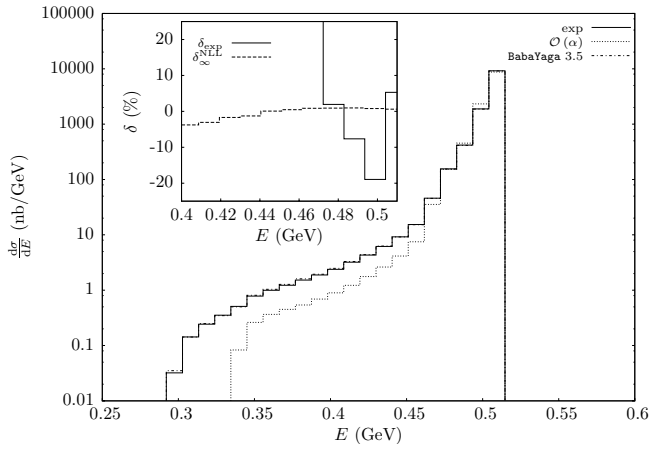

Fig. 19. Energy distribution of the most energetic photon in the process $e^+e^- \to \gamma\gamma$, according to the PS matched with $\mathcal{O}(\alpha)$ corrections denoted as exp (solid line), the exact $\mathcal{O}(\alpha)$ calculation (dashed line) and the pure all-order PS as in BabaYaga v3.5 (dashed-dotted line). lnset: relative effect (in per cent) of multiple photon corrections (solid line) and of non-log contributions of the matched PS algorithm (dashed line). From [227].

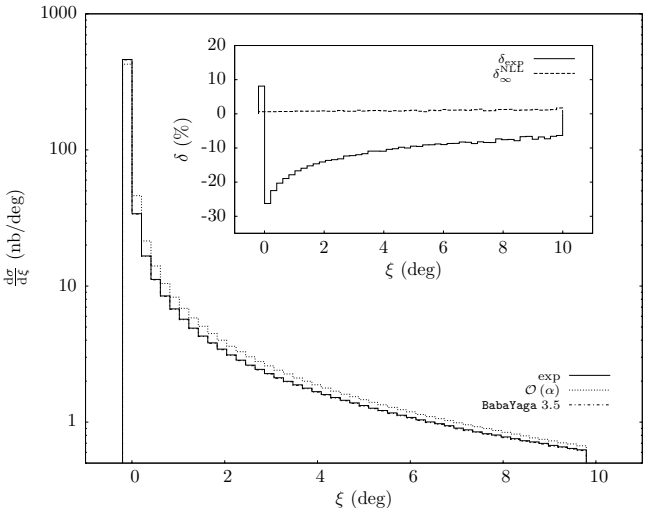

Fig. 20. Acollinearity distribution for the process $e^+e^- \to \gamma\gamma$, according to the PS matched with $\mathcal{O}(\alpha)$ corrections denoted as exp (solid line), the exact $\mathcal{O}(\alpha)$ calculation (dashed line) and the pure all-order PS as in BabaYaga v3.5 (dashed-dotted line). lnset: relative effect (in per cent) of multiple photon corrections (solid line) and of non-log contributions of the matched PS algorithm (dashed line). From [227].

line) and to all-order pure PS predictions of BabaYaga v3.5 (dashed-dotted line). In the inset of each plot, the relative effect due to multiple photon contributions ($\delta_{\rm HO}$) and non-logarithmic terms entering the improved PS algorithm ($\delta_\alpha^{\rm NLL}$) is also shown, according to the definitions given in Eq. (80).

For the energy distribution of the most energetic photon particularly pronounced effects due to exponentiation are present. In the statistically dominant region, HO corrections reduce the $\mathcal{O}(\alpha)$ distribution by about 20%, while they give rise to a significant hard tail close to the energy threshold of $0.3\sqrt{s}$ as a consequence of the higher photon multiplicity of the resummed calculation with respect to the fixed-order NLO prediction. Needless to say, the relative effect of multiple photon corrections below about 0.46 GeV not shown in the inset is finite but huge. This representation was chosen to make also visible in the inset the contribution of $\mathcal{O}(\alpha)$ non-log terms, that otherwise would be hardly seen in comparison with the multiple photon corrections. Concerning the acollinearity distribution, the contribution of higher-order corrections is positive and of about 10% for quasi-back-to-back photon events, whereas it is negative and decreasing from $\sim -30\%$ to $\sim -10\%$ for increasing acollinearity values. As far as the contributions of non-logaritmic effects dominated by next-to-leading $\mathcal{O}(\alpha)$ corrections are concerned, they contribute at the level of several per mille for the acollinearity distribution, while they lie in the several per cent range for the energy distribution.

As a whole, the results of the present Section emphasize that both exact $\mathcal{O}(\alpha)$ and HO photonic corrections are necessary, as well as taking into account the running of α, for a 0.1% theoretical precision in the calculation of both the cross sections and distributions.

1.7 Tuned comparisons

The typical procedure followed in the literature to establish the technical precision of the theoretical tools is to perform tuned comparisons between the predictions of independent programs using the same set of input parameters and experimental cuts. This strategy was initiated in the 90s during the CERN workshops for precision physics at LEP and is still in use when considering processes of interest for physics at hadron colliders demanding particularly accurate theoretical calculations. The tuning procedure is a key step in the validation of generators, because it allows to check that the different details entering the complex structure of the generators, e.g. implementation of radiative corrections, event selection routines, MC integration and event generation, are under control and to fix possible mistakes.

The tuned comparisons discussed in the following were performed switching off the vacuum polarization correction to the Bhabha scattering cross section. Actually, the generators implement the non-perturbative hadronic contribution to the running of α according to different parameterizations, which differently affect the cross section prediction (see Section 4 for discussion). Hence, this simplification is introduced to avoid possible bias in the interpretation of the results and allows to disentagle the effect of pure QED corrections. Also, the comparisons take into account *realistic* event selection cuts, in order to provide useful results for the experiments.

The present Section is a merge of results available in the literature [200] with those of new studies. The results refer to the Bhabha process at the energies of Φ, τ-charm

Table 6. Cross section predictions [nb] of BabaYaga@NLO and BHWIDE for the Bhabha cross section corresponding to two different angular acceptances, for the KLOE experiment at DAΦNE, and their relative differences (in per cent).

angular acceptance	BabaYaga@NLO	BHWIDE	δ(%)
$20^\circ \div 160^\circ$	6086.6(1)	6086.3(2)	0.005
$55^\circ \div 125^\circ$	455.85(1)	455.73(1)	0.030

and B factories. No tuned comparisons for the two photon production process have been carried out.

1.7.1 Φ and τ-charm factories

First we show comparisons between BabaYaga@NLO and BHWIDE according to the KLOE selection cuts of Eq. (12), considering also the angular range $20^\circ \leq \vartheta_\pm \leq 160^\circ$ for cross section results. The predictions of the two codes are reported in Tab. 6 for the two acceptance cuts together with their relative deviations. As can be seen the agreement is excellent, the relative deviations being well below the 0.1%. Comparisons between BabaYaga@NLO and BHWIDE at the level of differential distributions are given in Fig. 21 and Fig. 22 where the inset shows the relative deviations between the predictions of the two codes. As can be seen there is very good agreement between the two generators, as the predicted distributions appear at a first sight almost indistinguishable. Looking in more detail, there is a relative difference of a few per mille for the acollinearity distribution (Fig. 22) and of a few per cent for the invariant mass (Fig. 21), but only in the very hard tails, where the fluctuations observed are due to limited MC statistics. These configurations however contribute to the integrated cross section negligibly, their contribution being a factor $10^3 \div 10^4$ smaller than that around the very dominant peak regions. In fact these differences on differential distributions translate into agreement on the cross section values well below the one per mille, as shown in Tab. 6.

Similar tuned comparisons were performed between the results of BabaYaga@NLO, BHWIDE and MCGPJ in the presence of cuts modeling the event selection criteria of the CMD-2 experiment at the VEPP-2M collider, for a c.m. energy of $\sqrt{s} = 900$ MeV. The cuts used in this case are

$$
\begin{aligned}
&|\theta_- + \theta_+ - \pi| \leq \Delta\theta, \quad 1.1 \leq (\theta_+ - \theta_- + \pi)/2 \leq \pi - 1.1,\\
&||\phi_- + \phi_+| - \pi| \leq 0.15,\\
&p_- \sin(\theta_-) \geq 90 \text{ MeV}, \qquad p_+ \sin(\theta_+) \geq 90 \text{ MeV},\\
&(p_- + p_+)/2 \geq 90 \text{ MeV},
\end{aligned}
\tag{80}
$$

where θ_-, θ_+ are the electron/positron polar angles, respectively, $\phi_\pm$ their azimuthal angles, and $p_\pm$ the moduli of their three-momenta. $\Delta\theta$ stands for an acollinearity cut.

Figure 23 shows the relative differences between the results of BHWIDE and MCGPJ according to the criteria of Eq. (80), as a function of the acollinearity cut $\Delta\theta$. The relative deviations between the results of BabaYaga@NLO and MCGPJ for the same cuts are given in Fig. 24. It can be seen that the predictions of the three generators lie within a 0.2% band with differences of $\sim 0.3\%$ for extreme values of the acollinearity cut. This agreement can be considered satisfactory since for the acollinearity cut of real experimental interest ($\Delta\theta \approx 0.2$ rad) the generators agree within the one per mille.

Table 7. Cross section predictions [nb] of BabaYaga@NLO and MCGPJ for the Bhabha cross section at τ-charm factories ($\sqrt{s} = 3.5$ GeV) and their relative difference (in per cent).

BabaYaga@NLO	MCGPJ	δ(%)
35.20(2)	35.181(5)	0.06

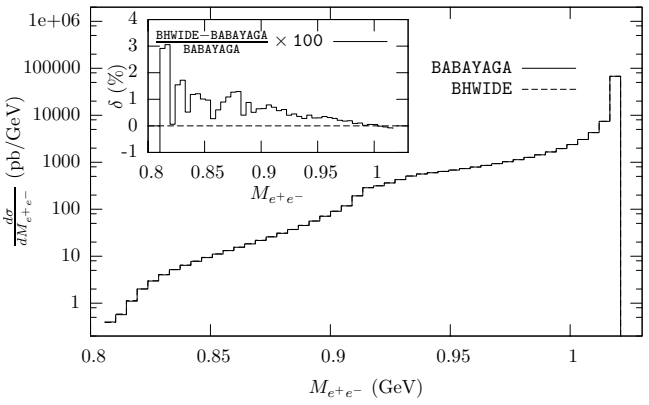

Fig. 21. Invariant mass distribution of the Bhabha process according to BHWIDE and BabaYaga@NLO, for the KLOE experiment at DAΦNE, and relative differences of the program predictions (inset). From [200].

A number of comparisons was also performed for a c.m. energy of 3.5 GeV relevant to the experiments at τ-charm factories. An example is given in Tab. 7 where the predictions of BabaYaga@NLO and MCGPJ are compared, using cuts similar to those of Eq. (80) and for an acollinearity cut of $\Delta\theta = 0.25$ rad. The agreement between the two codes is below one per mille. Comparisons between the two codes were also done at the level of differential cross sections, showing satisfactory agreement in the statistically relevant phase space regions. Preliminary results [228] for a c.m. energy on top of the J/Ψ resonance show good agreement between BabaYaga@NLO and BHWIDE predictions too.

1.7.2 B-factories

Concerning the B-factories, a considerable effort was done to establish the level of agreement between the generators BabaYaga@NLO and BHWIDE in comparison with BabaYaga v3.5 too. This study made use of the realistic luminosity cuts quoted in Section 1.3.3 for the BaBar experiment. The cross sections predicted by BabaYaga@NLO

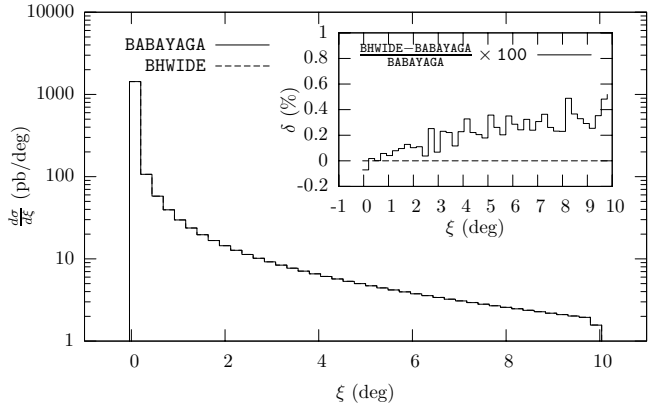

Fig. 22. Acollinearity distribution of the Bhabha process according to BHWIDE and BabaYaga@NLO, for the KLOE experiment at DAΦNE, and relative differences of the program predictions (inset). From [200].

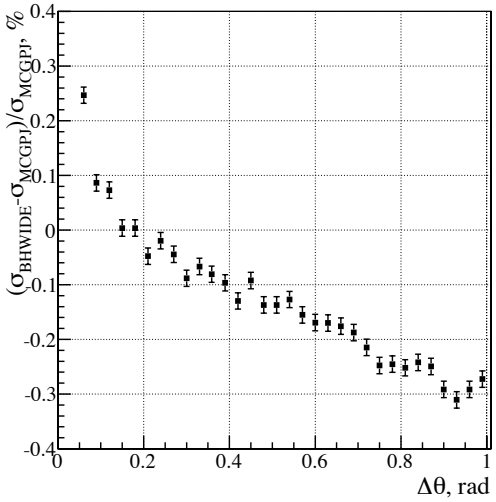

Fig. 23. Relative differences between BHWIDE and MCGPJ Bhabha cross sections as a function of the acollinearity cut, for the CMD-2 experiment at VEPP-2M.

and BHWIDE are shown in Tab. 8, together with the corresponding relative differences as a function of the considered angular range. The latter are also shown in Fig. 25, where the 1σ numerical error due to MC statistics is also quoted. As it can be seen, the two codes agree nicely, the predictions for the central value being in general in agreement at the 0.1% level or statistically compatible whenever a two to three per mille difference is present.

To further investigate how the two generators compare with each other a number of differential cross sections was studied. The results of this study are shown in Fig. 26 and Fig. 27 for the distribution of the electron energy and the polar angle, respectively, and in Fig. 28 for the acollinearity. For both the energy and scattering angle distribution the two programs agree within the statistical errors showing deviations not above the 0.5%. For the acollinearity dependence of the cross section, BabaYaga@NLO and BHWIDE agree within $\sim 1\%$. Therefore, the level of the agreement between the two codes around 10 GeV is the same as that observed at the Φ factories.

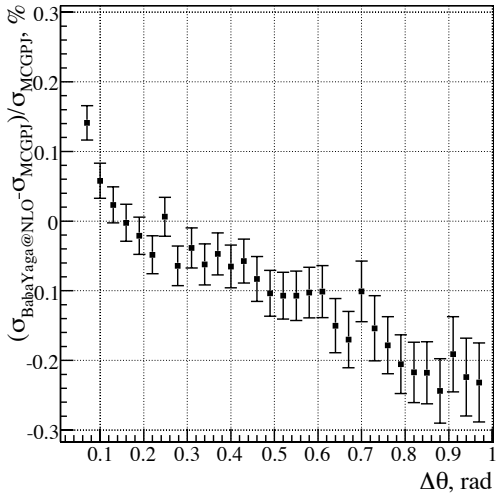

Fig. 24. Relative differences between BabaYaga@NLO and MCGPJ Bhabha cross sections as a function of the acollinearity cut, for the CMD-2 experiment at VEPP-2M.

Table 8. Cross section predictions [nb] of BabaYaga@NLO and BHWIDE for the Bhabha cross section as a function of the angular selection cuts for the BaBar experiment at PEP-II and absolute value of their relative differences (in per cent).

angular range (c.m.s.)	BabaYaga@NLO	BHWIDE	$\lvert\delta(\%)\rvert$
$15^\circ \div 165^\circ$	119.5(1)	119.53(8)	0.025
$30^\circ \div 150^\circ$	24.17(2)	24.22(2)	0.207
$40^\circ \div 140^\circ$	11.67(3)	11.660(8)	0.086
$50^\circ \div 130^\circ$	6.31(3)	6.289(4)	0.332
$60^\circ \div 120^\circ$	1.928(2)	1.931(3)	0.141
$70^\circ \div 110^\circ$	3.554(6)	3.549(3)	0.155
$80^\circ \div 100^\circ$	0.824(2)	0.822(1)	0.243

The main conclusions emerging from the tuned comparisons discussed in the present Section can be summarized as follows:

– The predictions for the Bhabha cross section of the most precise tools, i.e. BabaYaga@NLO, BHWIDE and MCGPJ, generally agree within 0.1%. If (slightly) larger differences are present they show up for particularly tight cuts or are due to limited MC statistics. When statistically meaningful discrepancies are observed they can be ascribed to the different theoretical recipes for the treatment of radiative corrections and their technical implementation. For example, as already emphasized, BabaYaga@NLO and BHWIDE adopt a fully factorized prescription for the matching of NLO and HO corrections, whereas MCGPJ implement some pieces

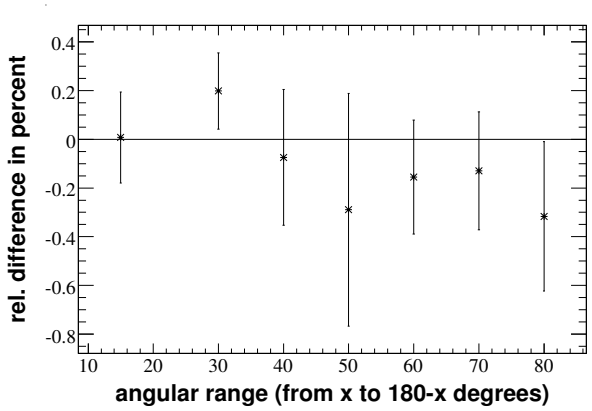

Fig. 25. Relative differences between BabaYaga@NLO and BHWIDE Bhabha cross sections as a function of the angular acceptance cut for the BaBar experiment at PEP-II. From [14].

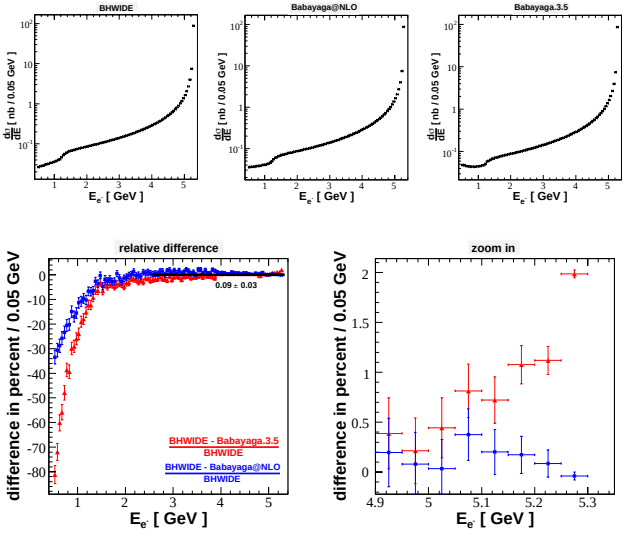

Fig. 26. Electron energy distributions according to BHWIDE, BabaYaga@NLO and BabaYaga v3.5 for the BaBar experiment at PEP-II and relative differences of the predictions of the programs. From [14].

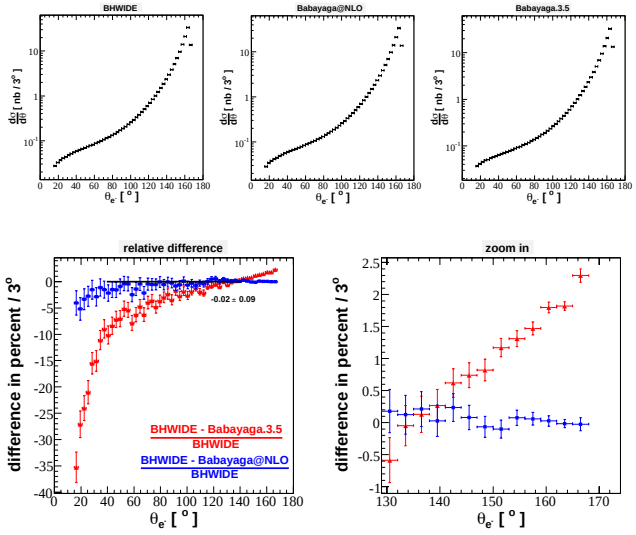

Fig. 27. Electron polar angle distributions according to BHWIDE, BabaYaga@NLO and BabaYaga v3.5 for the BaBar experiment at PEP-II and relative differences of the predictions of the programs. From [14].

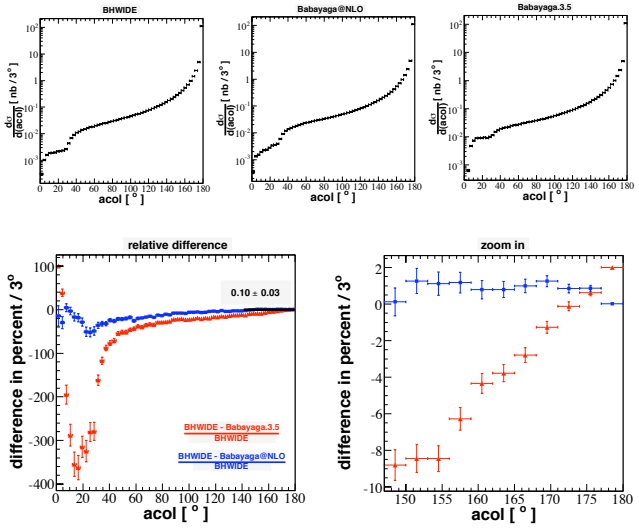

Fig. 28. Acollinearity distributions according to BHWIDE, BabaYaga@NLO and BabaYaga v3.5 for the BaBar experiment at PEP-II and relative differences of the predictions of the programs. From [14].

of the radiative corrections in additive form. This can give rise to discrepancies between the programs predictions especially in the presence of tight cuts enhancing the effect of soft radiation. Furthermore different choices are adopted in the generators for the scale entering the collinear logarithms in HO corrections beyond $\mathcal{O}(\alpha)$, that are another possible source of the observed differences. To go beyond the present situation a further non trivial effort should be done by comparing, for instance, the programs in the presence of NLO corrections only (technical test) and by analyzing their different treatment of the exponentiation of soft and collinear logarithms. This would certainly

shed light on the origin of the (small) discrepancies still registered at present.
– Also the distributions predicted by the generators agree well, with relative differences below the 1% level. Slightly larger discrepancies are only seen in sparsely populated phase space regions corresponding to very hard photon emission and which do not influence noticeably the luminosity measurement.

1.8 Theoretical accuracy

As discussed in Section 1.1, the total luminosity error crucially depends on the theoretical accuracy of the MC programs used by the experimentalists. As emphasized in Section 1.5, some of these generators like BHAGENF, BabaYaga v3.5 and BKQED miss theoretical ingredients which are unavoidable for cross section calculation with a precision at the per mille level. Therefore, they are inadequate for a highly accurate luminosity determination. BabaYaga@NLO, BHWIDE and MCGPJ include, however, both NLO and multiple photon corrections and their accuracy aims at a precision tag of 0.1%. But also these generators are affected by uncertainties which must be carefully considered in the light of the very stringent criteria of per mille accuracy. The most important components of the theoretical error of BabaYaga@NLO, BHWIDE and MCGPJ, mainly due to approximate or partially included pieces of radiative corrections, come from the following sources:

1. the non-perturbative light quark contribution to the running of α. It can be reliably evaluated only using the data of the hadron cross section at low energies. Hence, the vacuum polarization correction receives a data driven error which affects in turn the prediction of the Bhabha cross section, as emphasized in Section 4.
2. the complete set of $\mathcal{O}(\alpha^2)$ QED corrections. In spite of the impressive progress in this area, as reviewed in Section 1.3, an important piece of NNLO corrections, i.e. the exact NLO SV QED corrections to the single hard bremsstrahlung process $e^+e^- \to e^+e^-\gamma$, is still missing for the full $s+t$ Bhabha process [9]. However, partial results obtained for t-channel small-angle Bhabha scattering [229,11] and large-angle annihilation processes are available [230,231].
3. the $\mathcal{O}(\alpha^2)$ contribution due to real and virtual (lepton and hadron) pairs. The virtual contributions originate from the NNLO electron, heavy flavor and hadronic loop corrections discussed in Section 1.3, while the real corrections are due to the conversion of an external photon into pairs. The latter, as discussed in Section 1.3.3, gives rise to a final state with four particles, two of which to be considered as undetected to contribute to the Bhabha signature.

[9] As already remarked and further discussed in the following the complete calculation of the NLO corrections to hard photon emission in Bhabha scattering was performed during the completion of this report [65].

The uncertainty relative to the first point can be estimated by using the routines available in the literature for the calculation of the non-perturbative hadronic contribution $\Delta\alpha^{(5)}_{\rm hadr}(q^2)$ to the vacuum polarization. Actually these routines return, in addition to $\Delta\alpha^{(5)}_{\rm hadr}(q^2)$, an error $\delta_{\rm hadr}$ on its value. Therefore an estimate of the induced error can be simply obtained by computing the Bhabha cross section with $\Delta\alpha^{(5)}_{\rm hadr}(q^2) \pm \delta_{\rm hadr}$ and taking the difference as the theoretical uncertainty due to the hadronic contribution to vacuum polarization. In Tab. 9, the Bhabha cross sections, as obtained in the presence of the vacuum polarization correction according to the parameterizations of [224,225,226] (denoted as J) and of [129] (denoted as HMNT), respectively, are shown for Φ, τ-charm and B factories. The applied angular cuts refer to the typically adopted acceptance $55^\circ \le \theta_\pm \le 125^\circ$.

Table 9. Bhabha scattering cross section in the presence of the vacuum polarization correction, according to [224,225,226] (J) and [129] (HMNT), at meson factories. The notation $\rm J_-/HMNT_-$, J/HMNT and $\rm J_+/HMNT_+$ indicates minimum, central and maximum value of the two parametrizations.

Parametrization	Φ	τ-charm	B
$\rm J_-$	542.662(4)	46.9600(1)	5.85364(2)
J	542.662(4)	46.9658(1)	5.85529(2)
$\rm J_+$	542.662(4)	46.9715(1)	5.85693(2)
$\rm HMNT_-$	542.500(5)	46.9580(1)	5.85496(1)
HMNT	542.391(5)	46.9638(1)	5.85621(1)
$\rm HMNT_+$	542.283(5)	46.9697(1)	5.85746(2)

From Tab. 9 it can be seen that the two treatments of $\Delta\alpha^{(5)}_{\rm hadr}(q^2)$ induce effects on the Bhabha cross section in very good agreement, the relative differences between the central values being 0.05% (Φ-factories), 0.005% (τ-charm factories) and 0.02% (B-factories). This can be understood in terms of the dominance of t-channel exchange for large-angle Bhabha at meson factories. Indeed, the two routines provide results in excellent agreement for space-like momenta, as we explicitly checked, whereas different predictions show up for time-like momenta which, however, contribute to the Bhabha cross section only marginally. Also the spread between the minimum/maximum values and the central one as returned by the two routines agrees rather well, also a consequence of the dominance of t-channel exchange. This spread amounts to a few units in 10^{-4} and is presented in detail in Tab. 10 in the next Section.

Concerning the second point a general strategy to evaluate the size of missing NNLO corrections consists in deriving a cross section expansion up to $\mathcal{O}(\alpha^2)$ from the theoretical formulation implemented in the generator of interest. It can be cast in general into the following form

$$\sigma^{\alpha^2} = \sigma^{\alpha^2}_{\rm SV} + \sigma^{\alpha^2}_{\rm SV,H} + \sigma^{\alpha^2}_{\rm HH}, \qquad (81)$$

where in principle each of the $\mathcal{O}(\alpha^2)$ contributions is affected by an uncertainty to be properly estimated. In Eq.

(81) the first contribution is the cross section including $\mathcal{O}(\alpha^2)$ SV corrections, whose uncertainty can be evaluated through a comparison with some of the available NNLO calculations reviewed in Section 1.3. In particular, in [200] the $\sigma^{\alpha^2}_{\rm SV}$ of the BabaYaga@NLO generator was compared with the calculation of photonic corrections by Penin [99, 100] and the calculations by Bonciani *et al.* [104,105,115, 116,117] who computed two-loop fermionic corrections (in the one-family approximation $N_F = 1$) with finite mass terms and the addition of soft bremsstrahlung and real pair contributions [10]. The results of such comparisons are shown in Fig. 29 and Fig. 30 for realistic cuts at the Φ-factories. In Fig. 29 $\delta\sigma$ is the difference between $\sigma^{\alpha^2}_{\rm SV}$ of BabaYaga@NLO and the cross sections of the two $\mathcal{O}(\alpha^2)$ calculations, denoted as photonic (Penin) and $N_F = 1$ (Bonciani *et al.*), as a function of the logarithm of the infrared regulator ϵ. It can be seen that the differences are given by flat functions, demonstrating that such differences are infrared-safe, as expected, as a consequence of the universality and factorization properties of the infrared divergences. In Fig. 30, $\delta\sigma$ is shown as a function of the logarithm of a fictitious electron mass and for a fixed value of $\epsilon = 10^{-5}$. Since the difference with the calculation by Penin is given by a straight line, this indicates that the soft plus virtual two-loop photonic corrections missing in BabaYaga@NLO are $\mathcal{O}(\alpha^2 L)$ contributions, as already remarked. On the other hand, the difference with the calculation by Bonciani *et al.* is fitted by a quadratic function, showing that the electron two-loop effects missing in BabaYaga@NLO are of the order of $\alpha^2 L^2$. However, it is important to emphasize that, as shown in detail in [200], the sum of the relative differences with the two $\mathcal{O}(\alpha^2)$ calculations does not exceed the 2×10^{-4} level for experiments at Φ- and B-factories.

The second term in Eq. (81) is the cross section containing the one-loop corrections to single hard photon emission and its uncertainty can be estimated by relying on partial results existing in the literature. Actually the exact perturbative expression of $\sigma^{\alpha^2}_{\rm SV,H}$ is not yet available for full $s+t$ Bhabha scattering but using the results valid for small-angle Bhabha scattering [229,11] and large-angle annihilation processes [230,231] the relative uncertainty of the theoretical tools in the calculation of $\sigma^{\alpha^2}_{\rm SV,H}$ can be conservatively estimated at the level of 0.05%. Indeed the papers [229,11,230,231] show that a YFS matching of NLO and HO corrections gives SV one-loop results for the t-channel process $e^+e^- \to e^+e^-\gamma$ and s-channel annihilation $e^+e^- \to f\bar{f}\gamma$ (f = fermion) differing from the exact perturbative calculations by a few units in 10^{-4} at most. This conclusion holds also when photon energy cuts are varied. It is worth noting that during the completion of the present work a complete calculation of the NLO QED

[10] To provide meaningful results the contribution of the vacuum polarization was switched off in BabaYaga@NLO to compare with the calculation by Penin consistently. For the same reason the real soft and some pieces of virtual electron pair corrections were neglected in the comparison with the calculation by Bonciani *et al.*.

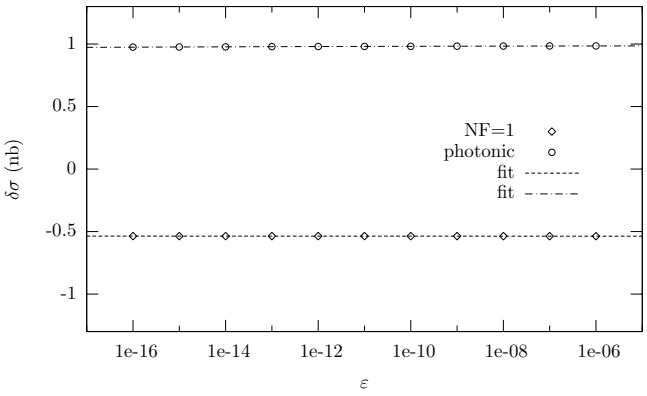

Fig. 29. Absolute differences (in nb) between the $\sigma^{\alpha^2}_{\rm SV}$ prediction of BabaYaga@NLO and the NNLO calculations of the photonic corrections [99,100] (photonic) and of the electron loop corrections [104,105,115,116,117] ($N_F = 1$) as a function of the infrared regulator ϵ for typical KLOE cuts. From [200].

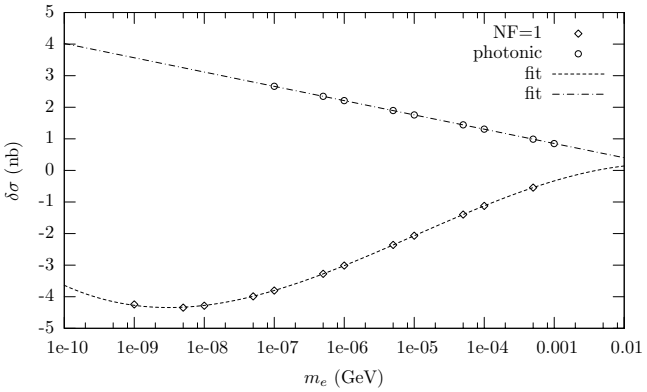

Fig. 30. Absolute differences (in nb) between the $\sigma^{\alpha^2}_{\rm SV}$ prediction of BabaYaga@NLO and the NNLO calculations of the photonic corrections [99,100] (photonic) and of the electron loop corrections [104,105,115,116,117] ($N_F = 1$) as a function of a fictitious electron mass for typical KLOE cuts. From [200].

corrections to hard bremsstrahlung emission in full $s+t$ Bhabha scattering appeared in the literature [65], along the lines described in Section 1.3.2. Explicit comparisons between the results of such an exact calculation with the predictions of the most accurate MC tools according to the typical luminosity cuts used at meson factories would be worthwhile to make the present error estimate related to the calculation of $\sigma^{\alpha^2}_{\rm SV,H}$ more robust.

The third contribution in Eq. (81) is the double hard bremsstrahlung cross section whose uncertainty can be directly evaluated by explicit comparison with the exact $e^+e^- \to e^+e^-\gamma\gamma$ cross section. In [200] was shown that the differences between $\sigma^{\alpha^2}_{\rm HH}$ as in BabaYaga@NLO and the matrix element calculation which exactly describes the contribution of two hard photons are really negligible, being at the 10^{-5} level.

The relative effect due to lepton (e, μ, τ) and hadron (π) pairs has been numerically analyzed in Section 1.3.3,

in the presence of realistic selection cuts. This evaluation makes use of the complete NNLO virtual corrections combined with an exact matrix element calculation of the four-particle production processes. It supersedes previous approximate estimates which underestimated the impact of those corrections. According to this new evaluation, the pair contribution dominated by the electron pair correction amounts to about 0.3% for KLOE and 0.1% for BaBar. These contributions are partially included in the BabaYaga@NLO code, as well as in other generators, through the insertion of the vacuum polarization correction in the NLO diagrams and detailed comparisons between the exact calculation and the BabaYaga@NLO predictions are in progress [232].

1.9 Conclusions and open issues

During the last few years a remarkable progress occurred in reducing the error of the luminosity measurements at flavour factories.

Dedicated event generators like BabaYaga@NLO and MCGPJ were developed in 2006 to provide predictions for the cross section of the large-angle Bhabha process, as well as for other QED reactions of interest, with a theoretical accuracy at the level of 0.1%. In parallel codes well-known since the time of LEP/SLC operation such as BHWIDE were extensively used by the experimentalists in data analyses. These MC programs all include, albeit according to different formulations, exact $\mathcal{O}(\alpha)$ QED corrections matched with LL contributions describing multiple photon emission. Such ingredients together with the vacuum polarization correction are strictly necessary to achieve a physical precision down to the per mille level. Indeed when considering typical selection cuts the NLO photonic corrections amount to about $15\div20\%$, the vacuum polarization contributes at the several per cent level and HO effects lie between $1\div2\%$.

The generators mentioned are, however, affected by an uncertainty due to HO effects neglected in their formulation such as light pair corrections or exact perturbative contributions present in NNLO calculations. From this point of view the great progress in the calculation of two-loop corrections to the Bhabha scattering cross section was essential to establish the theoretical accuracy of the existing generators and will be crucial if an improvement of the precision below the one per mille will be required.

A particular effort was done to compare the predictions of the generators consistently in order to assess the technical precision obtained by the implementation of radiative corrections and related computational details. These comparisons were performed in the presence of realistic event selection criteria and at different c.m. energies. For the KLOE and CMD-2 experiments around the Φ-resonance, where the statistics of Bhabha events is the highest and the experimental luminosity error at a few per mille level, the cross section results of BabaYaga@NLO, BHWIDE and MCGPJ agree within $\sim 0.1\%$. If (slightly) larger discrepancies are observed, they show up only for particularly tight cuts or exclusive distributions in specific phase space regions which do not influence the luminosity determination. Very similar results were obtained for τ-charm and B-factories. The main conclusion of the work on tuned comparisons is that the technical precision of MC programs is well under control, the discrepancies being due to different details in the treatment of the same sources of radiative corrections and their technical implementation. For example, BabaYaga@NLO and BHWIDE adopt a fully factorized prescription for the matching of NLO and HO corrections, whereas MCGPJ implement some radiative corrections pieces in additive form. This can give rise to some discrepancies between their predictions especially in the presence of tight cuts enhancing the effect of soft radiation. Furthermore different choices are adopted in the generators for the energy scale in the treatment of HO corrections beyond $\mathcal{O}(\alpha)$, that are another possible source of the observed differences. To go beyond the present situation a further, non trivial effort should be done by comparing, for instance, the programs in the presence of NLO corrections only (technical test) and for the specific effect due to the exponentiation of soft and collinear logarithms. This would certainly shed light on the origin of the (minor) discrepancies still registered at present.

On the theoretical side a new exact evaluation of lepton and hadron pair corrections to the Bhabha scattering cross section was carried out taking into account realistic cuts. This calculation provides results in substantial agreement with estimates based on singlet SF but supersedes previous evaluations in the soft-photon approximation. The results of the new exact calculation were preliminarily compared with the predictions of BabaYaga@NLO, that includes the bulk of such correction (due to reducible contributions) through the insertion of the vacuum polarization correction in the NLO diagrams but neglects the effect of real pair radiation and two-loop form factors. It turns out that the error induced by the approximate treatment of pair corrections amount to a few units in 10^{-4} both at KLOE and BaBar. Further work is in progress to arrive at a more solid and quantitative error estimate for these corrections when considering other selection criteria and c.m. energies too [232]. Also, the contribution induced by the uncertainty related to the non-perturbative contribution to the running of α was revisited making use of and comparing the two independent parameterizations derived in [224,225,226] and [129].

A summary of the different sources of theoretical error and their relative impact on the Bhabha cross section is given in Tab. 10. In Tab. 10, $|\delta^{\rm err}_{\rm VP}|$ is the error induced by the hadronic component of the vacuum polarization, $|\delta^{\rm err}_{\rm pairs}|$ the error due to missing pair corrections, $|\delta^{\rm err}_{\rm SV}|$ the uncertainty coming from SV NNLO corrections, $|\delta^{\rm err}_{\rm HH}|$ the uncertainty in the calculation of the double hard bremsstrahlung process and $|\delta^{\rm err}_{\rm SV,H}|$ the error estimate for one-loop corrections to single hard bremsstrahlung. As it can be seen pair corrections and exact NLO corrections to $e^+e^- \to e^+e^-\gamma$ are the dominant sources of error.

The total theoretical uncertainty as obtained by summing the different contributions linearly is $0.12\div0.14\%$

Table 10. Summary of different sources of theoretical uncertainty for the most precise generators used for luminosity measurements and the corresponding total theoretical errors for the calculation of the large-angle Bhabha cross section at meson factories.

Source of error (%)	Φ	τ-charm	B
$\lvert\delta^{\rm err}_{\rm VP}\rvert$ [224,225,226]	0.00	0.01	0.03
$\lvert\delta^{\rm err}_{\rm VP}\rvert$ [129]	0.02	0.01	0.02
$\lvert\delta^{\rm err}_{\rm SV}\rvert$	0.02	0.02	0.02
$\lvert\delta^{\rm err}_{\rm HH}\rvert$	0.00	0.00	0.00
$\lvert\delta^{\rm err}_{\rm SV,H}\rvert$	0.05	0.05	0.05
$\lvert\delta^{\rm err}_{\rm pairs}\rvert$	0.05	0.1	0.02
$\lvert\delta^{\rm err}_{\rm total}\rvert$	0.12÷0.14	0.18	0.11÷0.12

at the Φ factories, 0.18% at the τ-charm factories and $0.11 \div 0.12$% at the B factories. The slightly larger uncertainty at the τ-charm factories is mainly due, as can be seen, to the pair contribution error presently based on a very preliminary evaluation and for which a deeper analysis is ongoing [232]. The total uncertainty is slightly affected by the particular choice of the routine for the calculation of $\Delta\alpha^{(5)}_{\rm hadr}(q^2)$, since the two parameterizations considered here give rise to similar errors, with the exception of the Φ-factories for which the two recipes return uncertainties differing by 2×10^{-4}. However the "parametric" error induced by the hadronic contribution to the vacuum polarization may become a relevant source of uncertainty when considering predictions for a c.m. energy on top of and closely around very narrow resonances. For such a specific situation of interest for instance for the BES experiment, the appropriate treatment of α running in the calculation of the Bhabha cross section should be deeper scrutinized because of the differences observed between the predictions for $\Delta\alpha^{(5)}_{\rm hadr}(q^2)$ obtained by means of the available parameterization routines (see Section 4 for a more detailed discussion).

Albeit the theoretical uncertainty quoted in Tab. 10 could be put on firmer grounds thanks to further studies in progress, it appears to be quite robust and sufficient for present and planned precision luminosity measurements at meson factories, the experimental error currently being about a factor of two or three larger. Adopting the strategy followed during LEP/SLC operation one could arrive at a more aggressive error estimate by summing the relative contributions in quadrature. However, for the time being this does not seem to be necessary in the light of the current experimental errors.

Concluding the precision presently reached by large-angle Bhabha programs used in the luminosity measurement at meson factories is comparable with that achieved about ten years ago for luminosity monitoring through small-angle Bhabha scattering at LEP/SLC.

Some issues are still left open. In the context of tuned comparisons no effort was done to compare the available codes for the process of photon pair production. Since it contributes relevantly to the luminosity determination and precise predictions for its cross section can be obtained by means of the codes BabaYaga@NLO and MCGPJ this work should be definitely carried out. This would lead to a better understanding of the luminosity on the experimental side. In the framework of new theoretical advances an evaluation of NNLO contributions to the process $e^+e^- \to \gamma\gamma$ would be worthwhile to better assess the precision of the generators which do not include for the time being such corrections exactly. More important the exact one-loop corrections to the radiative process $e^+e^- \to e^+e^-\gamma$ should be calculated going beyond the partial results scattered in the literature (and referring to selection criteria valid for high-energy e^+e^- colliders) or limited to the soft-photon approximation [11]. Furthermore the radiative Bhabha process at one-loop should be evaluated taking into account the typical experimental cuts used at meson factories to get a better control of the theoretical uncertainty in the sector of NNLO corrections to Bhabha scattering. Incidentally this calculation would be also of interest for other studies at e^+e^- colliders of moderately high energy, such as the search for new physics phenomena (e.g., dark matter candidates), for which radiative Bhabha scattering is a very important background.

Acknowledgments
A.A., C.M.C.C., G.F., G.M., O.N., F.P., L.T., E.R. and A.S. acknowledge partial supported by the INTAS project Nr 05-1000008-8328 "Higher-order effects in e^+e^- annihilation and muon anomalous magnetic moment". The work of J.G., T.R. and M.W. was supported in part by Sonderforschungsbereich/Transregio SFB/TRR 9 of DFG and by the European Community's Marie-Curie Research Training Networks MRTN-CT-2006-035505 "HEPTOOLS" and MRTN-CT-2006-035482 "FLAVIAnet". M.W. was also funded by the Initiative and Networking Fund of the Helmholtz Association, contract HA-101 ("Physics at the Terascale"). M.C. was funded by the Heisenberg Programme of the Deutsche Forschungsgemeinschaft. The work of B.F.L.W. was supported in part by the US DOE contract DE-FG02-09ER41600, and by the EU Marie Curie Research Training Network grant under the contract No. MRTN-CT-2006-035505. We thank J. Libby for useful correspondence about the luminosity measurement at CLEO-c. We are grateful to T. Teubner for providing us with the routine for the evaluation of the hadronic contribution to vacuum polarization according to the HMNT parameterization.

2 Scan

scan

[11] As already remarked in Section 1.8 during the completion of the present work a complete calculation of the NLO QED corrections to hard bremsstrahlung emission in full s+t Bhabha scattering was performed in [65]. However, explicit comparisons between the predictions of this new calculation and the corresponding results of the most precise luminosity tools are still missing and would be needed to better assess the theoretical error induced by such contribution in the calculation of the luminosity cross section.

3 Radiative return

radiative return

4 Vacuum polarization

vacuum polarization

5 Tau physics

tau physics

6 Summary

References

1. KLOE Collaboration, F. Ambrosino et al., Eur. Phys. J. C47 (2006) 589–596, hep-ex/0604048.
2. N. Cabibbo and R. Gatto, Phys. Rev. 124 (1961) 1577–1595.
3. H. Bhabha, Proc. Roy. Soc. A154 (1936) 195.
4. G. Barbiellini et al., Nucl. Instrum. Meth. 123 (1975) 125.
5. H. C. Dehne, M. A. Preger, S. Tazzari, and G. Vignola, Nucl. Instrum. Meth. 116 (1974) 345–359.
6. S. Jadach et al., hep-ph/9602393.
7. A. B. Arbuzov et al., Nucl. Phys. B485 (1997) 457–502, hep-ph/9512344.
8. G. Montagna, O. Nicrosini, and F. Piccinini, Phys. Lett. B385 (1996) 348–356, hep-ph/9605252.
9. A. Arbuzov et al., Phys. Lett. B383 (1996) 238–242, hep-ph/9605239.
10. G. Montagna, O. Nicrosini, and F. Piccinini, Riv. Nuovo Cim. 21N9 (1998) 1–162, hep-ph/9802302.
11. B. F. L. Ward, S. Jadach, M. Melles, and S. A. Yost, Phys. Lett. B450 (1999) 262–266, hep-ph/9811245.
12. S. Jadach, hep-ph/0306083.
13. CLEO Collaboration, S. Dobbs et al., Phys. Rev. D76 (2007) 112001, 0709.3783.
14. A. Hafner, Diploma thesis, University of Karlsruhe, 2007.
15. D. M. Asner et al., 0809.1869.
16. L. M. Brown and R. P. Feynman, Phys. Rev. 85 (1952) 231.
17. F. Redhead, Proc. Roy. Soc. 220 (1953) 219.
18. R. Polovin, JETP 31 (1956) 449.
19. M. Consoli, Nucl. Phys. B160 (1979) 208.
20. M. Böhm, A. Denner, W. Hollik, and R. Sommer, Phys. Lett. B144 (1984) 414.
21. D. Bardin, W. Hollik, and T. Riemann, Z. Phys. C49 (1991) 485–490.
22. D. Bardin, P. Christova, M. Jack, L. Kalinovskaya, A. Olchevski, S. Riemann, and T. Riemann, Comput. Phys. Commun. 133 (2001) 229–395, hep-ph/9908433.
23. A. Arbuzov, M. Awramik, M. Czakon, A. Freitas, M. Grünewald, K. Mönig, S. Riemann, and T. Riemann, Comput. Phys. Commun. 174 (2006) 728–758, hep-ph/0507146.
24. G. Montagna, F. Piccinini, O. Nicrosini, G. Passarino, and R. Pittau, Nucl. Phys. B401 (1993) 3–66.
25. G. Montagna, F. Piccinini, O. Nicrosini, G. Passarino, and R. Pittau, Comput. Phys. Commun. 76 (1993) 328–360.
26. G. Montagna, O. Nicrosini, F. Piccinini, and G. Passarino, Comput. Phys. Commun. 117 (1999) 278–289, hep-ph/9804211.
27. A. Djouadi and C. Verzegnassi, Phys. Lett. B195 (1987) 265.
28. A. Djouadi, Nuovo Cim. A100 (1988) 357.
29. B. A. Kniehl, J. H. Kuhn, and R. G. Stuart, Phys. Lett. B214 (1988) 621.
30. J. J. van der Bij and F. Hoogeveen, Nucl. Phys. B283 (1987) 477.
31. R. Barbieri, M. Beccaria, P. Ciafaloni, G. Curci, and A. Vicere, Nucl. Phys. B409 (1993) 105–127.
32. J. Fleischer, O. V. Tarasov, and F. Jegerlehner, Phys. Lett. B319 (1993) 249–256.
33. J. Fleischer, O. V. Tarasov, and F. Jegerlehner, Phys. Rev. D51 (1995) 3820–3837.
34. R. Boughezal and M. Czakon, Nucl. Phys. B755 (2006) 221–238, hep-ph/0606232.
35. K. G. Chetyrkin, M. Faisst, J. H. Kuhn, P. Maierhofer, and C. Sturm, Phys. Rev. Lett. 97 (2006) 102003, hep-ph/0605201.
36. Y. Schroder and M. Steinhauser, Phys. Lett. B622 (2005) 124–130, hep-ph/0504055.
37. K. G. Chetyrkin, J. H. Kuhn, and M. Steinhauser, Phys. Lett. B351 (1995) 331–338, hep-ph/9502291.
38. K. G. Chetyrkin, J. H. Kuhn, and M. Steinhauser, Phys. Rev. Lett. 75 (1995) 3394–3397, hep-ph/9504413.
39. R. Barbieri, M. Beccaria, P. Ciafaloni, G. Curci, and A. Vicere, Phys. Lett. B288 (1992) 95–98, hep-ph/9205238.
40. J. J. van der Bij, K. G. Chetyrkin, M. Faisst, G. Jikia, and T. Seidensticker, Phys. Lett. B498 (2001) 156–162, hep-ph/0011373.
41. M. Faisst, J. H. Kuhn, T. Seidensticker, and O. Veretin, Nucl. Phys. B665 (2003) 649–662, hep-ph/0302275.
42. R. Boughezal, J. B. Tausk, and J. J. van der Bij, Nucl. Phys. B713 (2005) 278–290, hep-ph/0410216.
43. R. Boughezal, J. B. Tausk, and J. J. van der Bij, Nucl. Phys. B725 (2005) 3–14, hep-ph/0504092.
44. M. Awramik, M. Czakon, A. Freitas, and G. Weiglein, Phys. Rev. D69 (2004) 053006, hep-ph/0311148.
45. M. Awramik, M. Czakon, A. Freitas, and G. Weiglein, Phys. Rev. Lett. 93 (2004) 201805, hep-ph/0407317.
46. W. Hollik, U. Meier, and S. Uccirati, Nucl. Phys. B731 (2005) 213–224, hep-ph/0507158.
47. W. Hollik, U. Meier, and S. Uccirati, Nucl. Phys. B765 (2007) 154–165, hep-ph/0610312.
48. M. Awramik, M. Czakon, and A. Freitas, JHEP 11 (2006) 048, hep-ph/0608099.
49. M. Awramik, M. Czakon, and A. Freitas, Phys. Lett. B642 (2006) 563–566, hep-ph/0605339.
50. J. H. Kuhn, A. A. Penin, and V. A. Smirnov, Eur. Phys. J. C17 (2000) 97–105, hep-ph/9912503.
51. J. H. Kuhn, A. A. Penin, and V. A. Smirnov, Nucl. Phys. Proc. Suppl. 89 (2000) 94–99, hep-ph/0005301.
52. J. H. Kuhn, S. Moch, A. A. Penin, and V. A. Smirnov, Nucl. Phys. B616 (2001) 286–306, hep-ph/0106298.

53. B. Feucht, J. H. Kuhn, A. A. Penin, and V. A. Smirnov, Phys. Rev. Lett. 93 (2004) 101802, hep-ph/0404082.
54. B. Jantzen, J. H. Kuhn, A. A. Penin, and V. A. Smirnov, Phys. Rev. D72 (2005) 051301, hep-ph/0504111.
55. B. Jantzen, J. H. Kuhn, A. A. Penin, and V. A. Smirnov, Nucl. Phys. B731 (2005) 188–212, hep-ph/0509157.
56. A. Denner, B. Jantzen, and S. Pozzorini, Nucl. Phys. B761 (2007) 1–62, hep-ph/0608326.
57. A. Denner, B. Jantzen, and S. Pozzorini, 0801.2647.
58. F. Berends, K. Gaemers, and R. Gastmans, Nucl. Phys. B68 (1974) 541.
59. W. Beenakker, F. Berends, and S. van der Marck, Nucl. Phys. B349 (1991) 323.
60. M. Terentyev, Yad. Fiz. 9 (1969) 1212.
61. F. Berends and R. Gastmans, Nucl. Phys. B61 (1973) 414.
62. S. Eidelman and E. Kuraev, Nucl. Phys. B143 (1978) 353.
63. F. Berends, R. Kleiss, P. De Causmaecker, R. Gastmans, W. Troost, and T. Wu, Nucl. Phys. B206 (1982) 61.
64. M. Bohm and Z. Sack, Z. Phys. C33 (1986) 157.
65. S. Actis, P. Mastrolia, and G. Ossola, 0909.1750.
66. A. B. Arbuzov, E. A. Kuraev, N. P. Merenkov, and L. Trentadue, Phys. Atom. Nucl. 60 (1997) 591–600.
67. A. B. Arbuzov, E. A. Kuraev, N. P. Merenkov, and L. Trentadue, J. Exp. Theor. Phys. 81 (1995) 638–646, hep-ph/9509405.
68. A. B. Arbuzov, E. A. Kuraev, N. P. Merenkov, and L. Trentadue, Nucl. Phys. B474 (1996) 271–285.
69. S. Laporta and E. Remiddi, Phys. Lett. B379 (1996) 283–291, hep-ph/9602417.
70. S. Laporta, Int. J. Mod. Phys. A15 (2000) 5087–5159, hep-ph/0102033.
71. F. V. Tkachov, Phys. Lett. B100 (1981) 65–68.
72. K. Chetyrkin and F. Tkachov, Nucl. Phys. B192 (1981) 159–204.
73. A. V. Kotikov, Phys. Lett. B254 (1991) 158–164, note.
74. A. Kotikov, Phys. Lett. B259 (1991) 314–322.
75. A. V. Kotikov, Phys. Lett. B267 (1991) 123–127.
76. E. Remiddi, Nuovo Cim. A110 (1997) 1435–1452, hep-th/9711188.
77. M. Caffo, H. Czyz, S. Laporta, and E. Remiddi, Acta Phys. Polon. B29 (1998) 2627–2635, http://arXiv.org/abs/hep-th/9807119.
78. M. Caffo, H. Czyz, S. Laporta, and E. Remiddi, Nuovo Cim. A111 (1998) 365–389, http://arXiv.org/abs/hep-th/9805118.
79. M. Argeri and P. Mastrolia, Int. J. Mod. Phys. A22 (2007) 4375–4436, 0707.4037.
80. V. Smirnov, "Evaluating Feynman Integrals" (Springer Verlag, Berlin, 2004).
81. S. Friot, D. Greynat, and E. De Rafael, Phys. Lett. B628 (2005) 73–84, hep-ph/0505038.
82. N. Usyukina, Teor. Mat. Fiz. 22 (1975) 300–306 (in Russian).
83. V. Smirnov, Phys. Lett. B460 (1999) 397–404, hep-ph/9905323.
84. B. Tausk, Phys. Lett. B469 (1999) 225–234, hep-ph/9909506.
85. V. Smirnov and O. Veretin, Nucl. Phys. B566 (2000) 469–485, hep-ph/9907385.
86. V. A. Smirnov, Phys. Lett. B524 (2002) 129–136, hep-ph/0111160.
87. G. Heinrich and V. A. Smirnov, Phys. Lett. B598 (2004) 55–66, hep-ph/0406053.
88. M. Czakon, Comput. Phys. Commun. 175 (2006) 559–571, hep-ph/0511200.
89. J. Gluza, K. Kajda, and T. Riemann, Comput. Phys. Commun. 177 (2007) 879–893, arXiv:0704.2423.
90. A. Goncharov, Math. Res. Letters 5 (1998) 497.
91. D. J. Broadhurst, Eur. Phys. J. C8 (1999) 311–333, hep-th/9803091.
92. E. Remiddi and J. Vermaseren, Int. J. Mod. Phys. A15 (2000) 725–754, hep-ph/9905237.
93. T. Gehrmann and E. Remiddi, Comput. Phys. Commun. 141 (2001) 296–312, http://arXiv.org/abs/hep-ph/0107173.
94. T. Gehrmann and E. Remiddi, Comput. Phys. Commun. 144 (2002) 200–223, hep-ph/0111255.
95. D. Maitre, Comput. Phys. Commun. 174 (2006) 222–240, hep-ph/0507152.
96. D. Maitre, hep-ph/0703052.
97. J. Vollinga and S. Weinzierl, Comput. Phys. Commun. 167 (2005) 177, hep-ph/0410259.
98. S. Weinzierl, 0705.0900.
99. A. A. Penin, Phys. Rev. Lett. 95 (2005) 010408, hep-ph/0501120.
100. A. A. Penin, Nucl. Phys. B734 (2006) 185–202, hep-ph/0508127.
101. A. Mitov and S. Moch, JHEP 05 (2007) 001, hep-ph/0612149.
102. T. Becher and K. Melnikov, JHEP 06 (2007) 084, arXiv:0704.3582 [hep-ph].
103. Z. Bern, L. Dixon, and A. Ghinculov, Phys. Rev. D63 (2001) 053007, hep-ph/0010075.
104. R. Bonciani and A. Ferroglia, Phys. Rev. D72 (2005) 056004, hep-ph/0507047.
105. R. Bonciani, P. Mastrolia, and E. Remiddi, Nucl. Phys. B661 (2003) 289–343, hep-ph/0301170.
106. R. Bonciani, P. Mastrolia, and E. Remiddi, Nucl. Phys. B690 (2004) 138–176, hep-ph/0311145.
107. R. Bonciani, P. Mastrolia, and E. Remiddi, Nucl. Phys. B676 (2004) 399–452, hep-ph/0307295.
108. M. Czakon, J. Gluza, and T. Riemann, Phys. Rev. D71 (2005) 073009, hep-ph/0412164.
109. M. Czakon, J. Gluza, and T. Riemann, Nucl. Phys. B751 (2006) 1–17, hep-ph/0604101.
110. D. J. Broadhurst, J. Fleischer, and O. V. Tarasov, Z. Phys. C60 (1993) 287–302, hep-ph/9304303.
111. A. I. Davydychev and M. Y. Kalmykov, Nucl. Phys. B699 (2004) 3–64, hep-th/0303162.
112. A. B. Arbuzov, E. A. Kuraev, and B. G. Shaikhatdenov, Mod. Phys. Lett. A13 (1998) 2305–2316, hep-ph/9806215.
113. E. W. N. Glover, J. B. Tausk, and J. J. Van der Bij, Phys. Lett. B516 (2001) 33–38, hep-ph/0106052.
114. G. J. H. Burgers, Phys. Lett. B164 (1985) 167.
115. R. Bonciani, A. Ferroglia, P. Mastrolia, E. Remiddi, and J. van der Bij, Nucl. Phys. B681 (2004) 261–291, hep-ph/0310333.
116. R. Bonciani, A. Ferroglia, P. Mastrolia, E. Remiddi, and J. van der Bij, Nucl. Phys. B701 (2004) 121–179, hep-ph/0405275.
117. R. Bonciani, A. Ferroglia, P. Mastrolia, E. Remiddi, and J. J. van der Bij, Nucl. Phys. B716 (2005) 280–302, hep-ph/0411321.

118. S. Actis, M. Czakon, J. Gluza, and T. Riemann, Nucl. Phys. B786 (2007) 26–51, arXiv:0704.2400v.2 [hep-ph].
119. R. Bonciani, A. Ferroglia, and A. A. Penin, Phys. Rev. Lett. 100 (2008) 131601, 0710.4775.
120. R. Bonciani, A. Ferroglia, and A. A. Penin, JHEP 02 (2008) 080, arXiv:0802.2215.
121. S. Actis, M. Czakon, J. Gluza, and T. Riemann, Phys. Rev. Lett. 100 (2008) 131602, arXiv:0711.3847.
122. S. Actis, M. Czakon, J. Gluza, and T. Riemann, Phys. Rev. D78 (2008) 085019, arXiv:0807.4691.
123. J. Frenkel and J. C. Taylor, Nucl. Phys. B116 (1976) 185.
124. J. Fleischer, A. V. Kotikov, and O. L. Veretin, Nucl. Phys. B547 (1999) 343–374, hep-ph/9808242.
125. U. Aglietti and R. Bonciani, Nucl. Phys. B668 (2003) 3–76, hep-ph/0304028.
126. U. Aglietti and R. Bonciani, Nucl. Phys. B698 (2004) 277–318, hep-ph/0401193.
127. R. E. Cutkosky, J. Math. Phys. 1 (1960) 429–433.
128. M. Davier, S. Eidelman, A. Höcker, and Z. Zhang, Eur. Phys. J. C27 (2003) 497–521, hep-ph/0208177.
129. Private communications with T. Teubner. The Fortran program rintpl.F is based on the data compilation performed for [233,234]. The publication is in preparation. The routine is available upon request from the authors, E-mails: dnomura@post.kek.jp, thomas.teubner@liverpool.ac.uk.
130. R. V. Harlander and M. Steinhauser, Comput. Phys. Commun. 153 (2003) 244–274, hep-ph/0212294.
131. F. Berends and G. Komen, Phys. Lett. B63 (1976) 432.
132. B. Kniehl, M. Krawczyk, J. Kühn, and R. Stuart, Phys. Lett. B209 (1988) 337.
133. T. van Ritbergen and R. G. Stuart, Phys. Lett. B437 (1998) 201–208, hep-ph/9802341.
134. R. Barbieri, J. A. Mignaco, and E. Remiddi, Nuovo Cim. A11 (1972) 824–864.
135. R. Barbieri, J. A. Mignaco, and E. Remiddi, Nuovo Cim. A11 (1972) 865–916.
136. P. Mastrolia and E. Remiddi, Nucl. Phys. B664 (2003) 341–356, hep-ph/0302162.
137. S. Actis, M. Czakon, J. Gluza, and T. Riemann, Acta Phys. Polon. B38 (2007) 3517–3528, arXiv:0710.5111.
138. J. H. Kühn and S. Uccirati, Nucl. Phys. B806 (2009) 300–326, arXiv:0807.1284.
139. DESY Zeuthen webpage bhabha.html.
140. H. Burkhardt, TASSO-NOTE-192 (1981), and Fortran program repi.f (1986).
141. G. Passarino and M. Veltman, Nucl. Phys. B160 (1979) 151.
142. Z. Bern, L. J. Dixon, and D. A. Kosower, Ann. Rev. Nucl. Part. Sci. 46 (1996) 109–148, hep-ph/9602280.
143. L. J. Dixon, hep-ph/9601359.
144. T. Binoth, J. P. Guillet, and G. Heinrich, Nucl. Phys. B572 (2000) 361–386, hep-ph/9911342.
145. A. Denner and S. Dittmaier, Nucl. Phys. B658 (2003) 175–202, hep-ph/0212259.
146. T. Binoth, J. P. Guillet, G. Heinrich, E. Pilon, and C. Schubert, JHEP 10 (2005) 015, hep-ph/0504267.
147. A. Denner and S. Dittmaier, Nucl. Phys. B734 (2006) 62–115, hep-ph/0509141.
148. A. Denner and S. Dittmaier, Nucl. Phys. Proc. Suppl. 157 (2006) 53–57, hep-ph/0601085.
149. A. Davydychev, Phys. Lett. B263 (1991) 107–111.
150. O. V. Tarasov, Phys. Rev. D54 (1996) 6479–6490, http://arXiv.org/abs/hep-th/9606018.
151. J. Fleischer, F. Jegerlehner, and O. Tarasov, Nucl. Phys. B566 (2000) 423–440, http://arXiv.org/abs/hep-ph/9907327.
152. D. B. Melrose, Nuovo Cim. 40 (1965) 181–213.
153. T. Diakonidis, J. Fleischer, J. Gluza, K. Kajda, T. Riemann, and J. Tausk, arXiv:0807.2984.
154. T. Diakonidis, J. Fleischer, J. Gluza, K. Kajda, T. Riemann, and J. Tausk, 0812.2134.
155. Z. Bern, L. J. Dixon, and D. A. Kosower, Annals Phys. 322 (2007) 1587–1634, 0704.2798.
156. L. D. Landau, Nucl. Phys. 13 (1959) 181–192.
157. S. Mandelstam, Phys. Rev. 112 (1958) 1344–1360.
158. S. Mandelstam, Phys. Rev. 115 (1959) 1741–1751.
159. R. J. Eden, P. V. Landshoff, D. I. Olive, and J. C. Polkinghorne, Cambridge University Press (1966).
160. G. 't Hooft and M. Veltman, Nucl. Phys. B153 (1979) 365–401.
161. Z. Bern, L. J. Dixon, and D. A. Kosower, Phys. Lett. B302 (1993) 299–308, hep-ph/9212308.
162. Z. Bern, L. J. Dixon, and D. A. Kosower, Nucl. Phys. B412 (1994) 751–816, hep-ph/9306240.
163. G. Duplancic and B. Nizic, Eur. Phys. J. C35 (2004) 105–118, hep-ph/0303184.
164. R. K. Ellis and G. Zanderighi, JHEP 02 (2008) 002, 0712.1851.
165. R. Britto, F. Cachazo, and B. Feng, Nucl. Phys. B725 (2005) 275–305, hep-th/0412103.
166. P. Mastrolia, Phys. Lett. B644 (2007) 272–283, hep-th/0611091.
167. D. Forde, Phys. Rev. D75 (2007) 125019, 0704.1835.
168. N. E. J. Bjerrum-Bohr, D. C. Dunbar, and W. B. Perkins, JHEP 04 (2008) 038, 0709.2086.
169. R. Britto, E. Buchbinder, F. Cachazo, and B. Feng, Phys. Rev. D72 (2005) 065012, hep-ph/0503132.
170. R. Britto, B. Feng, and P. Mastrolia, Phys. Rev. D73 (2006) 105004, hep-ph/0602178.
171. C. Anastasiou, R. Britto, B. Feng, Z. Kunszt, and P. Mastrolia, Phys. Lett. B645 (2007) 213–216, hep-ph/0609191.
172. C. Anastasiou, R. Britto, B. Feng, Z. Kunszt, and P. Mastrolia, JHEP 03 (2007) 111, hep-ph/0612277.
173. R. Britto and B. Feng, Phys. Rev. D75 (2007) 105006, hep-ph/0612089.
174. E. W. Nigel Glover and C. Williams, JHEP 12 (2008) 067, 0810.2964.
175. R. Britto, B. Feng, and P. Mastrolia, Phys. Rev. D78 (2008) 025031, 0803.1989.
176. G. Ossola, C. G. Papadopoulos, and R. Pittau, Nucl. Phys. B763 (2007) 147–169, hep-ph/0609007.
177. G. Ossola, C. G. Papadopoulos, and R. Pittau, JHEP 07 (2007) 085, 0704.1271.
178. F. del Aguila and R. Pittau, JHEP 07 (2004) 017, hep-ph/0404120.
179. R. Pittau, hep-ph/0406105.
180. R. Pittau, Comput. Phys. Commun. 104 (1997) 23–36, hep-ph/9607309.
181. R. Pittau, Comput. Phys. Commun. 111 (1998) 48–52, hep-ph/9712418.
182. P. Mastrolia, G. Ossola, C. G. Papadopoulos, and R. Pittau, JHEP 06 (2008) 030, 0803.3964.

183. G. Ossola, C. G. Papadopoulos, and R. Pittau, JHEP 05 (2008) 004, 0802.1876.
184. A. Kanaki and C. G. Papadopoulos, Comput. Phys. Commun. 132 (2000) 306–315, hep-ph/0002082.
185. C. G. Papadopoulos, Comput. Phys. Commun. 137 (2001) 247–254, hep-ph/0007335.
186. C. G. Papadopoulos and M. Worek, Eur. Phys. J. C50 (2007) 843–856, hep-ph/0512150.
187. A. Cafarella, C. G. Papadopoulos, and M. Worek, 0710.2427.
188. H. Czyz and E. Nowak-Kubat, Acta Phys. Polon. B36 (2005) 3425–3434, hep-ph/0510287.
189. H. Czyz and E. Nowak-Kubat, Phys. Lett. B634 (2006) 493–497, hep-ph/0601169.
190. H. Czyz and M. Gunia, unpublished (2009).
191. M. Caffo and H. Czyz, Comput. Phys. Commun. 100 (1997) 99–118, hep-ph/9607357.
192. G. Montagna, M. Moretti, O. Nicrosini, A. Pallavicini, and F. Piccinini, Nucl. Phys. B547 (1999) 39–59, hep-ph/9811436.
193. E. Kuraev and V. Fadin, Sov. J. Nucl. Phys. 41 (1985) 466.
194. G. Altarelli and G. Martinelli, In *Ellis, J. (Ed.), Peccei, R.d. (Ed.): Physics At Lep, Vol. 1*, 47-57.
195. O. Nicrosini and L. Trentadue, Phys. Lett. B196 (1987) 551.
196. O. Nicrosini and L. Trentadue, Z. Phys. C39 (1988) 479.
197. D. Yennie, S. Frautschi, and H. Suura, Annals Phys. 13 (1961) 379.
198. C. M. Carloni Calame, C. Lunardini, G. Montagna, O. Nicrosini, and F. Piccinini, Nucl. Phys. B584 (2000) 459–479, hep-ph/0003268.
199. C. M. Carloni Calame, G. Montagna, O. Nicrosini, and F. Piccinini, Nucl. Phys. Proc. Suppl. 131 (2004) 48–55, hep-ph/0312014.
200. G. Balossini, C. M. Carloni Calame, G. Montagna, O. Nicrosini, and F. Piccinini, Nucl. Phys. B758 (2006) 227–253, hep-ph/0607181.
201. A. B. Arbuzov, G. V. Fedotovich, F. V. Ignatov, E. A. Kuraev, and A. L. Sibidanov, Eur. Phys. J. C46 (2006) 689–703, hep-ph/0504233.
202. S. Jadach, W. Placzek, and B. F. L. Ward, Phys. Lett. B390 (1997) 298–308, hep-ph/9608412.
203. V. Gribov and L. Lipatov, Sov. J. Nucl. Phys. 15 (1972) 675.
204. G. Altarelli and G. Parisi, Nucl. Phys. B126 (1977) 298.
205. Y. Dokshitzer, Sov. Phys. JETP 46 (1977) 641.
206. M. Cacciari, A. Deandrea, G. Montagna, and O. Nicrosini, Europhys. Lett. 17 (1992) 123.
207. M. Skrzypek, Acta Phys. Polon. B24 (1992) 123.
208. M. Przybycien, Acta Phys. Polon. B24 (1993) 1105.
209. A. B. Arbuzov, Phys. Lett. B470 (1999) 252.
210. A. Arbuzov, G. Fedotovich, E. Kuraev, N. Merenkov, V. Rushai, and L. Trentadue, JHEP 9710 (1997) 001, 9702262.
211. A. B. Arbuzov and E. Scherbakova, JETP Lett. 83 (2006) 427.
212. M. Greco and O. Nicrosini, Phys. Lett. B240 (1990) 219.
213. C. M. Carloni Calame, Phys. Lett. B520 (2001) 16–24, hep-ph/0103117.
214. A. B. Arbuzov and E. Scherbakova, Phys. Lett. B660 (2008) 37.
215. C. M. Carloni Calame, G. Montagna, O. Nicrosini, and M. Treccani, Phys. Rev. D69 (2004) 037301, hep-ph/0303102.
216. C. M. Carloni Calame, G. Montagna, O. Nicrosini, and M. Treccani, JHEP 05 (2005) 019, hep-ph/0502218.
217. C. M. Carloni Calame, G. Montagna, O. Nicrosini, and A. Vicini, JHEP 12 (2006) 016, hep-ph/0609170.
218. C. M. Carloni Calame, G. Montagna, O. Nicrosini, and A. Vicini, JHEP 10 (2007) 109, 0710.1722.
219. K. T. Mahanthappa, Phys. Rev. 126 (1962) 329–340.
220. M. Bohm, A. Denner, and W. Hollik, Nucl. Phys. B304 (1988) 687.
221. E. Drago and G. Venanzoni, KLOE note INFN/AE-97/48.
222. F. Berends and R. Kleiss, Nucl. Phys. B228 (1983) 537.
223. F. Berends and R. Kleiss, Nucl. Phys. B186 (1981) 22.
224. F. Jegerlehner, Z. Phys. C32 (1986) 195.
225. H. Burkhardt, F. Jegerlehner, G. Penso, and C. Verzegnassi, Z. Phys. C43 (1989) 497–501.
226. F. Jegerlehner, Nucl. Phys. Proc. Suppl. 162 (2006) 22–32, hep-ph/0608329.
227. G. Balossini et al., Phys. Lett. B663 (2008) 209–213, 0801.3360.
228. P. Rong-Gang, Private communication.
229. S. Jadach, M. Melles, B. F. L. Ward, and S. A. Yost, Phys. Lett. B377 (1996) 168–176, hep-ph/9603248.
230. C. Glosser, S. Jadach, B. F. L. Ward, and S. A. Yost, Phys. Lett. B605 (2005) 123–128, hep-ph/0406298.
231. S. Jadach, B. F. L. Ward, and S. A. Yost, Phys. Rev. D73 (2006) 073001, hep-ph/0602197.
232. C. Carloni Calame et al., in preparation.
233. K. Hagiwara, A. D. Martin, D. Nomura, and T. Teubner, Phys. Rev. D69 (2004) 093003, hep-ph/0312250.
234. K. Hagiwara, A. D. Martin, D. Nomura, and T. Teubner, Phys. Lett. B649 (2007) 173–179, hep-ph/0611102.